

UNIVERSITI MALAYSIA PAHANG



LAB2MARKET PROJECT

UIC161001

**INDUSTRIAL TESTING OF A 3-AXIS CNC TAILOR WELDED BLANK LASER
WELDING MACHINE USING PREDEFINED CLOSEST-DISTANCE VOLUME
INTERPOLATOR**

UMP
PROJECT LEADER:

IR. DR. FADHLUR RAHMAN BIN MOHD ROMLAY

TABLE OF CONTENT

TOPIC	PAGE NUMBER
INTRODUCTION	4
MILESTONE 1	8
Engineering Specification Design	
1.1 Conceptual Mechanical Design and Specification	
1.2 Conceptual Process Specification	
1.3 Conceptual Software Architecture	
MILESTONE 2	17
Detailed Engineering Design	
2.1 Detail Mechanical Design and Specification	
2.2 Detail Process Specification	
2.3 Software Architecture	
MILESTONE 3	36
Development and fabrication of prototype TWB machine	
3.1 Mechanical and Electrical Parts	
3.2 Main Framed as Based Structure	
3.3 CNC Gantry Structure Assembly	
3.2 GUI and Software Development	

MILESTONE 4**58**

PILOT PLAN LINE SETUP

- 4.1 Procure and Assemble of Laser Head with CNC Machine –Laser Integration.
- 4.2 Pre-Test TWB Machine – Part Welding Testing
- 4.3 Software Testing – Alfa Version

MILESTONE 5**74**

TRIAL RUN

- 5.1 Jig Tuned Up – TWB Part Fabrication
- 5.2 Performance Measurement – QC report on Mechanical Test by PHN
- 5.3 Software Finalizing – Release Version

FUTURE PROSPECT OF THE TWB TECHNOLOGY**117****REFERENCES****120****UMP**

INTRODUCTION

Tailor Welded Blank's (TWB's) technology was introduced and developed mainly for automotive industries which usually utilizing materials with different strength properties, different thicknesses, and also different surfaces coating [1]. Tailor Welded Blanks are made from individual steel sheets of different thickness, strength and coating which are joined together mostly by laser welding [2]. This manufacturing process allows for flexible part design and ensures the right material is used in the right place. Thicker or higher-strength material can be used in highly stressed areas while thinner sheets or deep drawing grades can be used in others. Expensive materials are only used where they are needed. There was some advantages drawn from the usage of this technology such as cost saving, weight reduction, and strength increment.

It was proved that when using TWB's, parts can be produced at reduced cost due to the usage of expensive materials only at the necessary location. The part weight also can be reduced since appropriate materials was utilized in the appropriate are. The most important features of this technology is to create a high strength at certain area, which is mostly at the crashed area with the utilization of high strength metals such as Advance High Strength Steels (AHSS) and Ultra High Strength Steels (UHSS).

High Strength Steels (HSS) and Advance High Strength Steel (AHSS)

Different components of a car body require many complicated forming operations where ductility of the material is very crucial. The automotive manufacturers are also continuously increasing the use of high strength steel (HSS) in order to comply with the safety norms of different geographic regions and also to reduce the weight of the car to make it more fuel efficient [3]. In a ways of combination of ductility and hardness, Boron steel (22MnB5) type was particularly used for supporting the body parts and safety relevant parts such as centre pillars, side impact protection, bumpers, even the chassis parts [4]. The type of Boron steel used today

was extremely high and was categorized in advance high strength steel (AHSS) which having characteristics of four times stronger than the average HSS. However, it could be applied in the mostly crashed parts, where it was joined with other parts consists of lower strength metals through TWB process which can be easy for the vehicle extrication rescue due to the cutting processes.

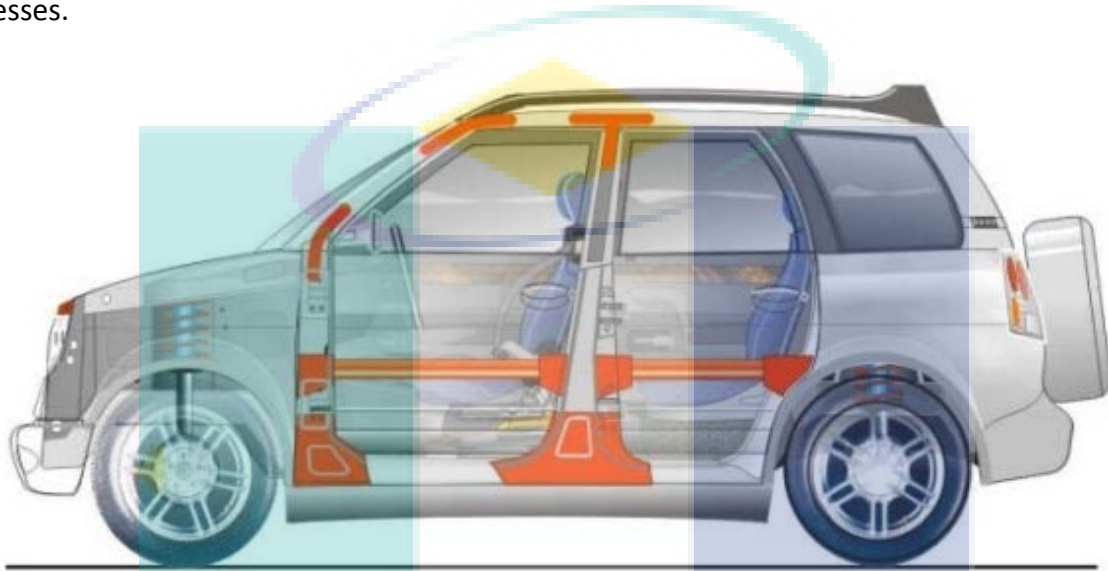


Fig.1 Strengthening Bars, Gussets, and Plates.

The introduction of this Boron steel was primarily found on European vehicles. Volvo probably uses this metal the most especially on bumper reinforcement, door beams, and seat recliner bracket as shown in Fig. 1. The application of Boron steel also to strengthen the weaker areas of the motor vehicle is obviously. Fig. 2 shows the results for the Boron parts after the crashed test which showing the strength of this material. However, appropriate tools was needed in order to cut this steel. It was proven that TWB technique plays important role where the soft part could be cut with normal rescue tools mostly after the deadly crashes.



Fig.2 Result from the Crashed Test.

Laser Welding in TWB

Lightweight design issue is the most important and challenging issue nowadays especially involving in automotive industries in order to produce light weight vehicle to improve the fuel efficiency [5]. TWB promising the combination of lightweight materials and the AHSS which applied not only for cars, but as well for transportation vehicles and cranes. In order to join the dissimilar steels characteristics, laser welding is the most valuable technique since there is no weld filler used compared to the conventional welding method such as metal inert gas (MIG), or tungsten inert gas (TIG) welding method. Fig. 3 shows the results of laser welding for a TWB part which shows that the smaller heat affected zone (HAZ) produce where this region was normally the weaker parts in welding joint [6].

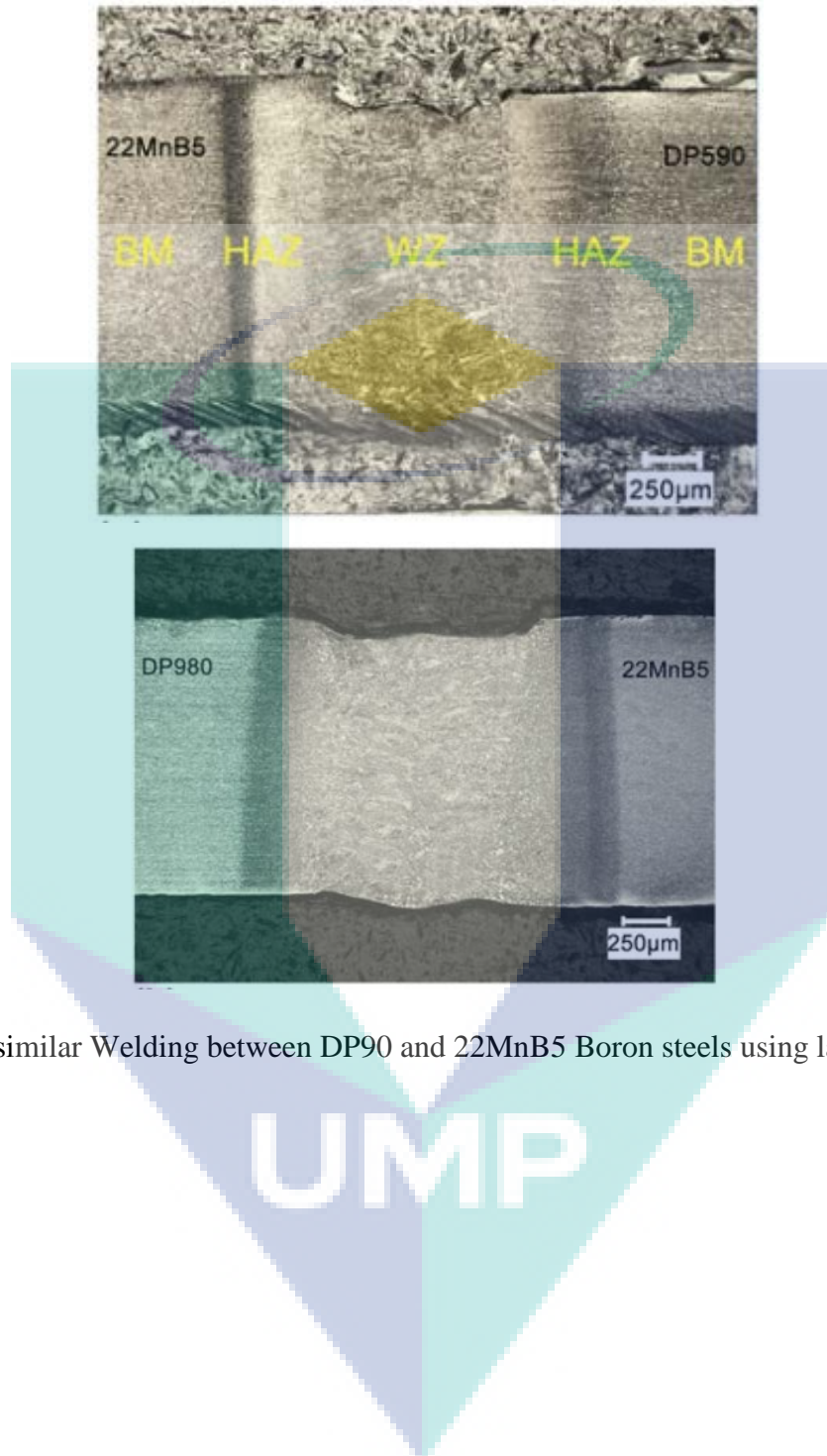


Fig. 3 Dissimilar Welding between DP90 and 22MnB5 Boron steels using laser welding.

MILESTONE 1 ENGINEERING SPECIFICATION DESIGN

1.1 CONCEPTUAL MECHANICAL DESIGN AND SPECIFICATION

Tailor welded products are primarily used in the automotive industry with popular applications including side frames, doors, pillars and rails. Whatever the application, TWB can help design solutions to reduce material cost and weight, improve quality and performance while optimizing your production processes. Potential applications outside automotive include solutions for industries such as: alternative energy, appliance, trucking, rail car, shipbuilding, construction, trailer, elevator/escalator, and furniture. Wherever steel and aluminium are used, tailored products can be applied to improve results. Fig. 1-1 to Fig. 1-3 show the applications of TWB in automobile parts which is car's side frame, door inner with header, and B- pillar, respectively.



Fig. 1-1. Car's Side Frame.



Fig. 1-2. Door Inner with Header.



Fig. 1-3. B-Pillar Outer.

Welded part of TWB was received from the PHN Company for the B-pillar parts before the hot stamping process. Materials was categorized to 3 parts which is A, B, and C since the information of the metals were unknown as shown in Fig. 1-4, Fig 1-5 and 1-6 shows the welded parts was shear cut in order to examine its welded cross section.

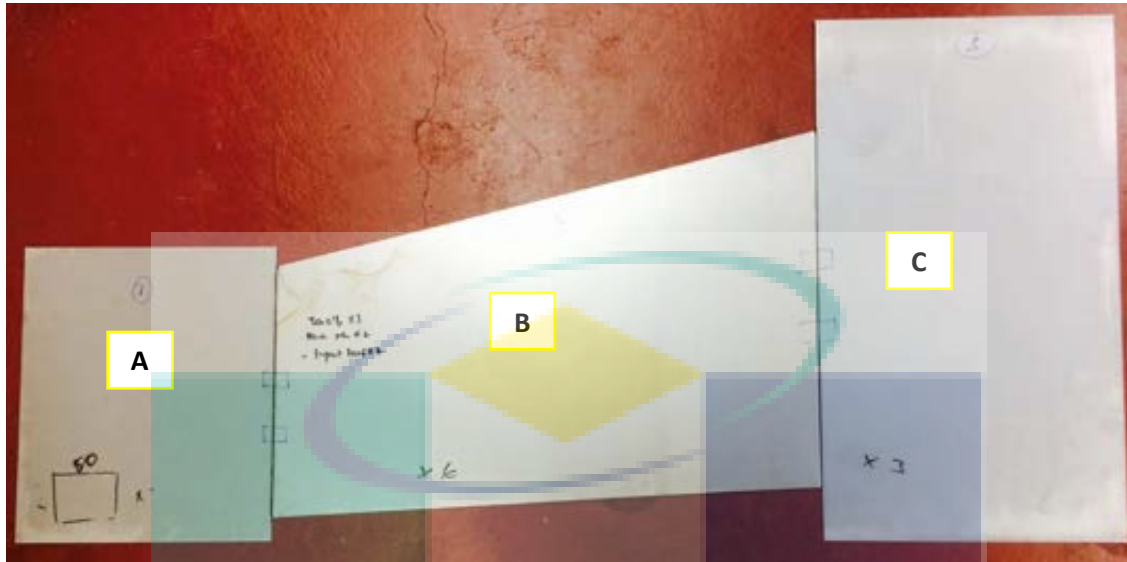


Fig. 1-4. B-pillar TWB welded part.

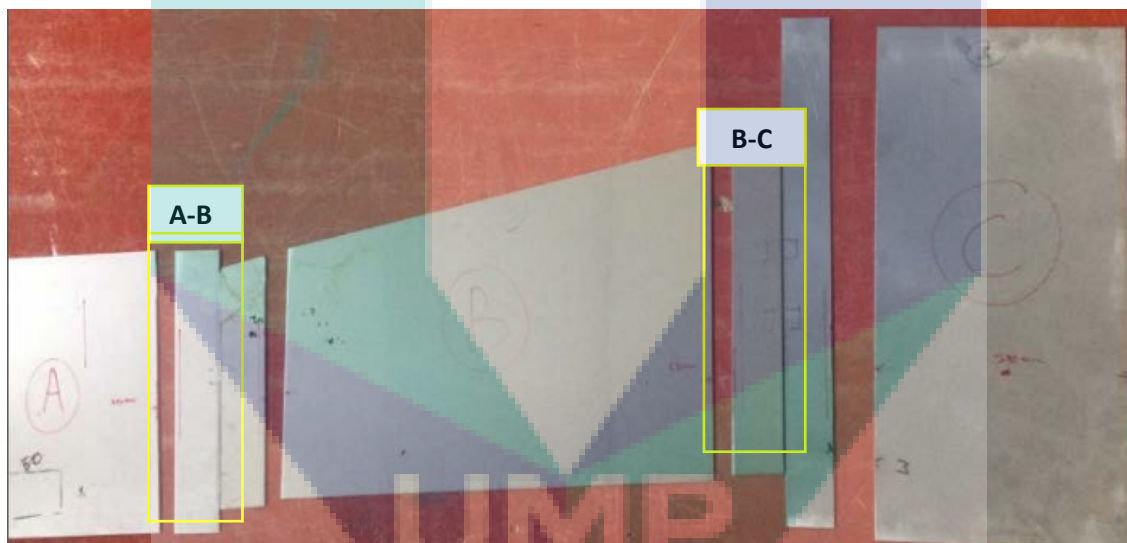


Fig. 1-5. Welded Part was Shear Cut at The Cross Section.

The idea to join the section A, B and C at different thickness of plate in order to get shape and geometry optimization according to the stress that applied to the structure. The shape optimization will provide cost effective and efficient.

1.2 CONCEPTUAL PROCESS SPECIFICATION

FIBER LASER MODULE

Fiber lasers deliver their energy through an integrated flexible optical fiber. Fiber lasers have a monolithic, entirely solid state, fiber-to-fiber design that does not require mirrors or optics to align or adjust. These features make fiber laser-based systems. Fiber lasers are typically smaller and lighter in weight than traditional lasers, saving valuable floor space. While conventional lasers can be delicate due to the precise alignment of mirrors, fiber lasers are more rugged and able to perform in variable working environments. These qualities permit fiber laser system to be transported easily. Main Features

- Excellent Beam Parameter Product (BPP)
- Constant BPP Over Entire Power Range
- Small Focus over Large Working Distance
- Over 30% Wall-Plug Efficiency

Maintenance-free Operation

- Modular 'Plug & Play' Design
- Compact, Rugged & Easy to Install Integrated Coupler or Beam Switch

Ytterbium Fiber Laser System

Low-order-mode Ytterbium fiber lasers range up to hundreds of kW output power, operating in CW/modulated modes up to 5kHz with wall-plug efficiencies >40%. The dynamic range is from 10% to full power with no change in beam divergence or beam profile, allowing a single laser to be used for both high and low power applications such as welding, drilling and cutting, a previously unheard of capability. The high brightness allows the use of long focal length processing lenses for vastly improved depth of field and minimal damage to optical

components. The unit must be equipped with fiber delivery module for the laser process application.

Ytterbium laser system mode of operation can be CW or modulated central wavelength. The wavelength ranges from 1070 ± 10 nm and the maximum average power is 2000 W. The laser system is housed in a closed compartment, air-conditioned and sealed cabinet adding to the robustness of the unit. This system must be controlled by either digital I/O, analog control or own software with the additional option to add either devicenet, profibus or ethernet interfaces. Developed as a completed system, this design features the widest range of fiber diameters, as well as the option to terminate to up to 6 ports from one power source

Output Feeding Fiber Core Terminating Diameter, μm : 50 Modulation Frequency, kHz: 0 – 5
Power Tunability, %: 10 – 100 Power Stability, % : ± 2 Beam Parameter Product, mm \times mrad:

Laser Welding Head

Laser welding head deliver accurate focusing within a modular design that supports a variety of setup and process options. The availability of tip extension lengths provides adaptability to almost any focal length. Offered par- focal versions can accommodate multiple focal lengths without changing the overall length of the head. In most configurations, a second lens drawer is included for the cover glass slide to allow easy, tool-less access. Adjustments are available for focus and standoff, as well as X-Y centering of the lens. Specification Clear Aperture (based on collimating lens choice) is 25.0 – 35.5 mm and fiber connection is HLC-8. The laser power is up to 8kW and support by water cooling system.

Laser Power Meter

The device utilizes disruptive technology to measure laser beam characteristics on very high power lasers. It measure a laser without coming in contact with its beam which allows it to be the laser quality measurement tool with no upper limit or constraint. The systems provides high-power industrial laser users with data never before seen such as the dynamic measurement of focus shift caused by thermal effects on the laser system. By not intercepting the beam and yet providing instantaneous measurements, we can monitor the beam at frequent intervals without having to shut down the process or remove tooling and fixtures to get access. In addition, we can now measure focal spot location at several times per second and know if there is any focal spot shift during those critical start-up moments.

The power meter is applicable for laser energy measurement. The power meter is capable as on-board features such as laser tuning, data logging, graphing, normalize, power or energy density units, attenuation scaling, max and min limits. The meter can also display the power or energy with a high resolution simulated analog needle display. The meter can be operated either by battery or from an AC source with the charger plugged in at all times. Its backlight allows illumination of the power meter in low light conditions. The built-in USB and RS232 interfaces and PC software allow on-line processing of data or processing previously stored data; results are displayed graphically on a PC. To support PC interfacing, LabVIEW drivers, Com Object Interface and ActiveX controls or related software must be provided.

It also provides an industrial laser user with measurement of other key laser operating parameters in real-time. The system measures the signal generated from Rayleigh scattering around the laser's beam waist, where the power density is the highest. Rayleigh scattering is a physical property of light caused by light scattering off of air molecules. Unlike traditional beam measurement systems, the beam passes directly through device and is not disrupted, mechanically or optically. In addition, the device has no moving parts so there is no need for cooling of any components. Specialized system software dynamically measures the signal multiple times per second, allowing the laser user to key in on critical operational laser attributes, such as beam waist size

1.3 CONCEPTUAL SOFTWARE ARCHITECTURE

Tailor Welded Blanks (TWB) CNC Laser Welding Controller Board

The TWB machine controller board is designed based on the recommendation of Panasonic Minas A5 Servo Drivers Manual. The controller board acts as an interface board for the Host Controller (PC) Parallel Port output to the Panasonic Minas A5 Servo Driver X4 Connector. The controller board also acts as limit switches hub which relay the limit switches signal to the X4 Connector input.

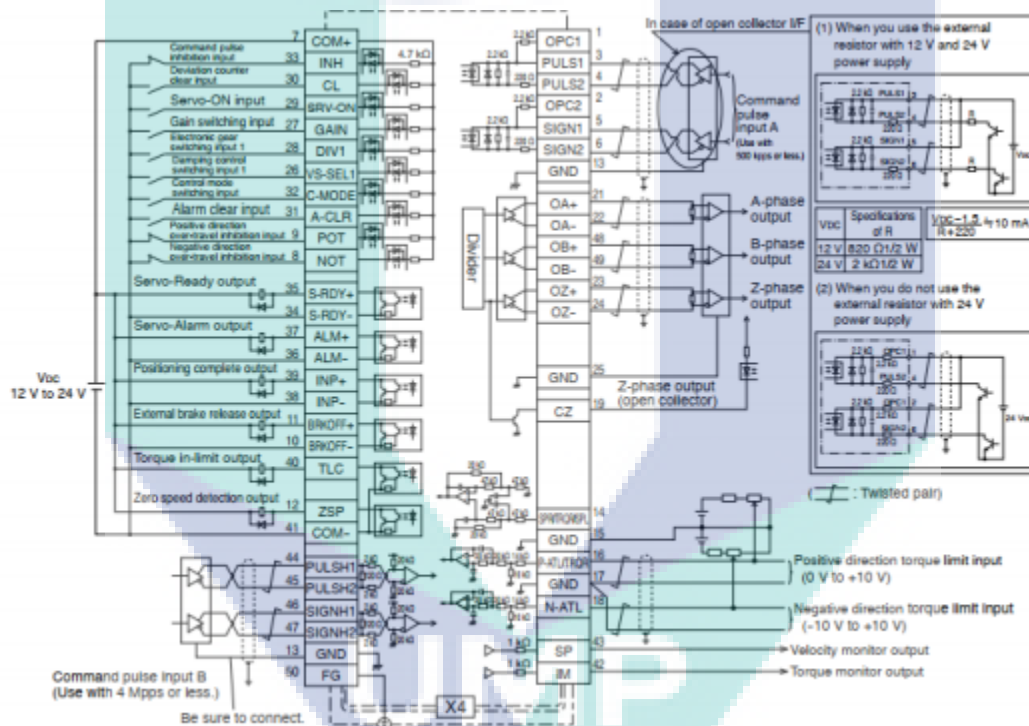


Figure 1.6. Minas A5 wiring example for Position Control Mode

Based on the recommendations of Minas A5 technical document in Figure 1.6, the controller board is designed for integration of all inputs and outputs signals in the system. The controller board also provide a terminal for the Laser module integration. Other features of the controller board is discussed in the next section.

Controller Board Architecture

The design of the controller board for TWB Machine is given the name Machmum Controller Board. Currently, it is the first iteration of the TWB Controller board design. The design will be further improved in the future to enhance its robustness, stability, and reliability. More features can be added such as on-board microcontroller unit (MCU) to process the incoming signals in any way since it can be reprogrammable to suit any applications.

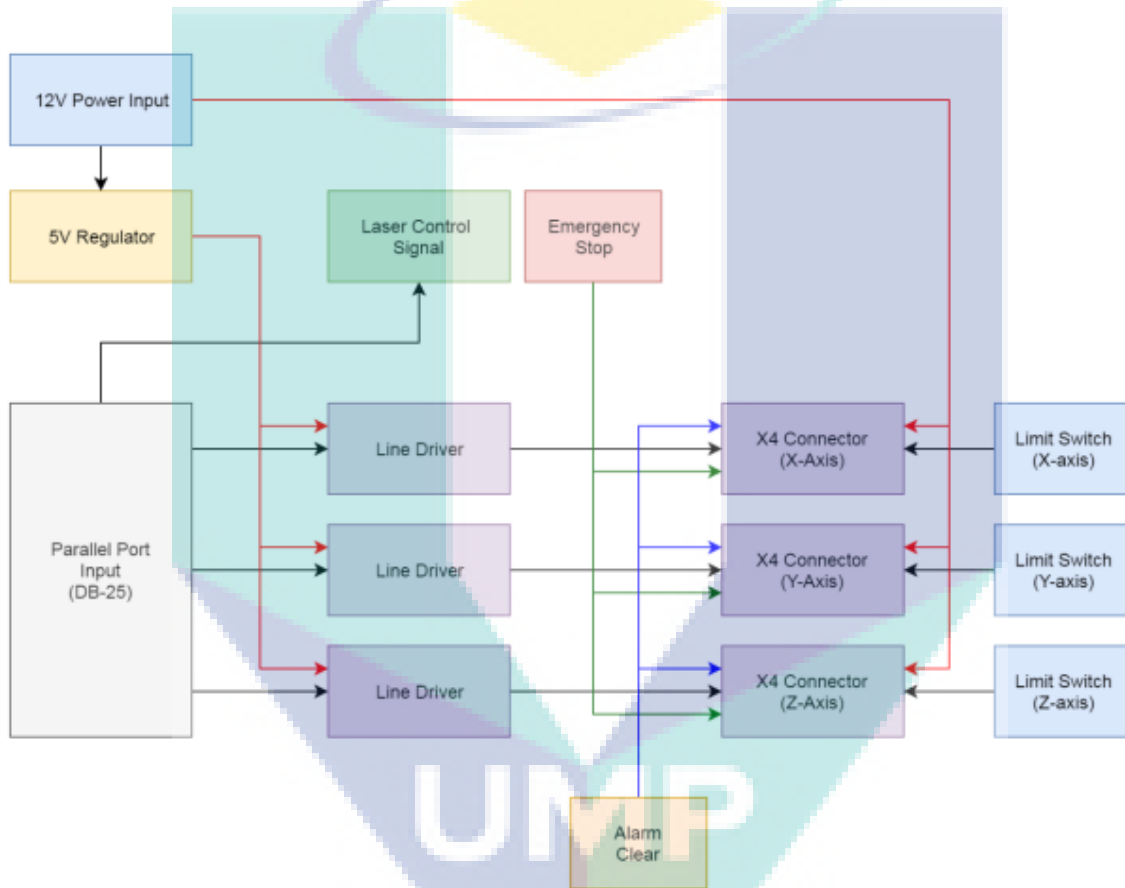


Figure 1.7. Architecture for Machmum Controller Board

As seen in Figure 1-7, the Machmum Controller Board requires 12V DC Power Input to operate. The 12V supply is shared with each axes X4 Connector pin for COM+ as specified by the Minas A5 Servo Driver manual. The 12V is also regulated to 5V to power up Line Driver ICs. Parallel Port output data pins are connected to its respective axes Line Driver ICs input for Pulse and Direction as shown. Two data pins are connected to

the terminal for Laser Control Signal. The two pins are allocated for Laser module integration process. Limit switches are directly connected to its respective axes of X4 Connector.

According to Minas A5 technical manual, there are two pins for limit switch connection for Minas A5 Servo Driver. One is Positive-Over-Travel (POT) pin, the other is Negative-Over-Travel (NOT) pin in the X4 Connector. The POT pin is for positive direction limit of the linear drive, and vice versa for NOT. Emergency Stop terminal is provided for the Emergency Stop button connection to the Machmum Controller Board. In the Controller Board, the Emergency Stop signal is connected to every SRV-ON pin of the X4 Connectors. This is purposely designed so that whenever the Emergency button is pressed, a signal will be sent to all servo drivers to immediately stop the driver by disabling it and prevent it from accidently receives anymore pulse command. Alarm Clear is an optional input signal for every Minas A5 Servo Drivers. This signal acts as Soft Reset for the Servo Drivers. However, not all alarm/error in Minas A5 can be cleared by soft-reset. Critical error might require the driver to be switched OFF to clear the Error notification in the Servo Drivers.

The logo for UMP (Universiti Malaysia Perlis) is a large, stylized letter 'U' composed of four overlapping triangles in shades of teal and light blue. The letters 'UMP' are printed in white, bold, sans-serif font across the center of the 'U' shape.

UMP

MILESTONE 2 DETAIL ENGINEERING DESIGN

2.1 DETAIL MECHANICAL DESIGN AND SPECIFICATION

Mechanical specification of TWB part from PHN Industry Sdn Bhd. are tabulated in Table 2-1 and Table 2-2 below. The thickness variation of materials are; 1 mm for SPRC 45, and 1.6 mm for SPRC 40. These types of materials are known as cold-reduced high strength steels.

Table 2-1 Chemical Composition of as-received materials

Material	Element	C	Mn	P	S	Si
SPRC 40	Wt %	0.03	0.254	0.069	0.01	0.104
SPRC 45	Wt %	0.08	0.72	0.065	0.05	0.09

Table 2-2 Mechanical Properties of as-received materials

Material	UTS (MPa)	YS (MPa)	E, 50 GL (%)
SPRC 40	401	281	39
SPRC 45	454	337	37

The geometry properties of the B-pillar panel is as shown in Fig. 2-1 which consists of three blanks of materials. The blanks were joint at weld line in a horizontal straight line.

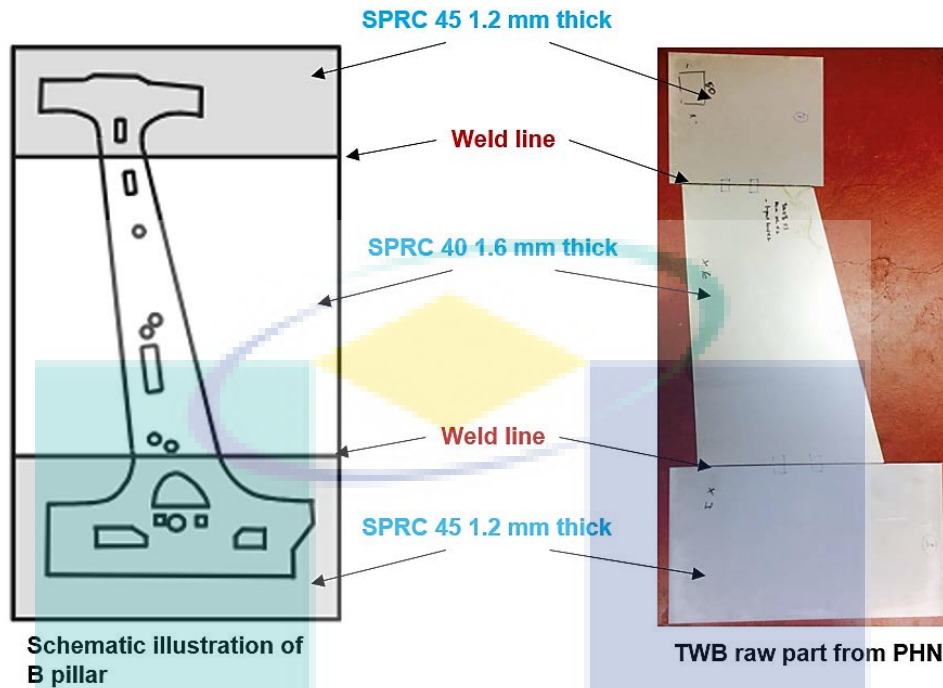


Fig. 2-1. SPRC 40 and 45 application in TWB raw products of B-pillar

The detail specifications of the pillar is discussed next which consist of material specification and joint characteristic.

2.2 DETAIL PROCESS SPECIFICATION

The conceptual laser process parameter that determined the quality of final laser product are the macrostructure and microstructure arrangement. Micro hardness can be measure using Virker hardness test while energy dispersive X-Ray (EDX) analysis can be applied to observe the element composition percentage in the weldment area.

Macrostructure

For this section, sample was divided to two parts which is part A-B and part B-C. Top surfaces and welded cross section was shown in this section.

Sample A-B

The macrostructures images was captured for this sample on top surface and at the weld cross section. Fig. 2-2 and 2-3 shows the macrostructures images for top surface and weld cross section, respectively.

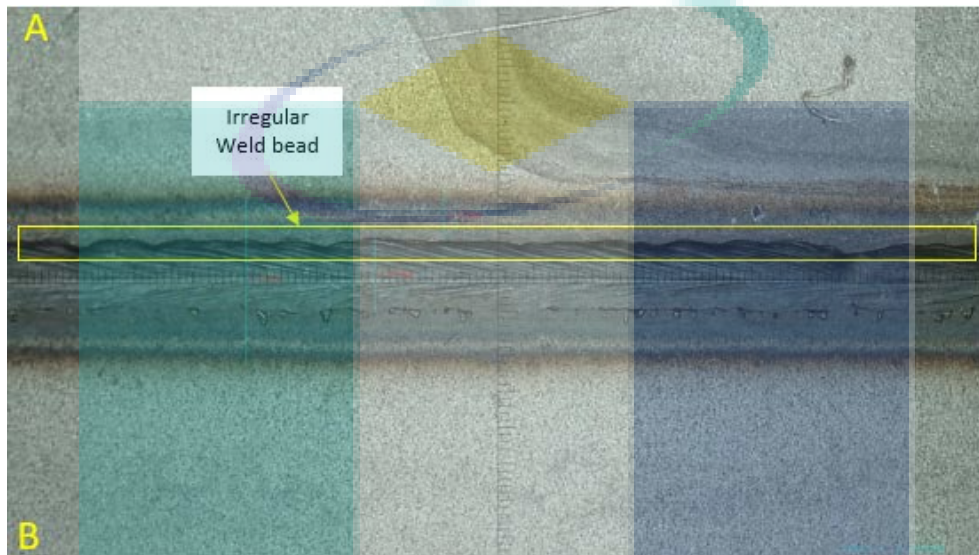


Fig. 2-2. Top Surface at Weld Region of Sample A-B.

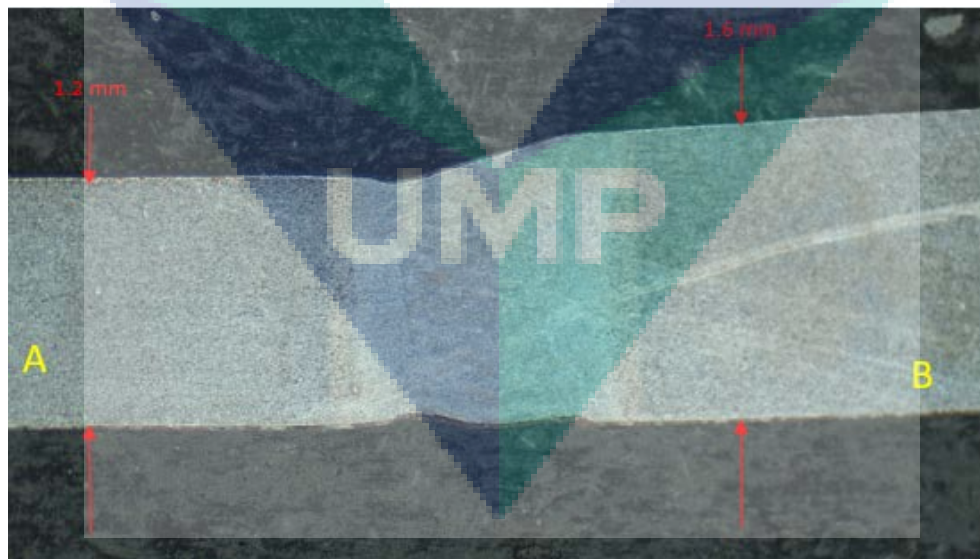


Fig. 2-3. Welded Cross Section of Sample A-B.

From Fig. 2-2, it was shown that irregular weld bead produced on the top surface of the welded part. There was no spatter or arc strike was found at the surface and the weld

bead also was smaller compared than using conventional welding method such as MIG and TIG. For Fig. 2-3, it was observed from the image captured that the parts was a dissimilar welded part, where material A and B having thicknesses of 1.2 and 1.6 mm, respectively. Full weld penetration with smaller HAZ was found at the weld region and it shows that one of the characteristics of a strong weld joint. It was observed that sample A and B having similar grain structure with same time taken for etching process.

Sample B-C

The macrostructures images was captured for this sample on top surface and at the weld cross section. Fig. 2-4 and 2-5 show the macrostructures images for top surface and weld cross section, respectively.

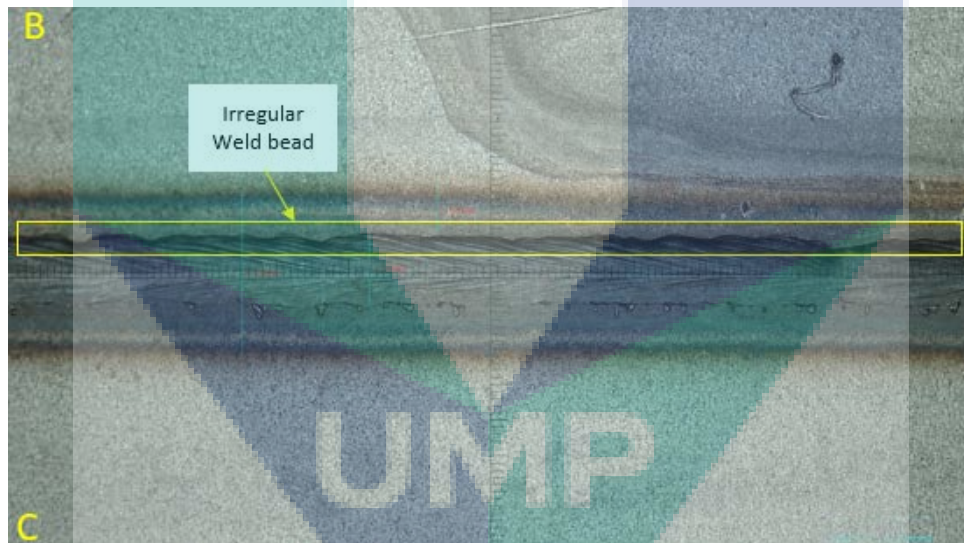


Fig. 2-4. Top Surface at Weld Region of Sample B-C.

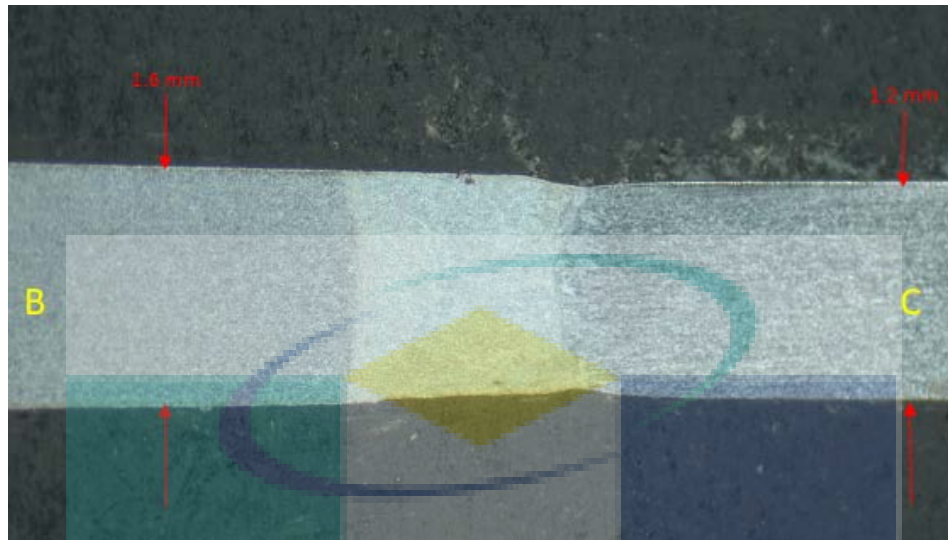


Fig. 2- 5. Welded Cross Section of Sample B-C.

From Fig. 2-4, it was shown that irregular weld bead produced on the top surface of the welded part. There was no spatter or arc strike was found at the surface and the weld bead also was smaller compared than using conventional welding method such as MIG and TIG. For Fig. 2-5, it was observed from the image captured that the parts was a dissimilar welded part, where material B and C having thicknesses of 1.6 and 1.2 mm, respectively. Full weld penetration with smaller HAZ was found at the weld region and it shows that one of the characteristics of a strong weld joint. Based on the macrostructure observation, it was observed that material B and C having different grains structure and sample C was etched with longer time compared to the sample A and B.

Microstructures

Microstructure images at the cross section area for both samples, A-B and B-C was observed using optical microscope (OM) and scanning electron microscope (SEM). Fig. 2-6 and 7 show the microstructure images captured for both samples.

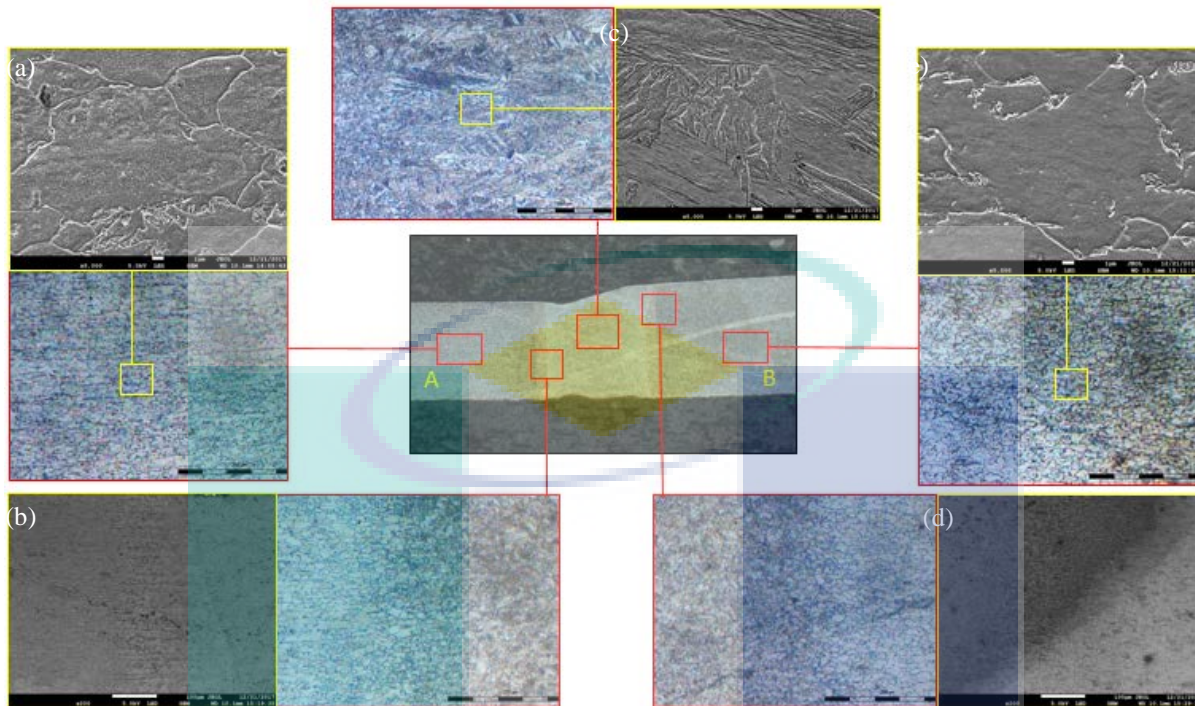


Fig. 2-6. Microstructure Images at (a) Base Metal A (b) Transition Region from A to FZ (C) Fusion Zone (d) Transition Region from FZ to BM B and (e) Base Metal B.

From Fig 2-6 (a), it was observed that there was inter and intradendritic structure in base metal A which represents by ferrite and pearlite. For Fig. 2-6 (b), it was shown that the transition region from the base metal A to the fusion zone (FZ) where the grain structure from ferrite and pearlite changing to fully martensitic. Fig. 2-6 (c) shows the images of grain structures which have fully changed to martensite in FZ. Meanwhile in Fig. 2-6 (d), the grains changing from the martensite to ferrite and pearlite towards base metal B. Base metal B was shown in Fig. 2-6 (e) where the grain structure also consists of inter and intradendritic grain which represent the ferrite and pearlite structure similarly with base metal A. It was proven when the etching solution and time was same used to etch sample A-B. Average grain size of base metal A was approximately $6.88 \mu\text{m}$ which is smaller compared to base metal B which is approximately $7.26 \mu\text{m}$.

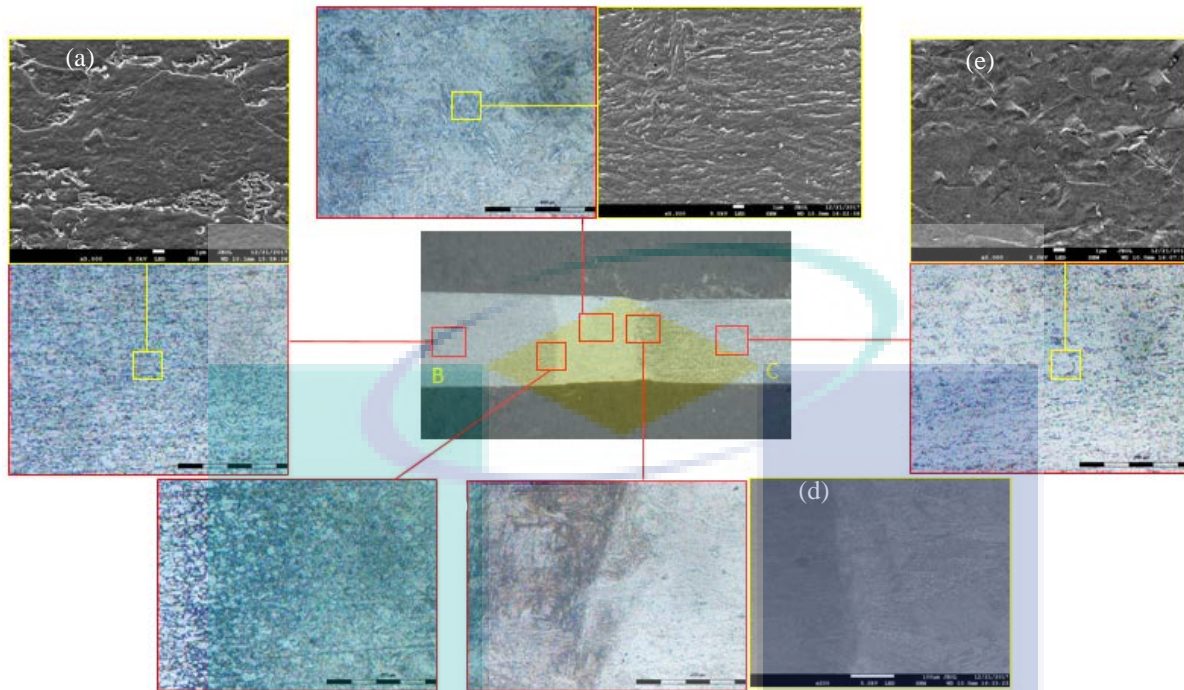


Fig.2-7 Microstructure Images at (a) Base Metal B (b) Transition Region from B to FZ (C) Fusion Zone (d) Transition Region from FZ to BM C and (e) Base Metal C.

Meanwhile, for Fig. 2-7 (a), it was observed that base metal B having the grain structure consists of ferrite and pearlite which is same as before (sample A-B) since this side come from the same material. Fig. 2-7 (b) shows the transition region from coarser grain structure to finer martensitic grain towards fusion zone. In fusion zone which is represented by Fig. 2-7 (c), it consists of fully fine martensite grain structures. In Fig. 2-7, it show the transition region from FZ to the base metal C. However, Fig. 2-7 (e) shows the grain structure of base metal C where the grain structure was unrecognised. The average gain size of base metal B was approximately $7.24 \mu\text{m}$ meanwhile for base metal C could not be measured for this sample.

Micro Hardness

Vickers hardness test was performed on this sample using 500 gf with 10 s dwell time. The indentation was done across the weld and measured with 40 times magnifications. Table 2 shows the data collected for the hardness value. Fig. 2-8 shows the illustration of hardness variation across the welding joint of sample A-B. Each point of indentation was range about 0.25 mm to another point. Total indentation for this sample was 13 points. Table 2-4 was constructed in order to calculate the region size for the HAZ and FZ, mostly. For HAZ 1, which is at the base metal A's side, the region size was approximately 0.5 mm. It was similar to the fusion zone and HAZ 2 which is also having same region size.

Table 2-3. Hardness Value for Sample A-B.

Points	Position (mm)	Vickers Hardness (Hv)
1	0	160
2	0.25	168.4
3	0.5	167
4	0.75	196.7
5	1	186
6	1.25	332.5
7	1.5	319.4
8	1.75	333.7
9	2	219.5
10	2.25	189.6
11	2.5	170.4
12	2.75	160.6
13	3	161.9

Table 1-4. Region Size Based on Hardness Variation in Sample A-B.

Location	Size (mm)
Base Metal A	0.75

HAZ 1	0.5
FZ	0.5
HAZ 2	0.5
Base Metal	0.75

B

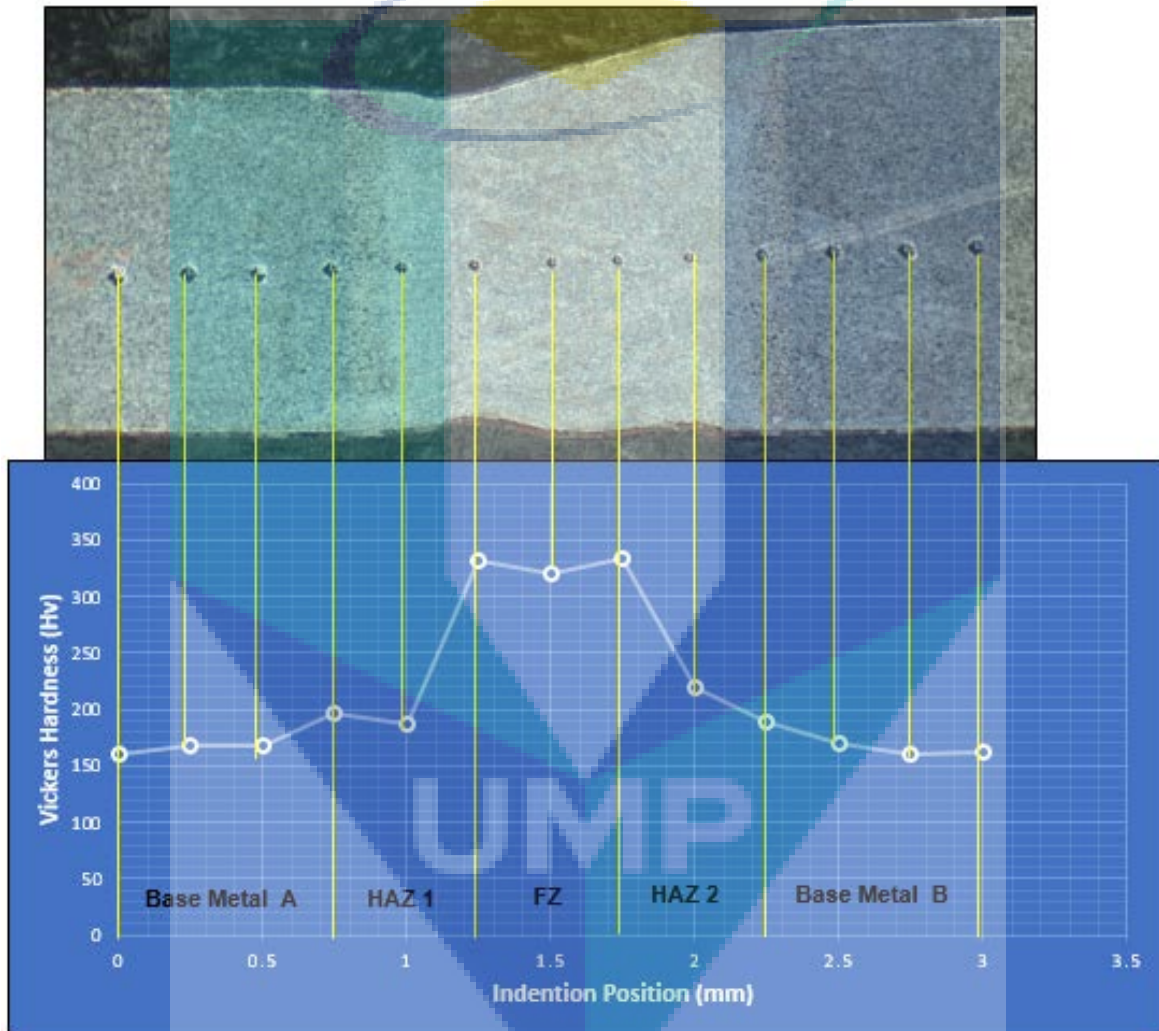


Fig. 2-8. Hardness Value versus Indention Positions for Sample A-B.

Graph of hardness value was constructed based on the data collected in Table 2-3. It was observed that base metal region of both metals, A and B was lower than its HAZ. Fusion Zone

possessed the highest hardness value which is maximum 333.7 Hv. The hardness value at FZ was high due to the fully martensitic grain structure produced after weld.

For sample B-C, the hardness was also performed and the data was collected as shown in Table 2-5. Eleven indentation points was done since the weld size was smaller compared to the weld region in sample A-B. Graph of hardness variation was constructed as shown in Fig. 16 based on data collected in Table 2-5. It was observed from Fig. 2-9 that the hardness was highest at the fusion zone also. However, the hardness was lower at the base metal of B and C. The size of the region was then calculated based on the indentation variation across the weld. All region starting from the base metal B until base metal C having same width based on the indentation points.

Table 2-5. Hardness Value for Sample B-C.

Points	Position (mm)	Vickers Hardness (Hv)
1	0	186.6
2	0.25	194.3
3	0.5	235.2
4	0.75	256.5
5	1	347.6
6	1.25	332.7
7	1.5	357.3
8	1.75	243.2
9	2	230.7
10	2.25	175.2
11	2.5	184.7

Table 2-6. Region Size Based on Hardness Variation in Sample B-C.

Location	Size (mm)
B Base Metal	0.5
HAZ 1	0.5

	FZ	0.5
	HAZ 2	0.5
C	Base Metal	0.5

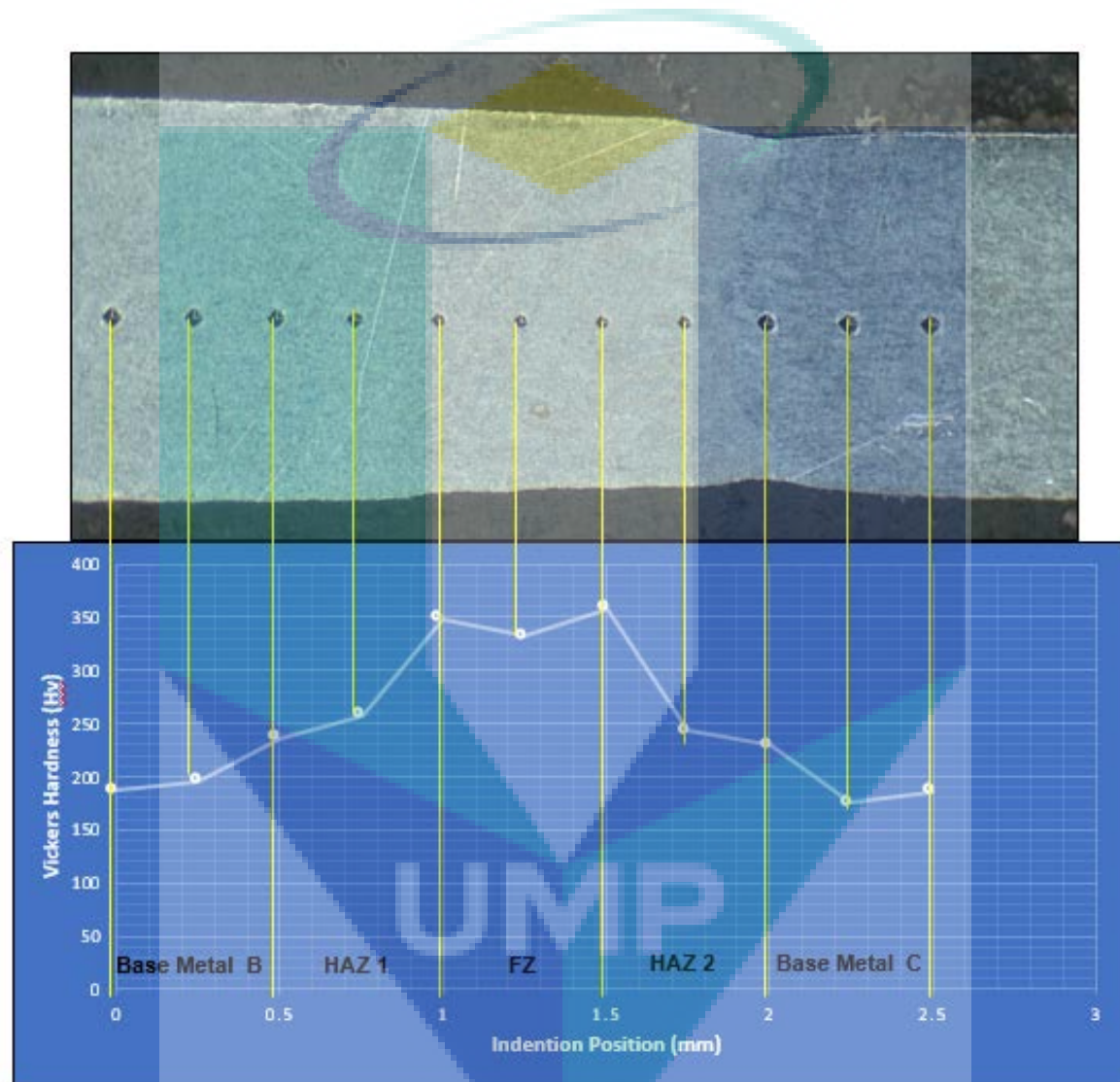


Fig. 2-9. Hardness Value versus Indentation Positions for Sample B-C.

Energy Dispersive X-Ray (EDX) Analysis

EDX analysis was performed on both samples A-B and B-C where 4 spectrums was done in order to observe the element composition percentage in the weld. For sample A-B, the EDX result

was shown in Fig. 2-10 where area scan was done for 4 spectrum at 4 different regions. EDX analysis for sample B-C was shown in Fig. 2-11 where only 3 area spectrum was done since only point spectrum was done to determine the element composition in the grain of fusion zone. The element composition was then summarized in Table 2-7 which consists of elements Boron, B, Carbon, C, Mangan, Mn, and Iron, Fe as balance composition in term of its weight percentages.

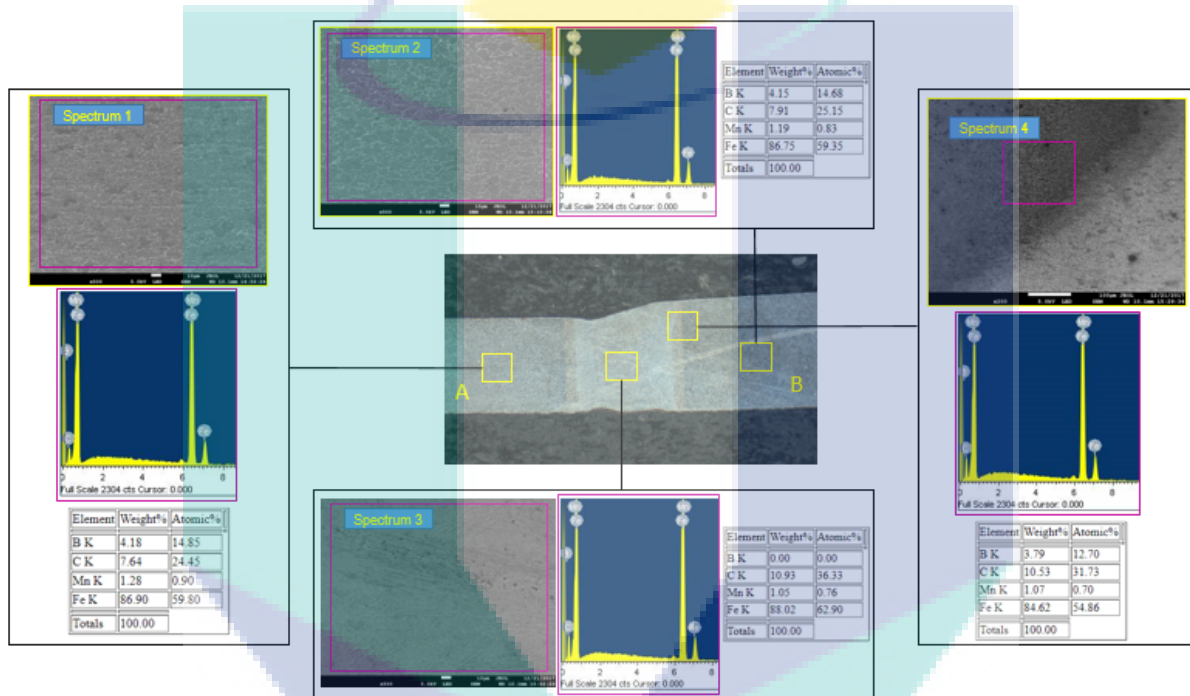


Fig.2-10. EDX Analysis for Sample A-B.

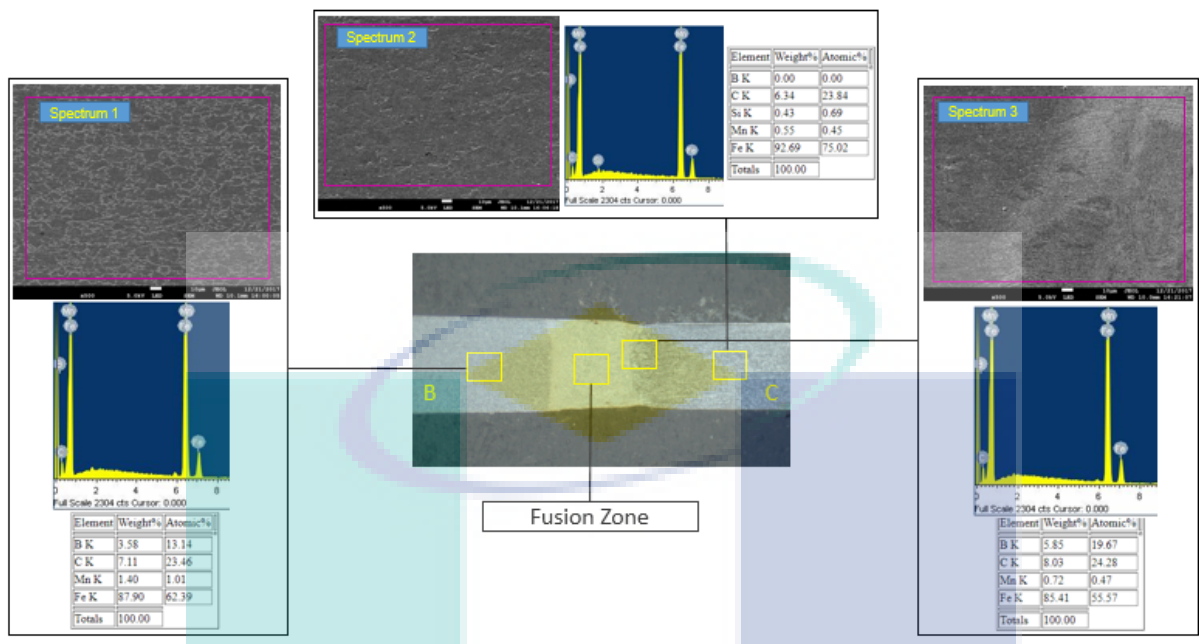


Fig.2-11. EDX Analysis for Sample B-C.

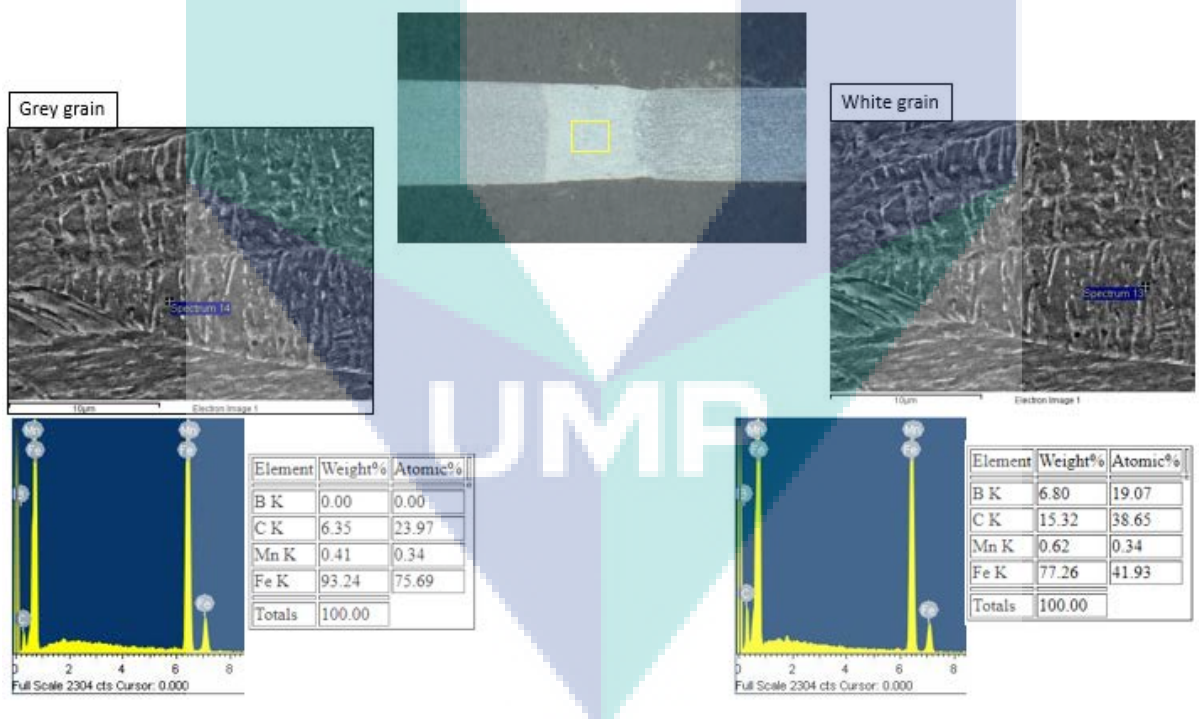


Fig.2-12. EDX Analysis for Fusion Zone in Sample B-C.

Based on Table 2-7, it was observed that boron element is in high percentage for A and B sample. The weight percentage of B is in range 3% - 5% while C also got in high weight

percentage about 7% and can reach up to 24%. However, sample C shows zero weight percentage of B but high in C composition about range 10% - 24%.

Table 2-7 Summary of EDX Results for Both Samples

Spectrum	Sample A-B		Sample B-C	
	Element	Composition , Wt %	Element	Composition , Wt %
1	Boron, B	4.18	Boron, B	3.58
	Carbon, C	7.64	Carbon, C	7.11
	Mangan, Mn	1.28	Mangan, Mn	1.40
	Iron, Fe	Bal.	Iron, Fe	Bal.
2	Boron, B	4.15	Boron, B	0.00
	Carbon, C	7.91	Carbon, C	23.8
	Mangan, Mn	1.19	Mangan, Mn	0.45
	Iron, Fe	Bal.	Iron, Fe	Bal.
	Silicon, Si	-	Silicon, Si	0.69
3	Boron, B	0.00	Boron, B	19.7
	Carbon, C	10.9	Carbon, C	24.3
	Mangan, Mn	1.05	Mangan, Mn	0.47
	Iron, Fe	Bal.	Iron, Fe	Bal.
4	Boron, B	3.79	-	-
	Carbon, C	10.5	-	-
	Mangan, Mn	1.07	-	-
	Iron, Fe	Bal.	-	-

2.3 SOFTWARE ARCHITECTURE

Open Architecture Control (OAC) is a well-known term in the field of machine control [7]. Since the early nineties several initiatives world-wide have worked on concepts for enabling control vendors, machine tool builders and end-users to benefit more from flexible and agile production facilities. The main aim was an easy implementation and integration of customer-specific controls by means of open interfaces and configuration methods in a vendor-neutral, standardized environment. An open-architecture is the definition of a set of components with well-defined behavior and well-defined relationship, and for which the definition is known to all. Often the definition is standardized, either through a standards body or through de facto adoption by a wide community. In some cases, component vendors provide the definition. Desktop computing is one of the most widely known examples of an open architecture, where components include display monitors, input devices, storage devices, and software functions

provided by the operating system or applications [8]. There are a lot of benefits for suppliers and users of using OAC [9].

The project presents the development of a new OAC system for Computerized Numerical Control (CNC) laser machine. The objectives of this development are: to reduce the time processing and the cost for production, while at the same time able to increase the safety of the machine operators. In particular, this development was motivated by the necessity of industrial sector. Due to their high initial costs, the laser wear must be reduced during cutting and their benefits must be fully explored in production. These PC-based monitoring controlling systems have, as the most important feature, the fully integrated possibilities of communication with the controller, getting and sending information from and to the Numerical Control (NC), acting on its up and low level routines. It allows the execution of corrective actions during the cutting or engraving, monitoring and adjusting the core cutting parameters, permitting the operation and the monitoring of the process through Ethernet/Internet.

This report is organized as followed: Section 2 describes the proposed OAC system to be developed for laser machine. In Section 3, we implement the proposed OAC system. We present the major characteristics of the system by focusing on operator graphical interface in server and also the benefits that can be obtained by its application in the cutting or engraving process.

PROPOSED OAC SYSTEM FOR LASER MACHINE

In this section, we present the OAC system for laser machine. The OAC system allows new monitoring and controlling operation in the cutting or engraving process, locally or remotely. In addition, it able to monitor or control the laser machine and make it available to the high management levels through Ethernet/Internet.

An overview of the OAC system is presented in Figure 2-13. There are two scenarios of the OAC system that include the remote scenario and machine scenarios. In the remote scenario, clients can perform monitoring and controlling actions and/or collect information sharing it with the management systems. The client's graphical user interface will be developed using web browsing. The client computers will be connected with the server via Ethernet. View and/or control can be performed, in which machine setup, diagnostic and operation will be performed remotely. Thus, it able to maximize the operation and reduces machine down time.

The machine scenario represents the connections design between the server, Fanuc CNC machine, IP Camera and laser machine. An IP camera will be installed around the machine. The PC - CNC communication is performed by using a parallel port cable to connect PC to the CNC. Operator interface is developed using the C++ language.

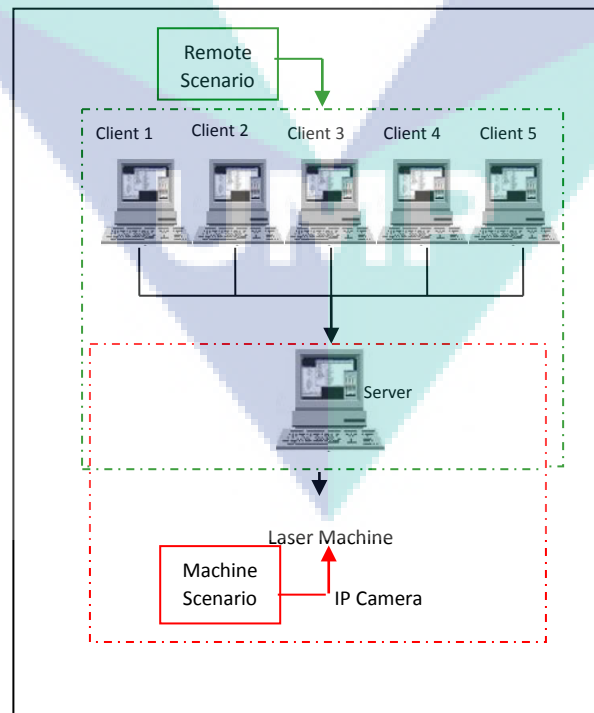


Figure 2-13. System overview

For the time being, the development of graphical user interface is being implemented in server in the Windows environment. Figure 6 shows the GUI that works in server. There are two panels to control different part. One is for laser moving and other is laser starting. For moving the laser, the user has to choose the direction and the laser speed as shown in Figure 6. The higher number of laser speed is the faster the laser will be move because we set the laser speed as an integer (int) so the higher number is the fastest. To start the moving process, click the start button. To stop the process, press the stop button.

To start the cutting or engraving process, the user need to insert the G-Code file that contain the information of the drawing that wanted by the user. The user can browse the file as presented in Figure 8 and add it or by creating a new file by clicking the new button. It will go directly to the drawing software, ArtCAM Pro software. The drawing information will be saving in form of axis-x and axis-y. The laser will be move accordingly to the coordinate position.

For laser strength selection, the higher number is the higher strength of laser. For engraving process, it is suggested to use the lower number. But it is depending on the material we are using to engraving the drawing. For example, if we are using wood as the medium to engrave, it is advisable to use lower strength rather than using an acrylic as the medium. This research to determine the laser strength to cut a various type of medium also has been made in University Malaysia Pahang (UMP) by my research colleague.

Phase 1: Develop GUI for Server PC

The implement OAC system is now being tested in order to develop new cutting and engraving strategies. New monitoring systems, based on the developed Graphical User Interface (GUI), will permit the most effective and reliable data processing. In order to make GUI, the

parameter for the machine has been identified. The lists of the parameter or selection in this laser machine are as in the Table 4 below.

Table 2-7. Parameter or selection to be considered

Parameter/Selection	Unit/Type	Calculation
Moving Direction	Forward, Forward & Left, Forward & Right, Left, Right, Backward, Backward & Right, Backward & Left	-
Moving Speed	5- 50 or higher	> higher, > faster
G-Code File	.txt file	-
Laser Strength	200 – 3000 or higher	> higher, > Strength

For the time being, the development of graphical user interface is being implemented in server in the Windows environment. Figure 6 shows the GUI that works in server. There are two panels to control different part. One is for laser moving and other is laser starting. For moving the laser, the user has to choose the direction and the laser speed as shown in Figure 6. The higher number of laser speed is the faster the laser will be move because we set the laser speed as an integer (int) so the higher number is the fastest. To start the moving process, click the start button. To stop the process, press the stop button. Figure 7 shows the selected items interface for laser moving.

To start the welding process, the user need to insert the G-Code file that contain the information of the drawing that wanted by the user. The user can browse the file as presented in Figure 8 and add it or by creating a new file by clicking the new button. It will go directly to the drawing software, such as; ArtCAM Pro software. The drawing information will be saving in form of axis-x and axis-y. The laser will be move accordingly to the coordinate position.

For laser strength selection, the higher number is the higher strength of laser. For welding process, it is suggested to use the lower number. But it is depending on the material that chosen to weld the profile. This research to determine the laser strength to cut a various type of medium also has been made in University Malaysia Pahang (UMP).

Phase 2: GUI Script Coding

The algorithm is using C++ language to develop the operator interface for server pc. The reasons for selection of this language are because:

C++ is easy to learn. C++ was designed to be easy to use and is therefore easy to write, compile, debug, and learn than other programming languages.

C++ is object-oriented. This allows user to create modular programs and reusable code.

C++ is easy-to-use interface library. C++ has Abstract Window Toolkit that enable programmer to uses native facilities to display windows.

C++ is low cost programming language because the tool is easy to get.

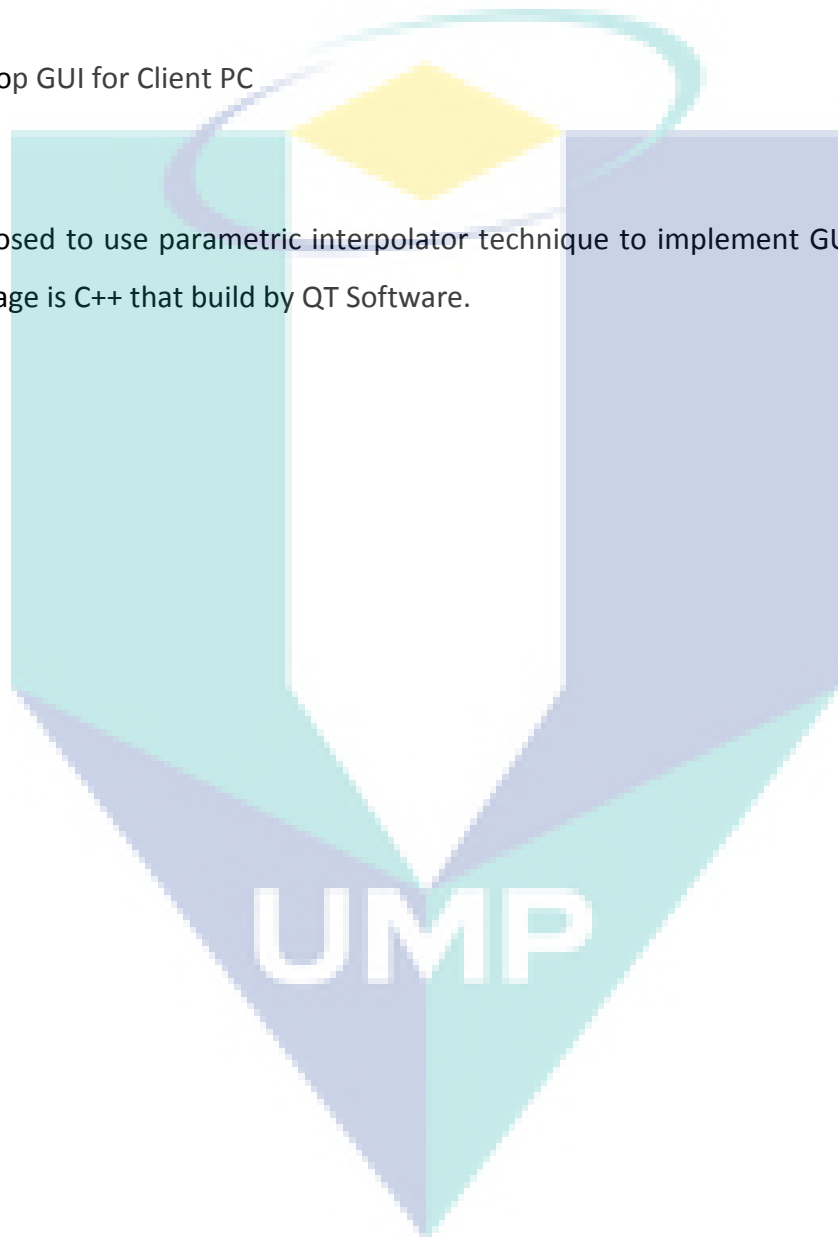
The primary advantage is developing windows applications more rapidly using Microsoft Founded Class (MFC) vs. Win32 while still using C++. In visual C++, there is a paltform for document/view architecture that eases the programming functionality. Visual C++ also gives MFC supports that make "everything possible" in windows programming.

Phase 3: Setup charge coupled device (CCD) Camera and Viewing Method

The laser system require a CCD camera viewing method from the machine controller. LAN communication protocol is utilized for data transfer.

Phase 4: Develop GUI for Client PC

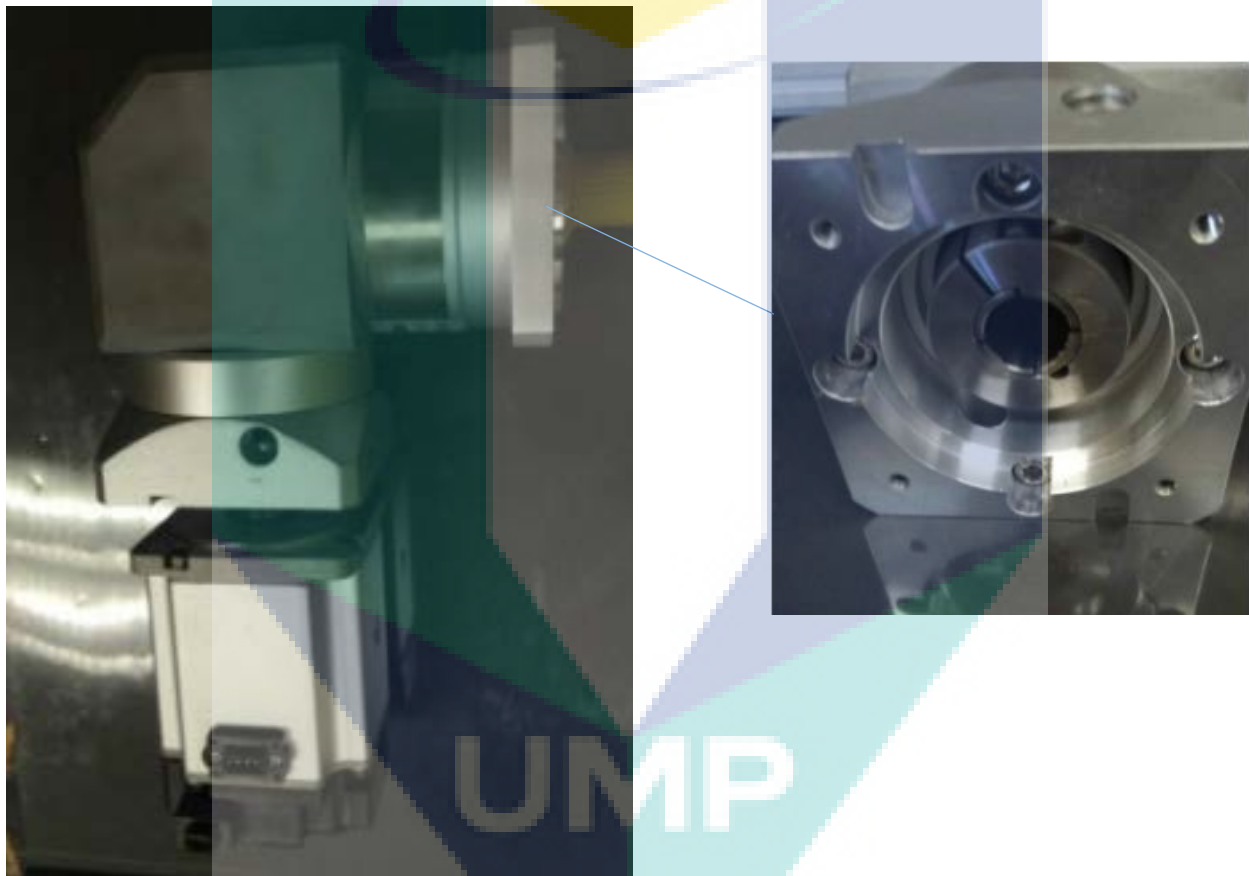
We have proposed to use parametric interpolator technique to implement GUI in clients. The choosen language is C++ that build by QT Software.



MILESTONE 3: DEVELOPMENT AND FABRICATION OF PROTOTYPE TWB MACHINE

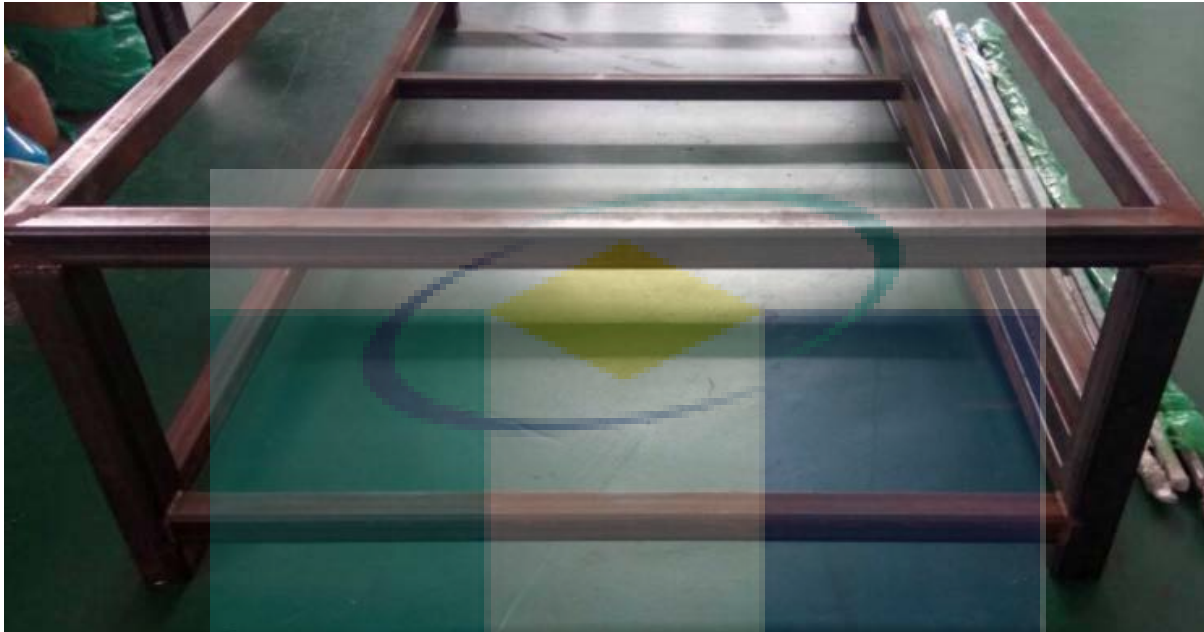
3.1 MECHANICAL AND ELECTRICAL PARTS

Machine Parts Fabrication



Motor bracket fabrication

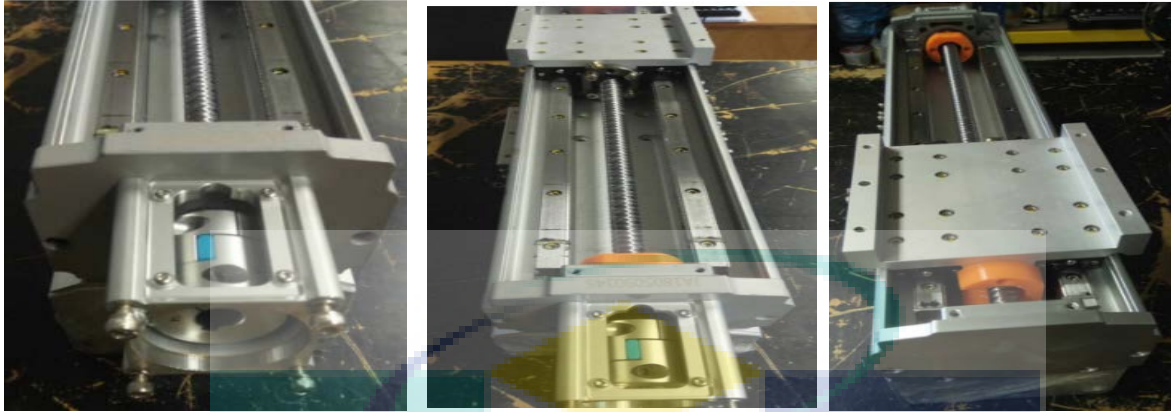
3.2 MAIN FRAMED AS BASED STRUCTURE



Main frame platform



Main frame constructed from hollow square 100 x 100 mm

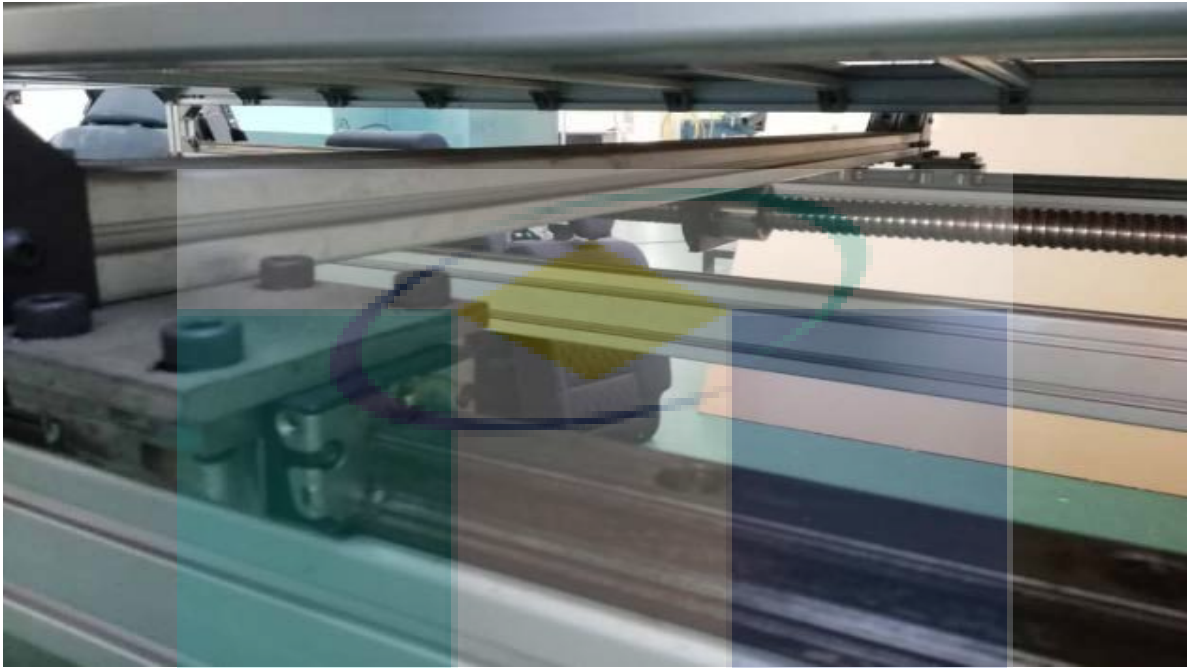


Z – axis travel



Y-axis travel platform

3.3 CNC GANTRY STRUCTURE ASSEMBLY

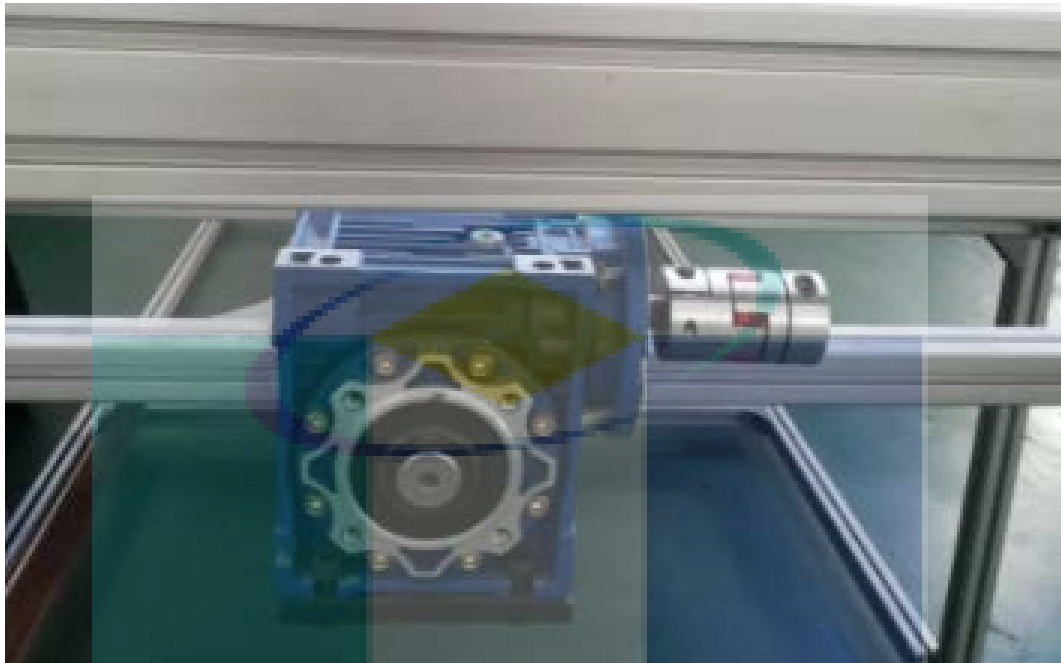


Ball-screw and linear guide assembly

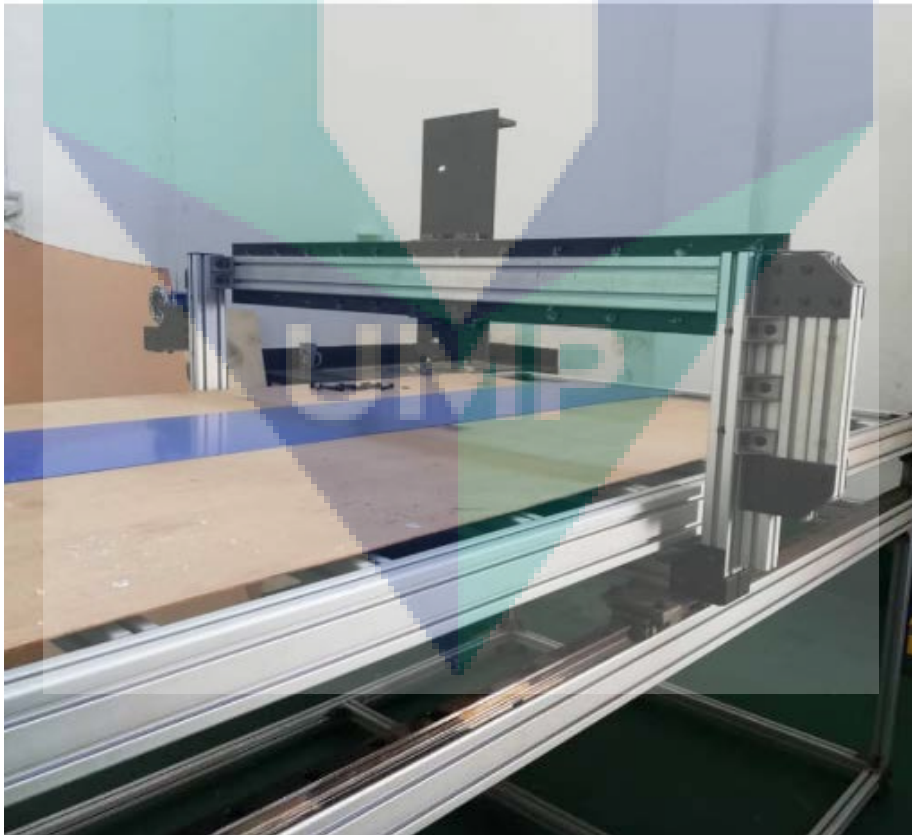


Pillow block and bearing assembly

1



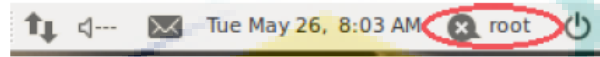
Gearbox mounting with flexible coupling



Y-axis and Z-axis gantry base

3.4 GUI AND SOFTWARE DEVELOPMENT

⚠ THIS SOFTWARE CAN ONLY BE EXECUTED IN 'ROOT' USER ENVIRONMENT.



Software Setup

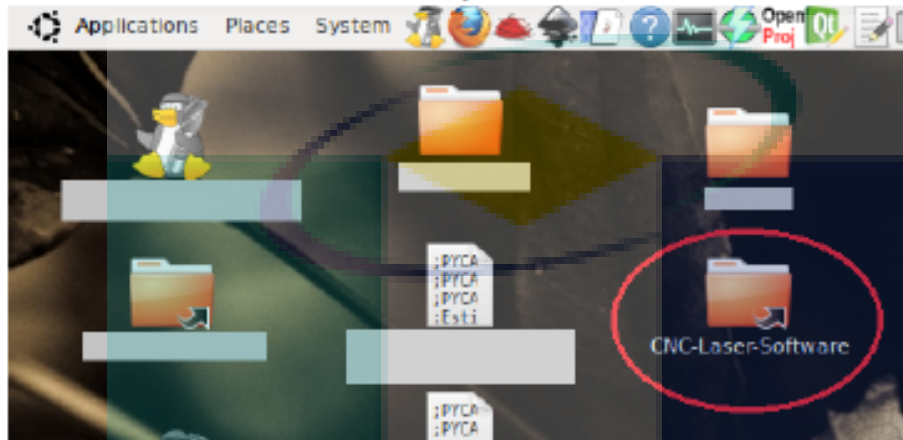
If this is the first time running this software on a new computer, please follow the steps 1-3 below, to remove/uninstall the software, follow step 4:

- (1) Check/Install all necessary Components
 - Make sure the Computer is Connected to the Internet
 - Run 'FIRST-RUN.sh' and select 'Run in Terminal'
 - Wait for the Program to Complete
- (2) Check if the Software is Working
 - Double-click on 'MMU-UMP' executable to Execute the Software
 - Check if all the Functions and Programs are working correctly
- (3) Install the Software onto the Computer
 - Double-click on 'MMU-UMP' executable to Execute the Software
 - Navigate to 'File->Install Software'
 - Wait for the Installation to Complete
 - Exit the Software
 - Navigate to 'Desktop->CNC-Laser-Software'
 - Double-click on 'CNC-Laser-Software' executable to Execute the Software
- (4) Uninstall the Software from the Computer
 - Navigate to 'File->Uninstall Software'
 - Wait for the Program to Complete
 - Exit the Software

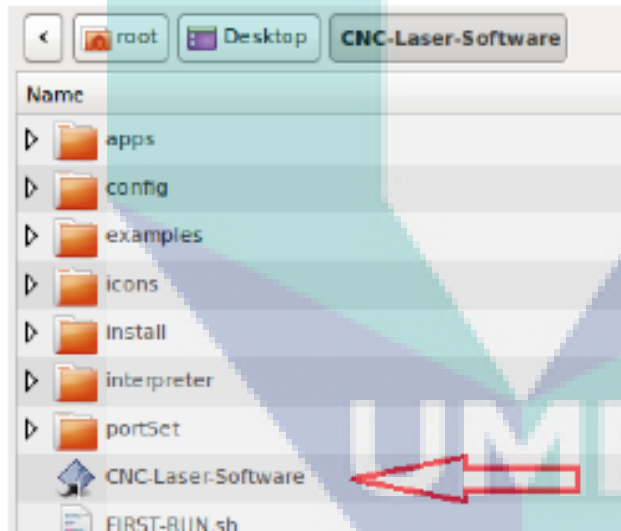
Using the Software

Initialization

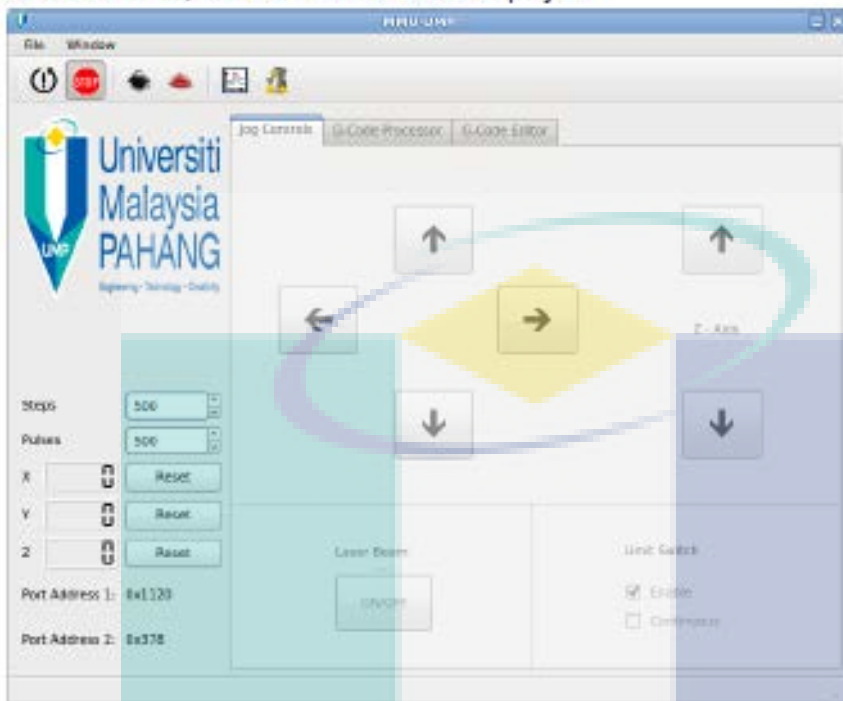
- Execute the Software from the Desktop Shortcut created



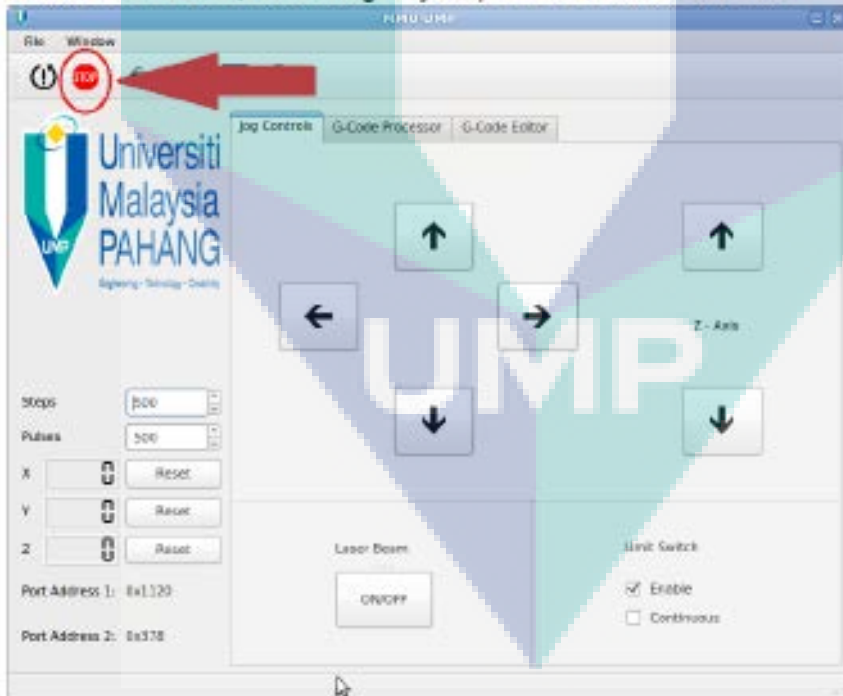
- Click on the Shortcut created on the Folder to Execute the Software



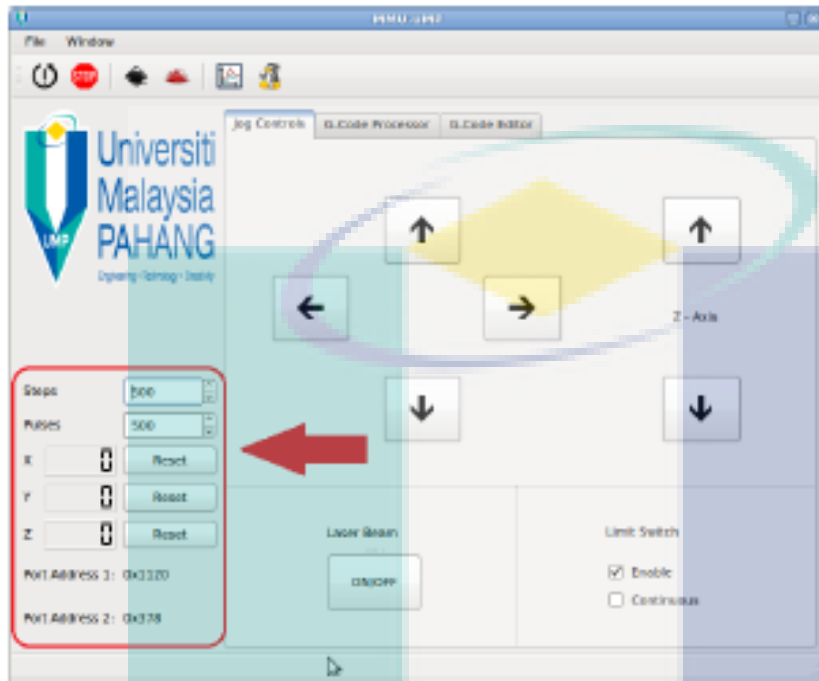
- When launched, the Main Screen will be displayed



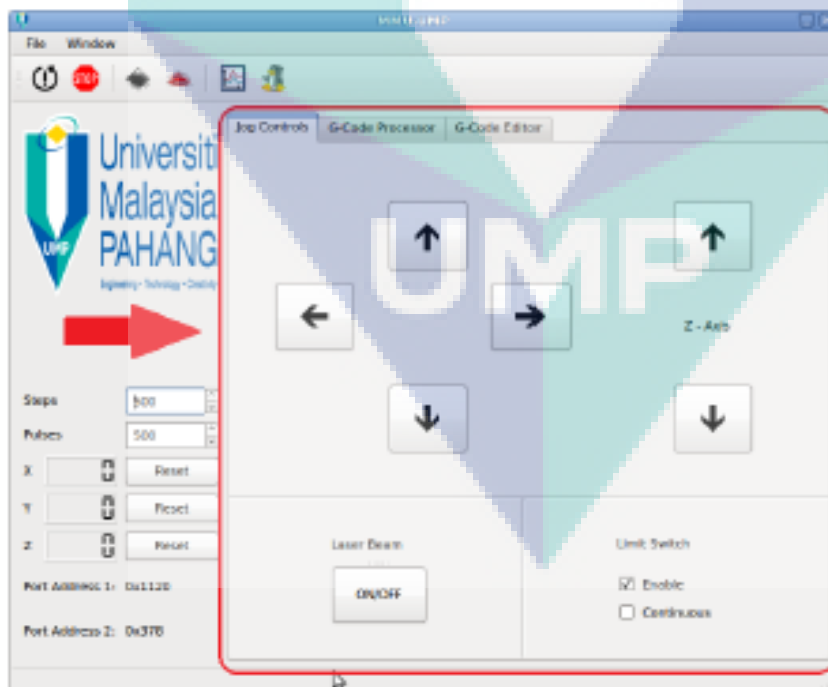
- To use the Software, the 'Emergency Stop' button has to be released



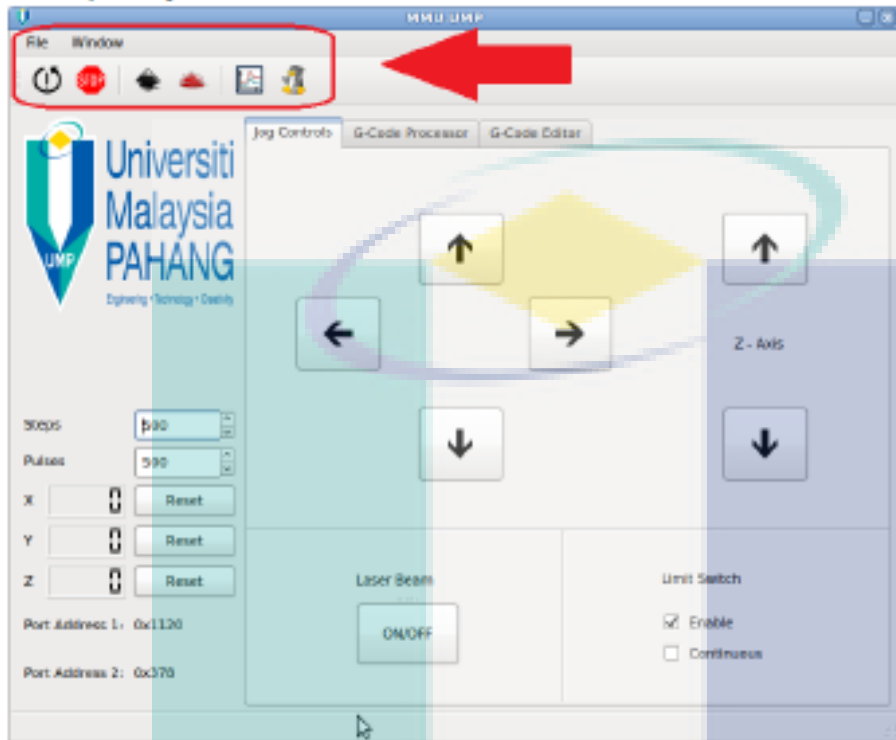
- On the Left side of the screen, there are Steps and Pulses settings that can be changed, Reset buttons for X, Y and Z position counter and the Base address of Parallel Port 1 and Parallel Port 2



- On the Right Side of the screen, there are Working tabs which are Jog Controls, G-Code Processor and G-Code Editor



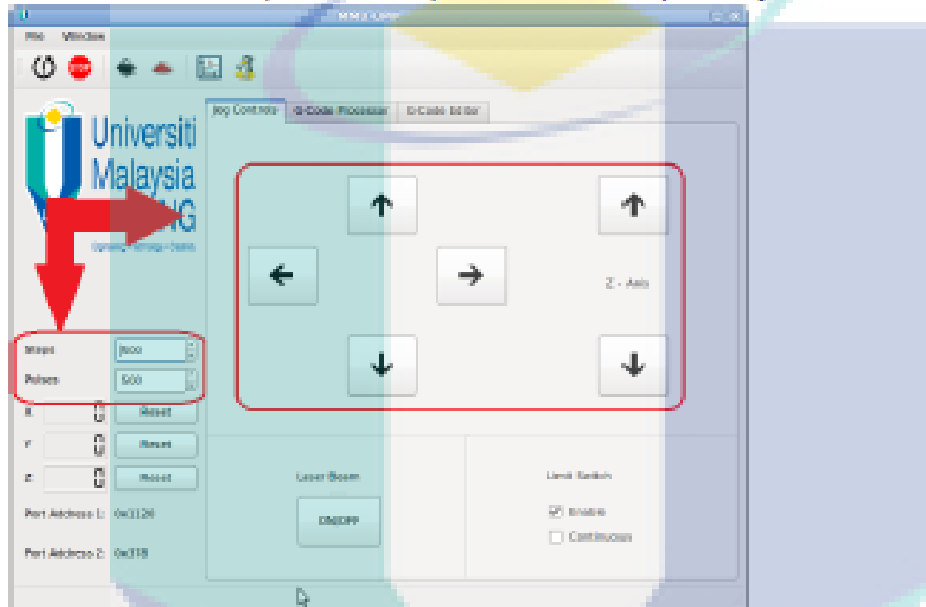
- On the Top of the screen, there is the Menu bar which consists of 'File' and 'Window' and a set of Shortcut Icons which consists of 'Emergency Reset', 'Emergency Stop', 'Inkscape', 'PyCam', 'G-Code Plotter' and 'G-Code Simulator'



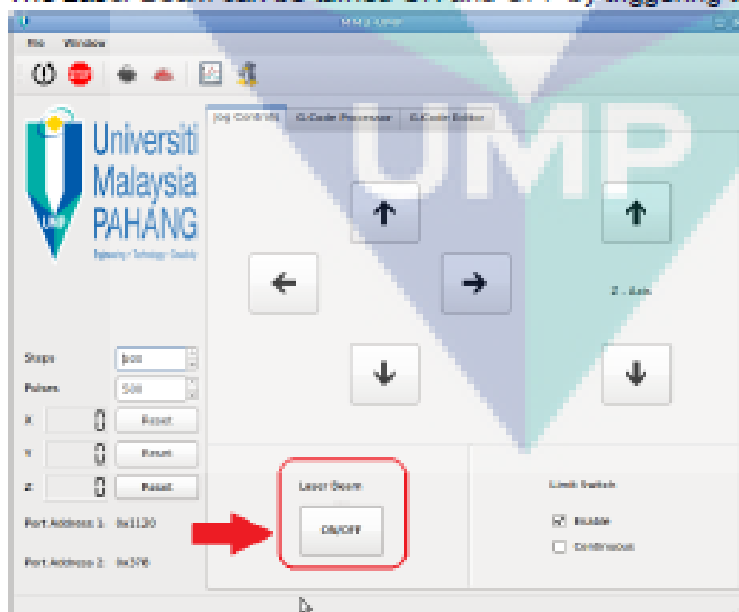
Working Tabs

Jog Controls

- This Tab is designed to allow the user to move the X, Y and Z axis to their Home Position
- The Distance travelled and the Speed of each of the Axis can be altered by changing the value of Pulses for Speed and Steps for Distance respectively



- The Laser Beam can be turned ON and OFF by triggering the Laser Beam button

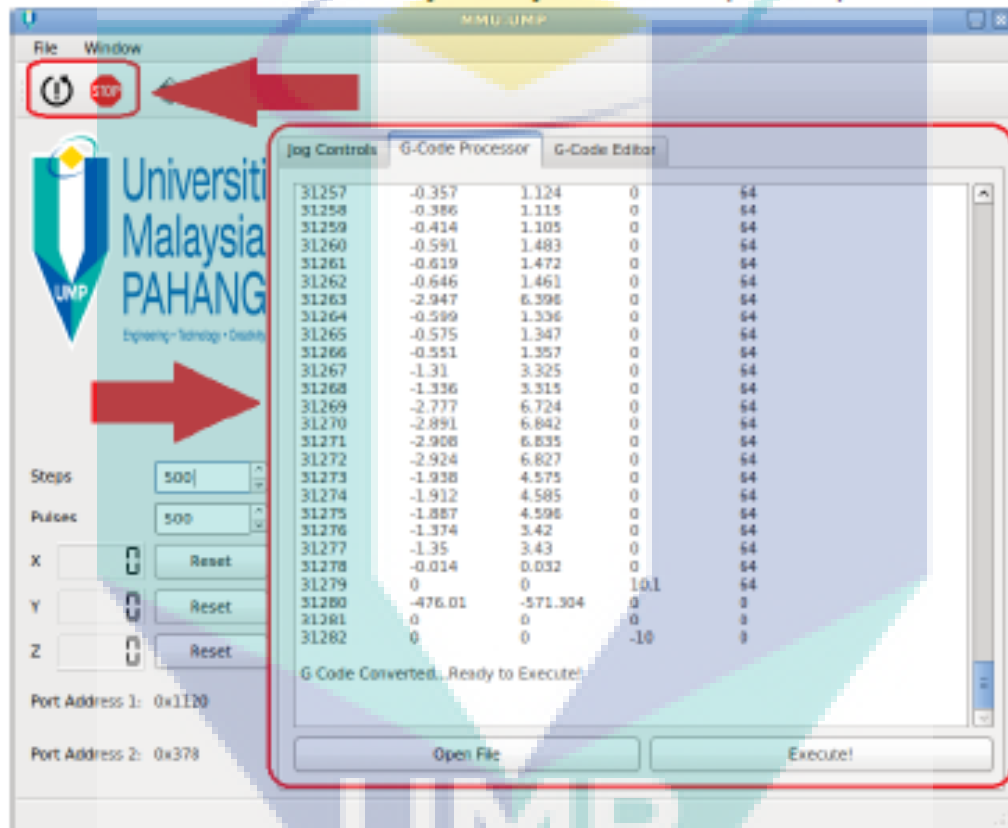


- Limit Switch can be activated or deactivated by triggering the Enable checkbox
- The Continuous option provides continuous movement of an Axis until it encounters a Limit Switch

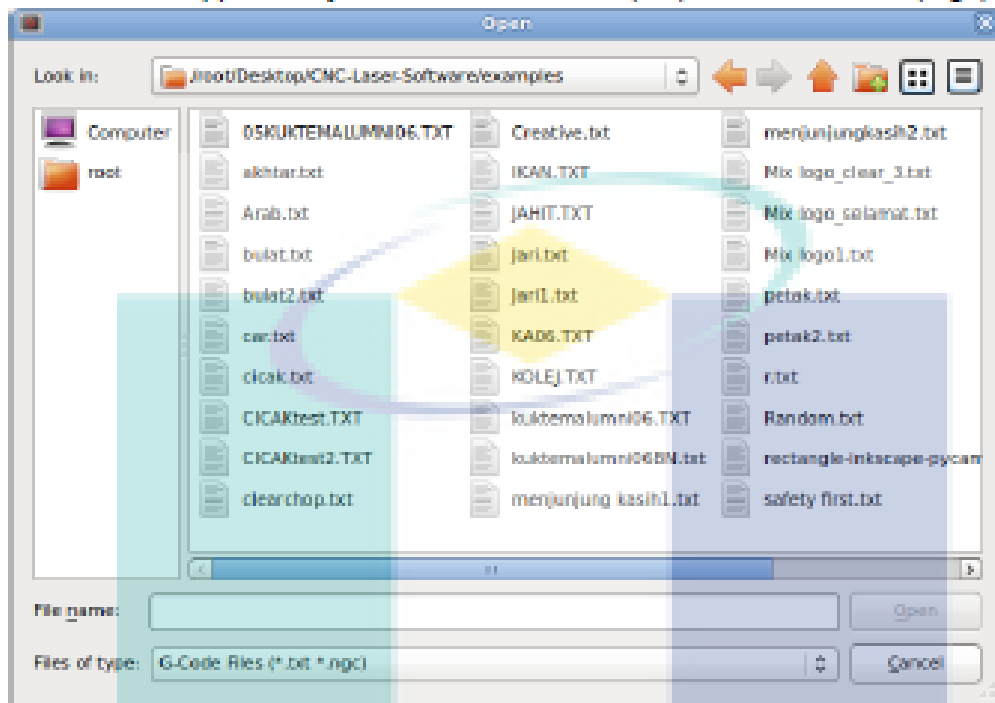


G-Code Processor

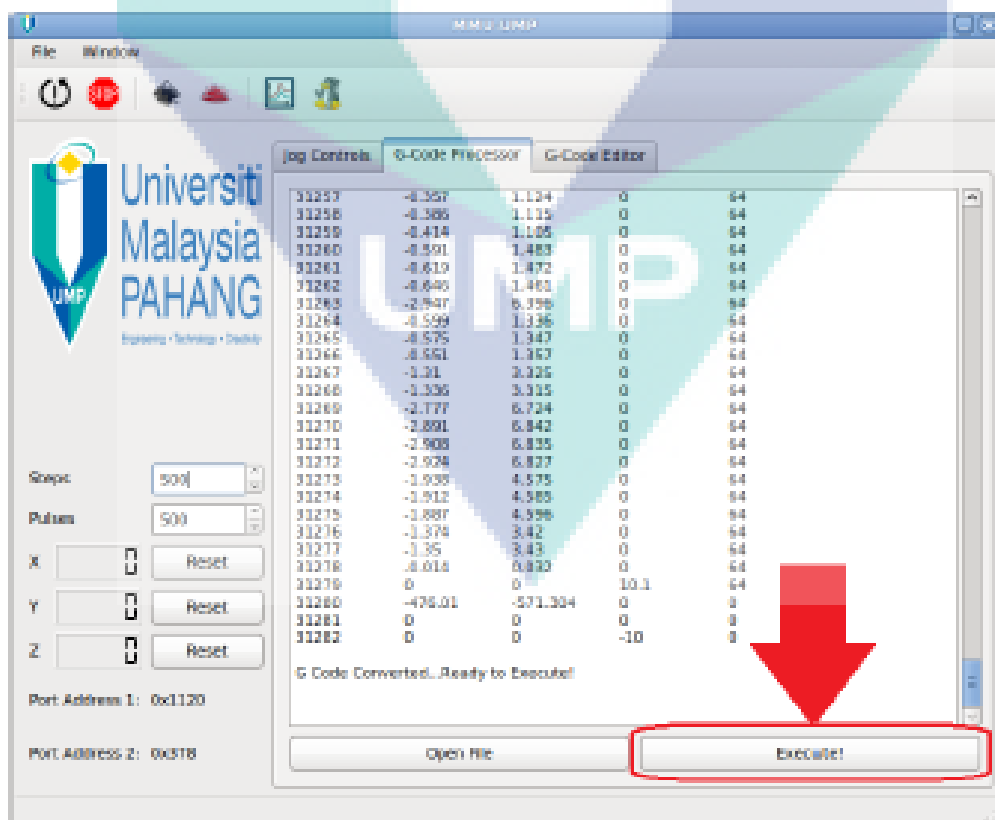
- The G-Code Processor uses Linear Interpolator to process G-Code for the CNC Machine
- The Distance travelled and the Speed of each of the Axis can be altered by changing the value of Pulses for Speed and Steps for Distance respectively
- In this Tab, the 'Emergency Stop' button can be triggered anytime to Halt any current processing of the G-Code
- In the event of Halting the process, it is advised to Reset the Software by triggering the 'Reset Software' button to clear any memory residue of the previous processes



- To Open a G-Code File, click on 'Open File' and choose the appropriate File
- The formats supported by the Software are Text(.txt) and G-Code files(.ngc)

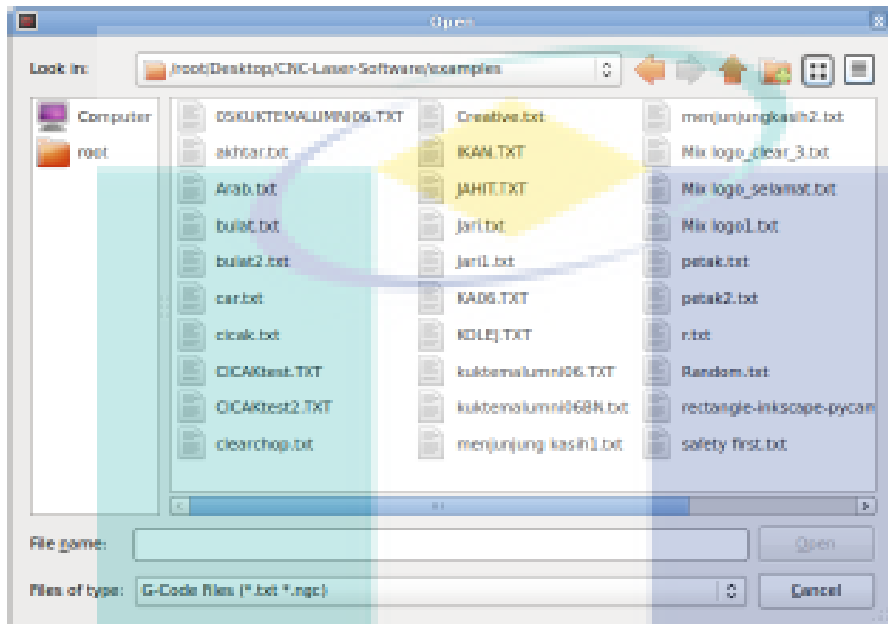


- After the G-Code has been loaded, click on 'Execute!' to execute the G-Code on the CNC Machine

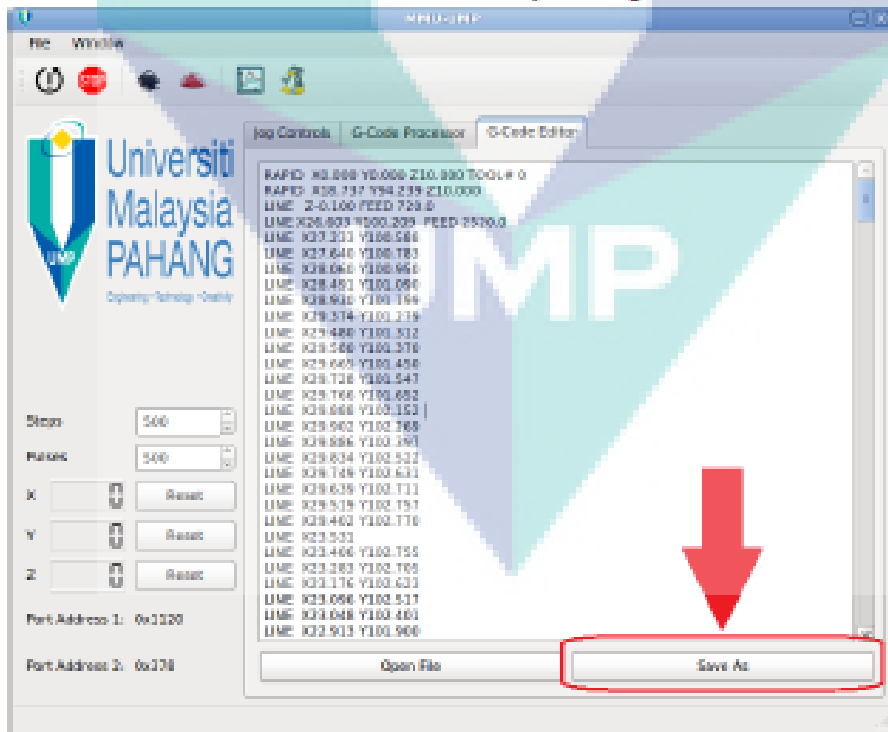


G-Code Editor

- The G-Code Editor is a text editor that can be used to make minor adjustments to the G-Code file before Executing it on the CNC Machine
- To Open a G-Code File, click on 'Open File' and choose the appropriate File
- The formats supported by the Software are Text(.txt) and G-Code files(.ngc)



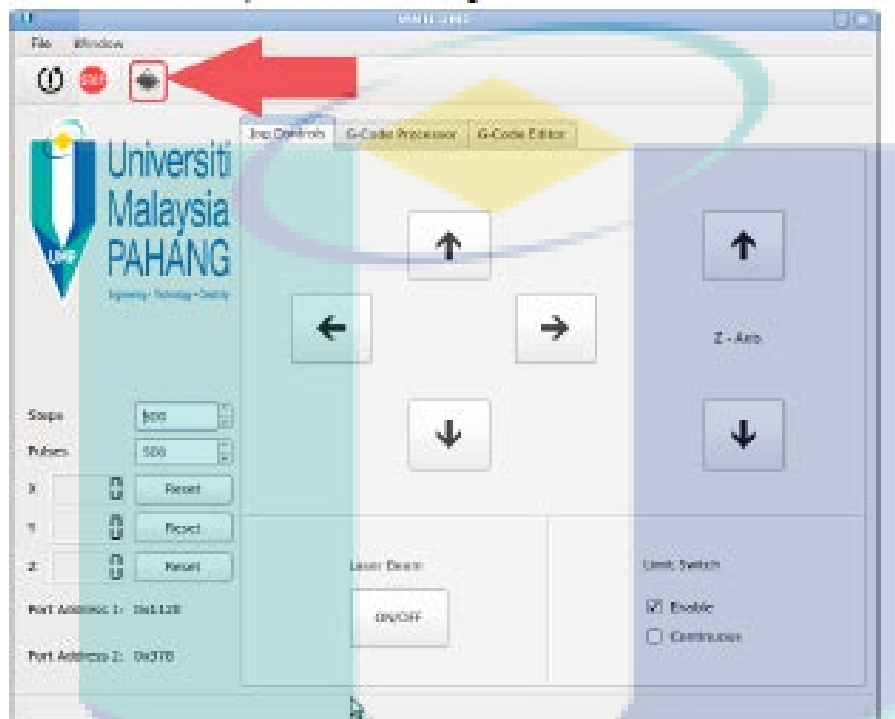
- Once the G-Code is Edited, Save the file by clicking on Save As



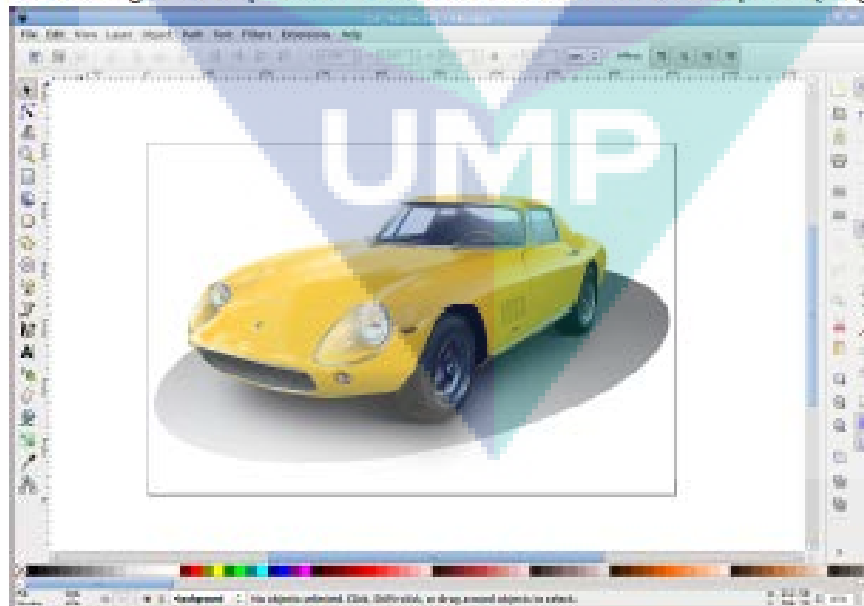
External Software

Inkscape

- To Execute 'Inkscape', click on the logo

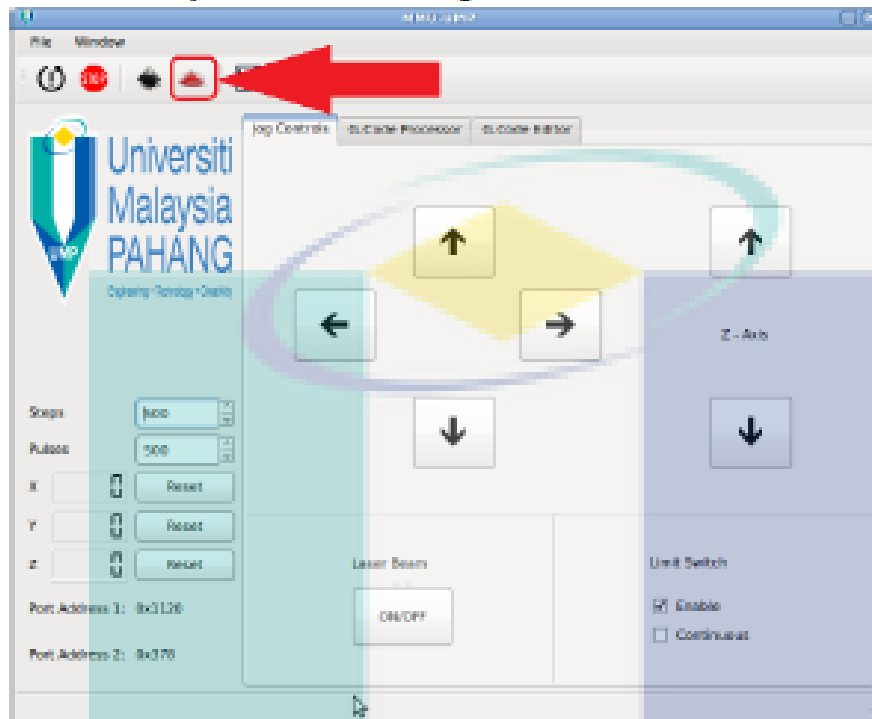


- Draw Image as Required and Save As Scalable Vector Graphics (.svg)

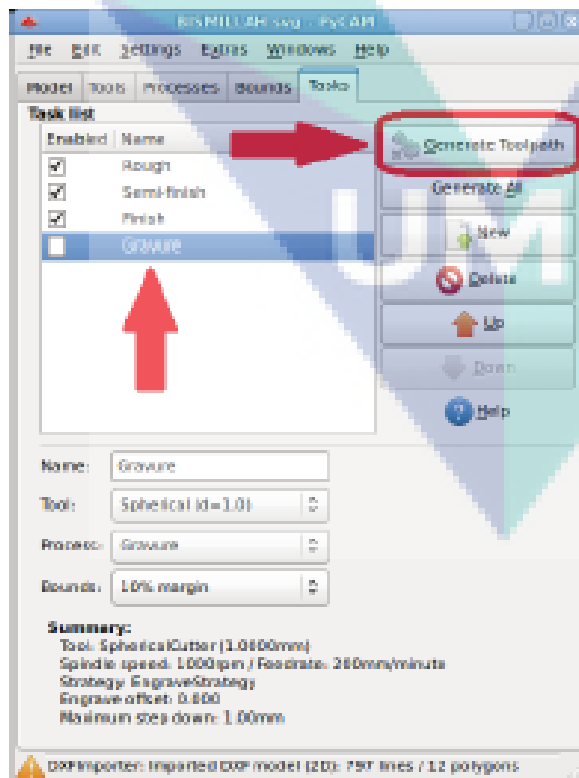


PyCam

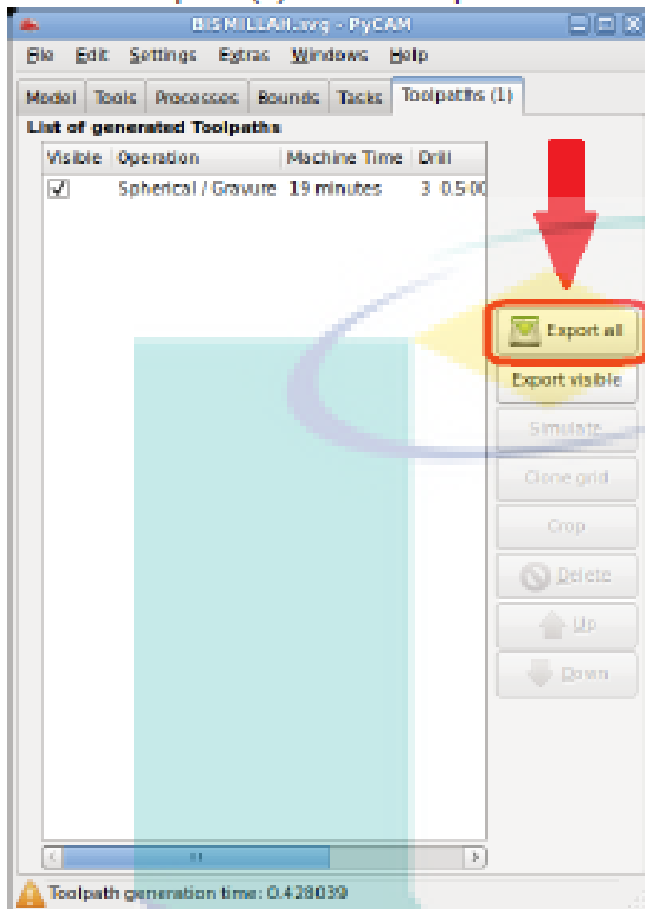
- To Execute 'PyCam, click on the logo



- Import the (.svg) file created earlier using Inkscape
- Click on 'Tasks', select 'Gravure' and click on 'Generate Toolpath'



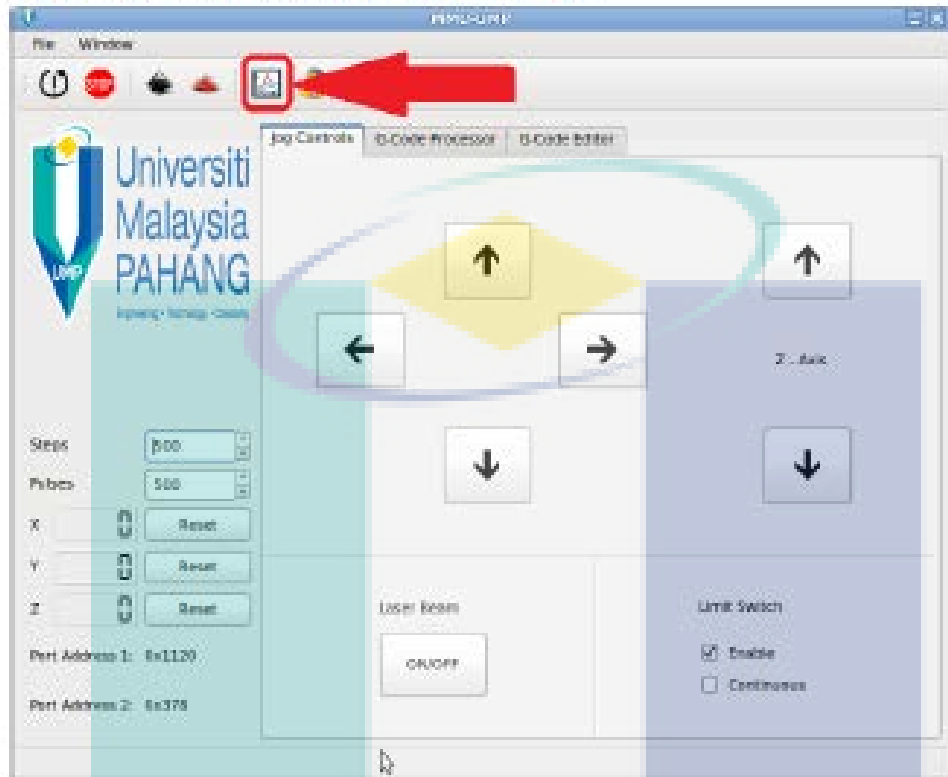
- Click on 'Toolpaths (1)' and click 'Export all' to save the converted file into G-Code(.ngc)



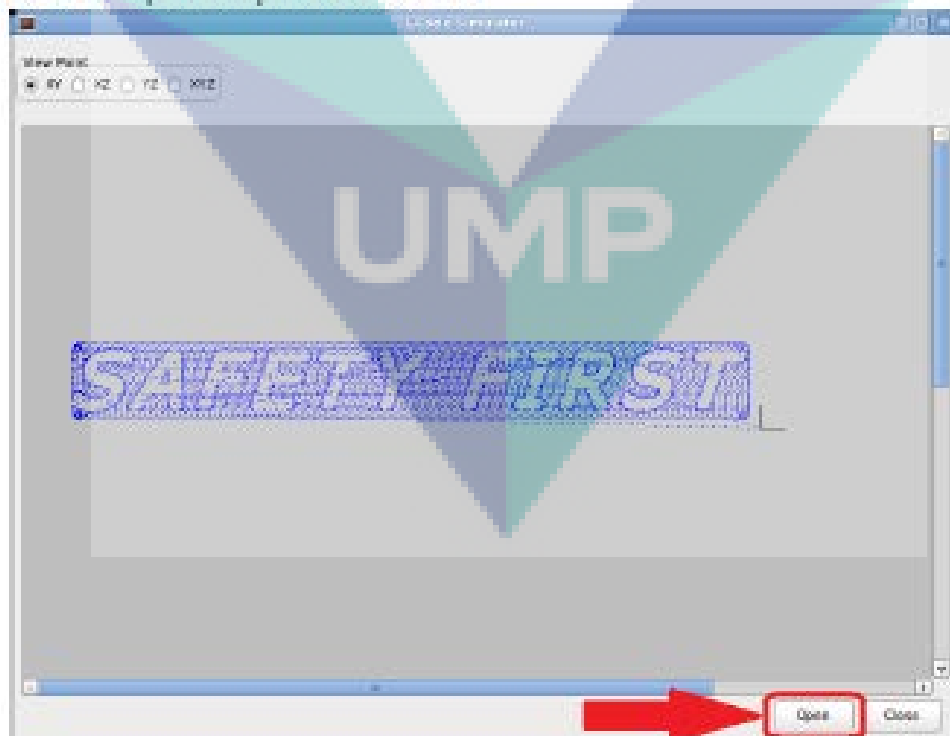
UMP

G-Code Plotter

- To Execute 'G-Code Plotter', click on the logo

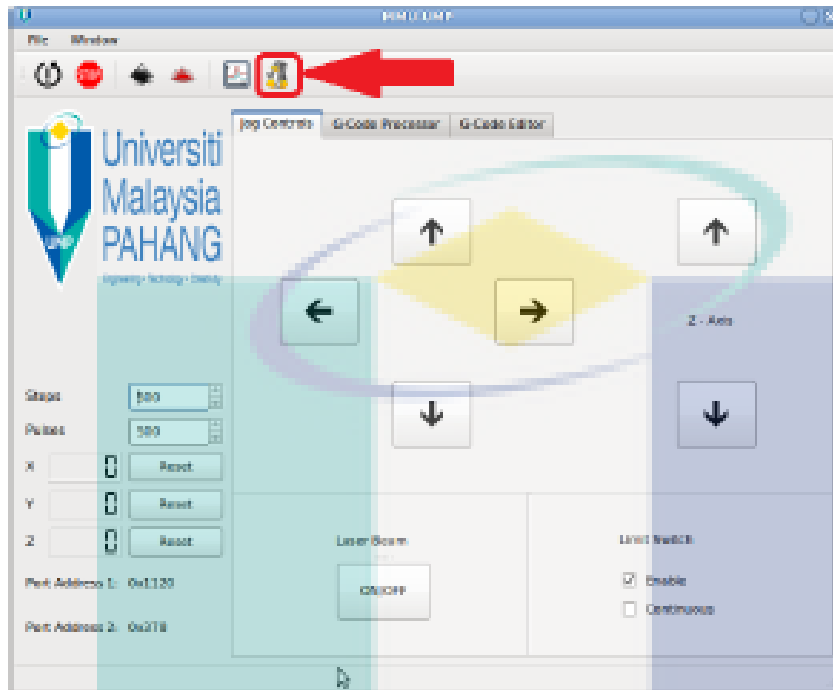


- Click on 'Open' to open a G-Code file

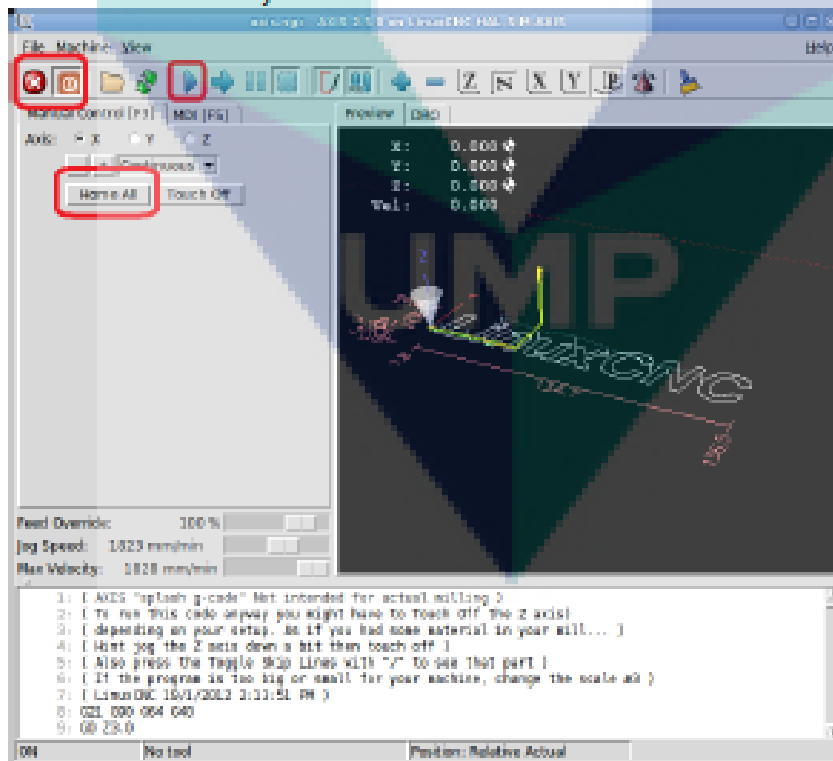


G-Code Simulator

- To Execute 'G-Code Simulator, click on the logo



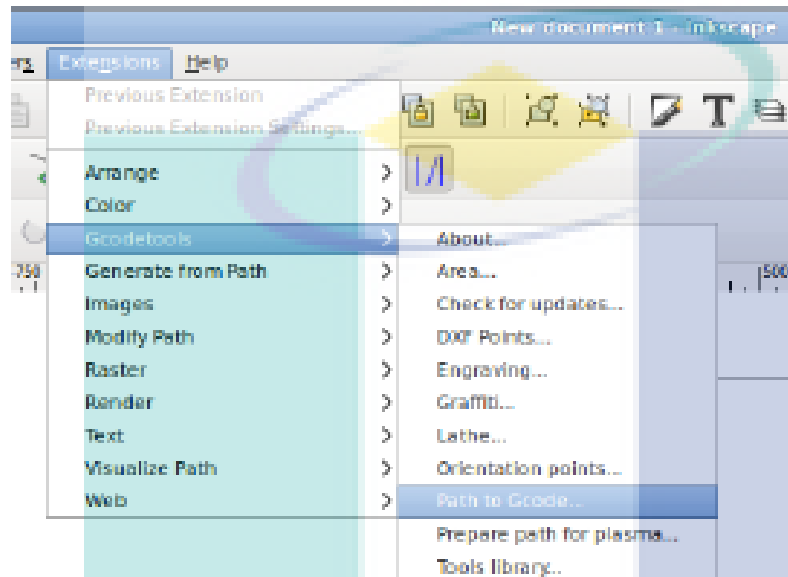
- Open the G-Code File created previously (.ngc) and select the 'Machine On' and 'Home All'. Click on the 'Play' button to see the Simulation



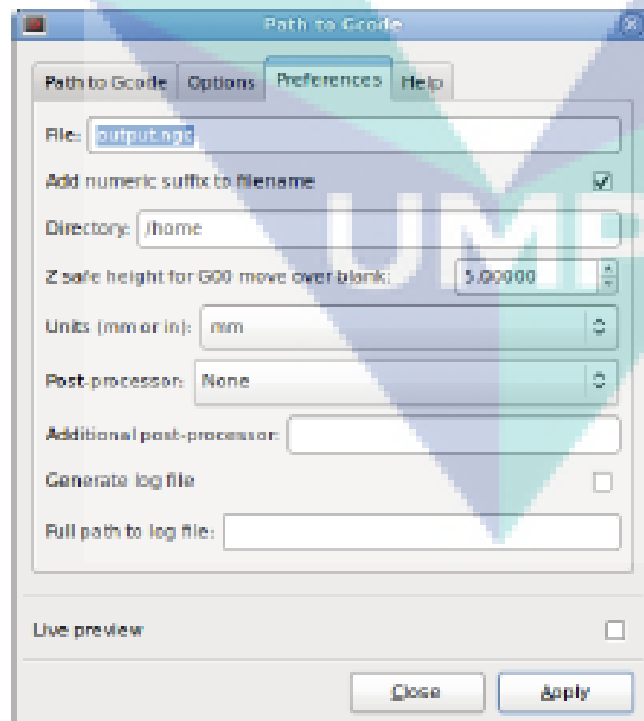
Admin Guide

G-Code using Inkscape (will NOT work on Software)

- Navigate to 'Extensions', select 'Goodetools' and click on 'Path to Gcode...'



- Select 'Preferences' and set the attributes



MILESTONE 4: PILOT PLAN LINE SETUP

4.1 PROCURE AND ASSEMBLE OF LASER HEAD WITH CNC MACHINE – LASER INTEGRATION.



Fig 4-1. 2 kWatt Ytterbium Fiber Laser Laser Source

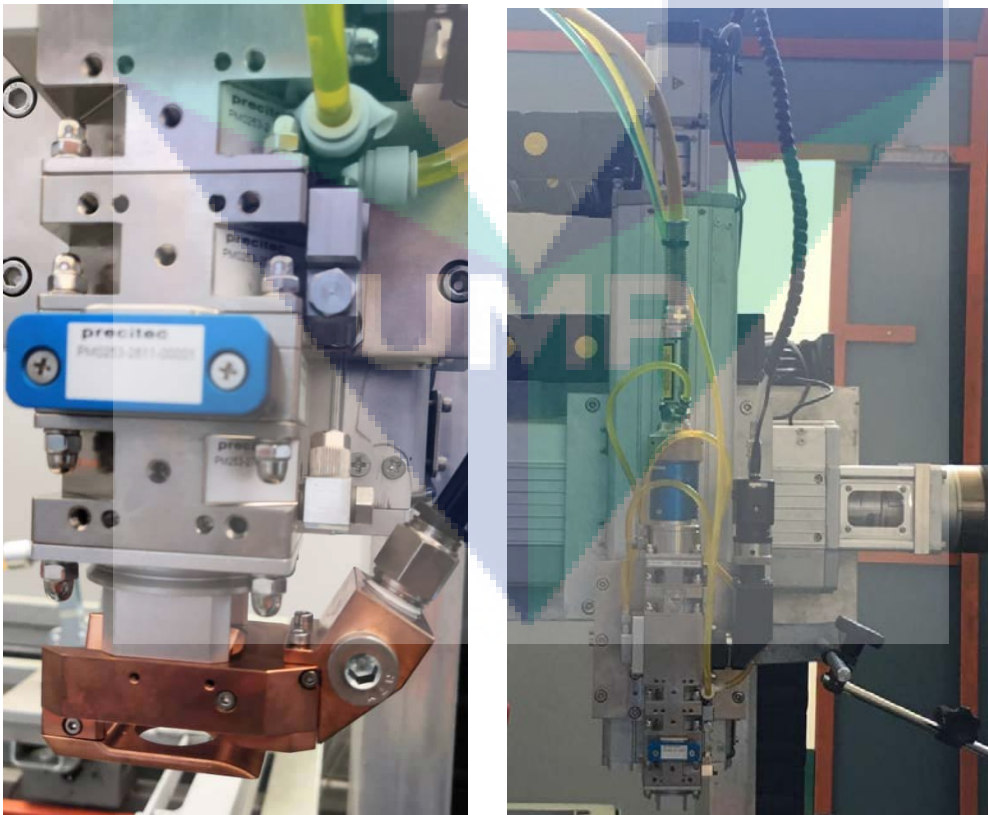


Fig 4-2. Laser Head Installed to CNC Machine



Fig 4-3. Argon Inert Gas with Flow and Dry Filter



Fig 4-4. Chiller Set with Water Inlet and Outlet

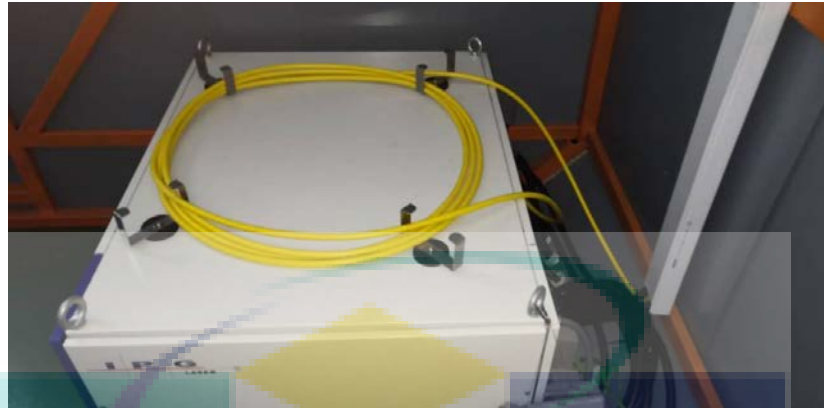


Fig 4-5. Laser Transmission Fiber Cable

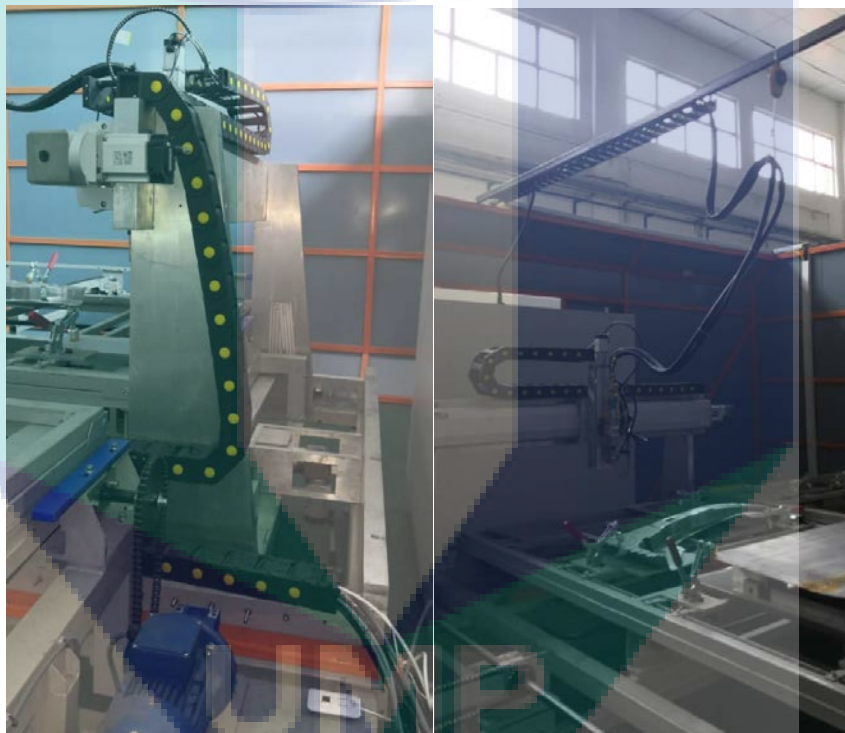


Fig 4-6. Fiber Cable from Laser Source to Laser Head

4.2 Pre-Test TWB Machine – Part Welding Testing

Before welding process, test samples were prepared by dimension of 300 × 100 mm. The Materials which is Galvanized Iron (GI), Boron steel (22MnB5), and low carbon steel/mild steel (LCS) with thicknesses of 3, 2, 1.6, and 1.2 mm, respectively were selected for this work. Table 4-1 shows the details of experiment orders for the materials, which is used in this pre-experiment. Prior to laser weld, the experiment was conducted using coated materials in order to observe the ability of this laser machine to weld the steels.

Table 4-1. Details of Pre-experiment.

Experiment	Material	Thickness (mm)
1	GI + GI (Zn coated)	3, 3
2	GI + GI (Zn coated)	2, 2
3	GI + GI (Zn coated)	2, 2
4	22MnB5 (uncoated) + LCS (Zn Coated)	1.6, 1.2

The materials were cleaned using Ethanol for the last preparation. Once the materials have already been prepared, the samples were clamped onto the welding jig in butt joint configuration. Figure 4-7 shows the experiment setup for the butt joint at the fiber laser machine.

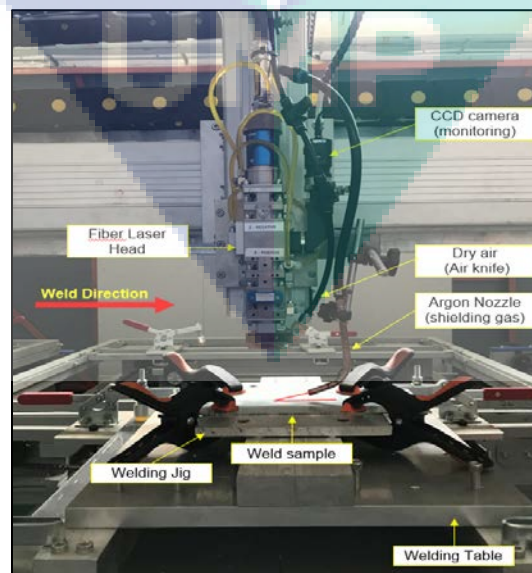


Figure 4-7. Experiment Setup

From Figure 1, samples to be welded were placed on the welding jig which in fixed position on the welding table in butt joint configuration. Argon gas was used as the shielding gas for laser welding steels. Dry compressed air was used as air knife, where to prevent from the plasma/plume smoke going up and attack the laser protective mirror. CCD camera was attached to the laser head for the monitoring system. For the weld line alignment, the laser head was moved along the weld line and monitored at CCD camera monitor as shown in Figure 4.8.



Figure 4.8. Monitoring Weld Line Alignment.

Table 4-2. Laser Welding Parameters

Experiment	Focal Length (mm)	Argon gas (L/min)	Scanning Speed (mm/min)	Laser Power, Watt (W)
1	82 (focused)	15	400	1000 W
2	90	10		
3	82	10		
4	82	12	800	

Table 4-2 shows the welding parameters used for the experiments accordingly. From this table, laser power of 1 kW was used. Focal length of 82 mm was used measured from the surface of the samples to the end section of laser head as advised to be the most focused point. The focal length was increased for experiment 2 using 90 mm, which the weld condition is in defocused position. For the shielding gas, first experiment used 15 L/min Argon flowrate, which resulting some spark/spatter during the welding process. The gas flowrate was reduced for experiment 2 and 3 and increase by 2 L/min for experiment 4. Laser scanning speed used to weld GI steels was constant at 400 mm/min, and was increased to 800 mm/min to weld 1.6 and 1.2 mm thickness of 22MnB5 and LCS, respectively in order to reduce the heat input.

Figure 4-9 to 4-12 show the weld appearance for welded samples from experiment number 1 to 4. It was observed that full weld penetration achieved for all welded samples using laser power of 1 kW with scanning speed of 400 mm/min. From the weld appearance of experiment 2 (Fig 4), it was observed that the weld bead (top surface) was slightly larger compared to the weld bead of samples welded by focused focal length. For the effect of shielding gas flowrates, it was observed that fine weld bead appearance produced for experiment 1 (Fig 3) compared to experiment 3 (Fig 5). It shows that the shielding gas flowrates is suitable to be set at 15 L/min. Lastly, dissimilar welding between boron and mild steel was successful using 1 kW laser power with 600 mm/min (Fig 6) with full penetration weld. However, poor weld bead appearance produced due to the lower shielding gas flowrate used (12 L/min).

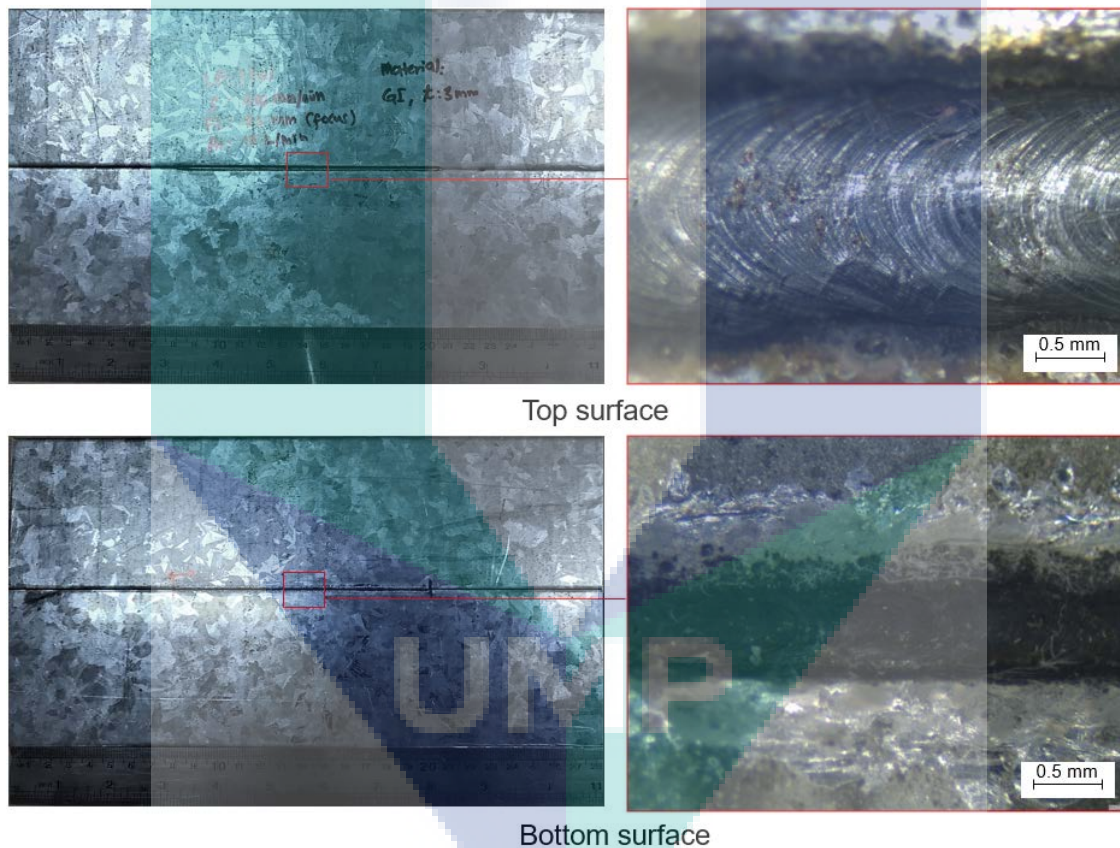


Figure 4-9. Weld Appearance for Experiment 1 (GI + GI, thickness 3 mm).

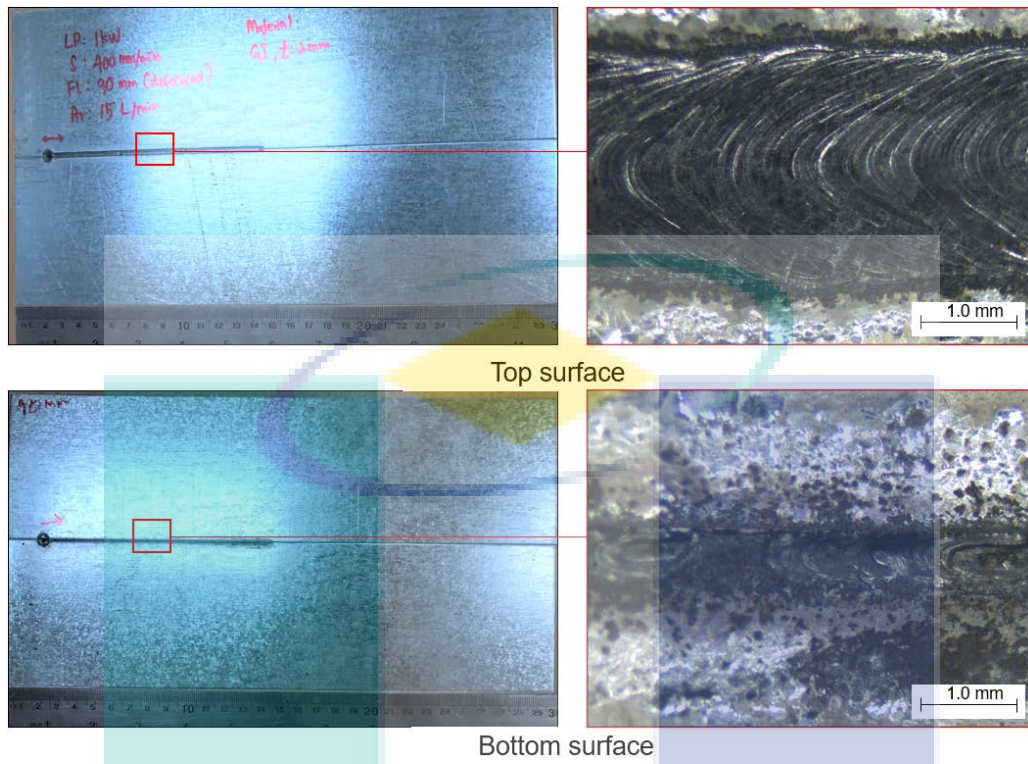


Figure 4-10. Weld Appearance for Experiment 2 (GI + GI, thickness 2 mm)

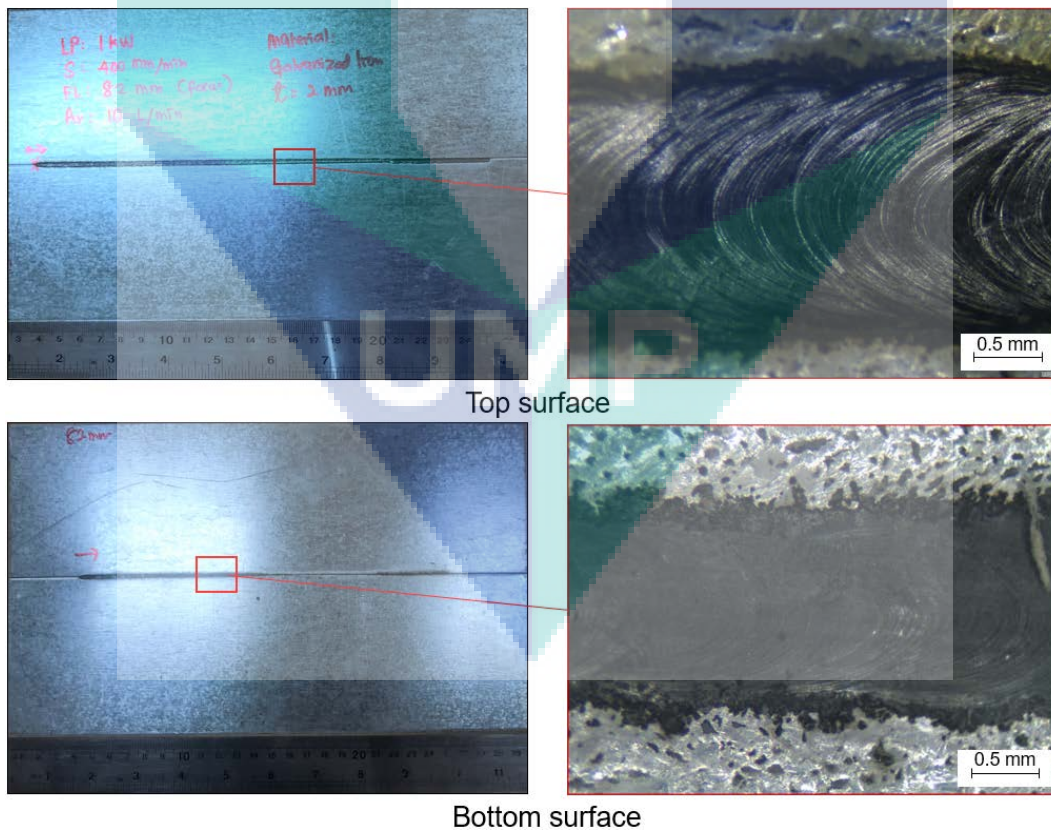


Figure 4-11. Weld Appearance for Experiment 3 (GI + GI, thickness 2 mm).

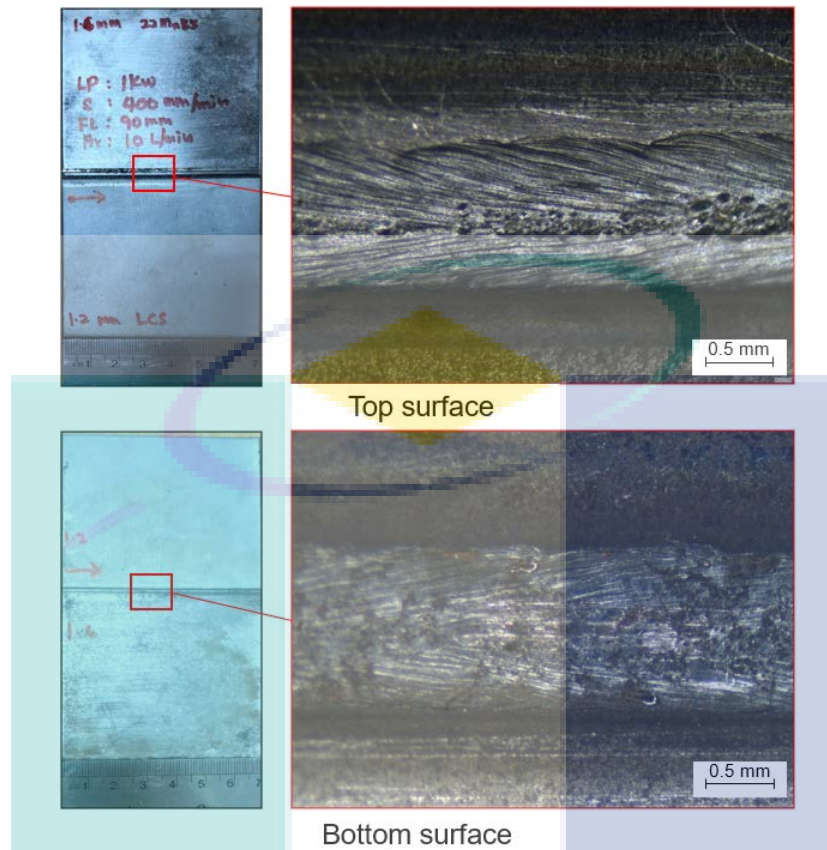


Figure 4-12. Weld Appearance for Experiment 4 (22MnB5 (uncoated) + LCS (Zn Coated), 1.6, 1.2 mm thickness).

WELDED PARTS FROM 2 KW CW FIBER LASER

For further test, the sample was prepared to be weld using 2 KW laser with continuous wave (CW) mode. Fig. 4-13 shows the welded sample where the top surfaces and the cross section was observed.

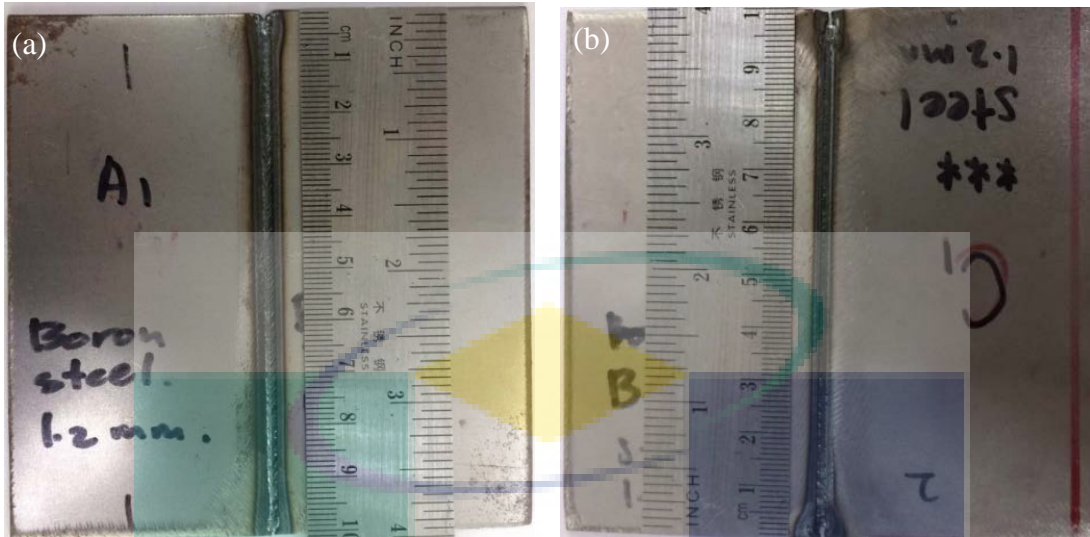


Fig.4-13 Welded Sample using 2 KW CW Fiber Laser (a) Sample A-B (b) Sample B-C.

Macrostructures

For this section, sample was divided to two parts which is part A-B and part B-C. Top surfaces and welded cross section was shown in this section.

Sample A-B

The macrostructures images was captured for this sample on top surface and at the weld cross section. Fig. 4-14 and 4-15 show the macrostructures images for top surface and weld cross section, respectively. From Fig. 4-14, the top surface of sample A-B indicates some defects such as undercut, pores, and slag inclusions. However, the weld bead was good observed from the top view. For the cross section as shown in Fig. 4-15, the undercut defect can be observed clearly at the position of transition region between base metal A and fusion zone. Complete penetration was achieved for this weld. However, the FZ and HAZ was larger. It was clearly shown from Fig. 4-15 where the phase can be observed clearly since there was a comparison between the changes of colours and grain at the weld region starting from both base metals. Sample A and B were having different thicknesses which is 1.2 and 1.6 mm, respectively.

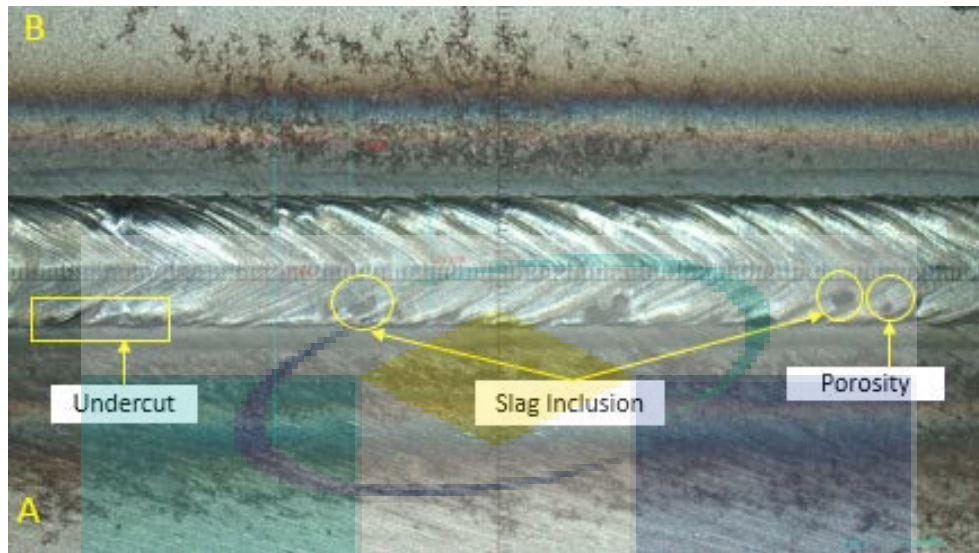


Fig.4-14 Top Surface at Weld Region of Sample A-B.

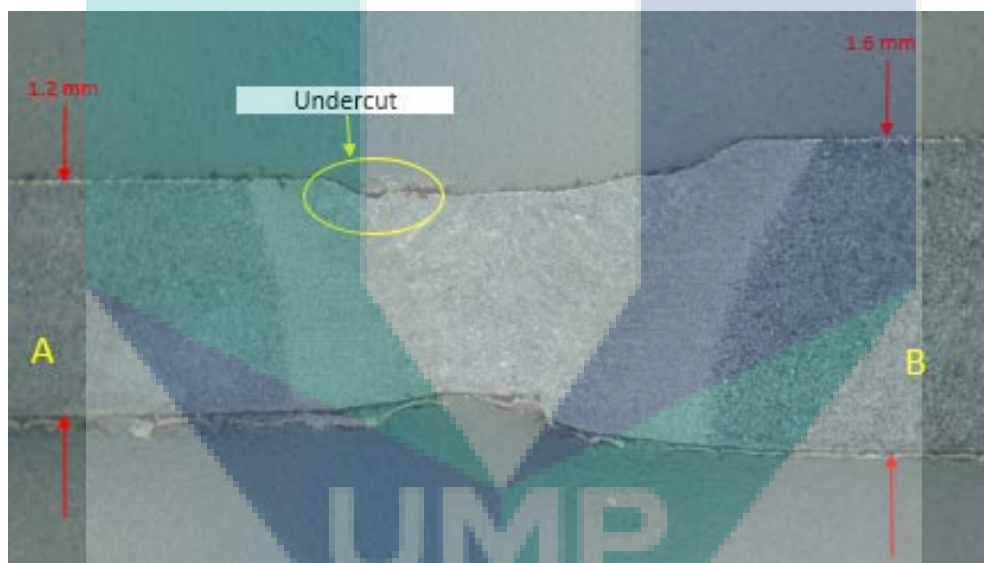


Fig. 4-15 Cross Section at Weld Region of Sample A-B.

Sample B-C

The macrostructures images was captured for this sample on top surface and at the weld cross section. Fig. 4-16 and 4-17 show the macrostructures images for top surface and weld cross section, respectively. From Fig. 4-16, the top surface of sample B-C indicates some defects such as spatters, pores, and slag inclusions. However, the weld bead was good observed from the top view. For the cross section as shown in Fig. 4-17, incomplete penetration or

known as lack of root fusion was observed for this weld. The FZ and HAZ also was larger. It was clearly shown from Fig. 4-17 where the phase can be observed clearly since there was a comparison between the changes of colours and grain at the weld region starting from both base metals. Sample B and C were having different thicknesses which is 1.6 and 1.2 mm, respectively.

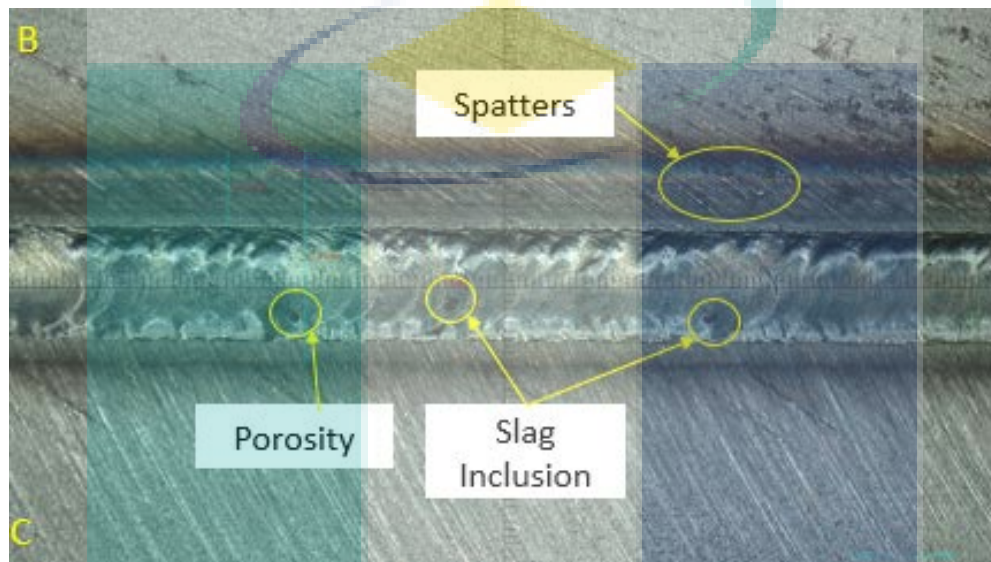


Fig. 4-16. Top Surface at Weld Region of Sample B-C

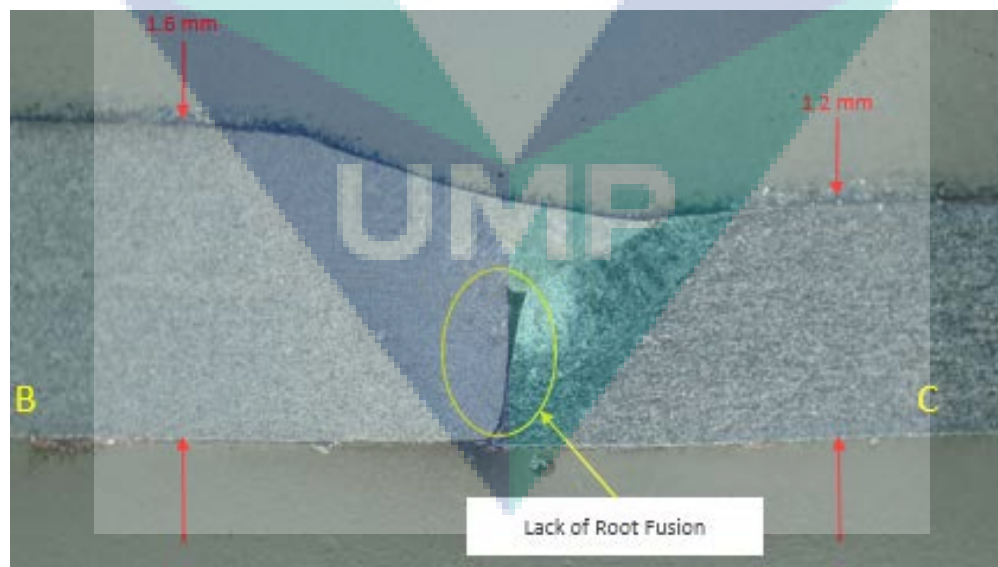


Fig.4.17. Cross Section at Weld Region of Sample B-C.

TEST FINDING SUMMARY

As a conclusion, the sample A, B and C from PHN were successfully undergo metallurgical process in order to justify the composition of the steel. All the results were being observed and recorded and are illustrate in comparison table below.

POSITION	SAMPLE	Width of Region, mm		
		HAZ 1	FZ	HAZ 2
PHN	A – B	0.384	0.540	0.683
	B – C	0.400	0.735	0.570
XYZ	A – B	1.055	1.635	1.426
	B – C	0.992	1.246	0.738

POSITION	SAMPLE	Average Grain Size			
		Base Metal A , μm	Base Metal B , μm	Base Metal C , μm	Fusion Zone , μm^2
PHN	A – B	6.88	7.26	-	0.49
	B – C	-	7.34	2.26	0.57
XYZ	A – B	7.34	7.24	-	1.62
	B – C	-	7.95	0.738	0.67

Weight of Element (%)

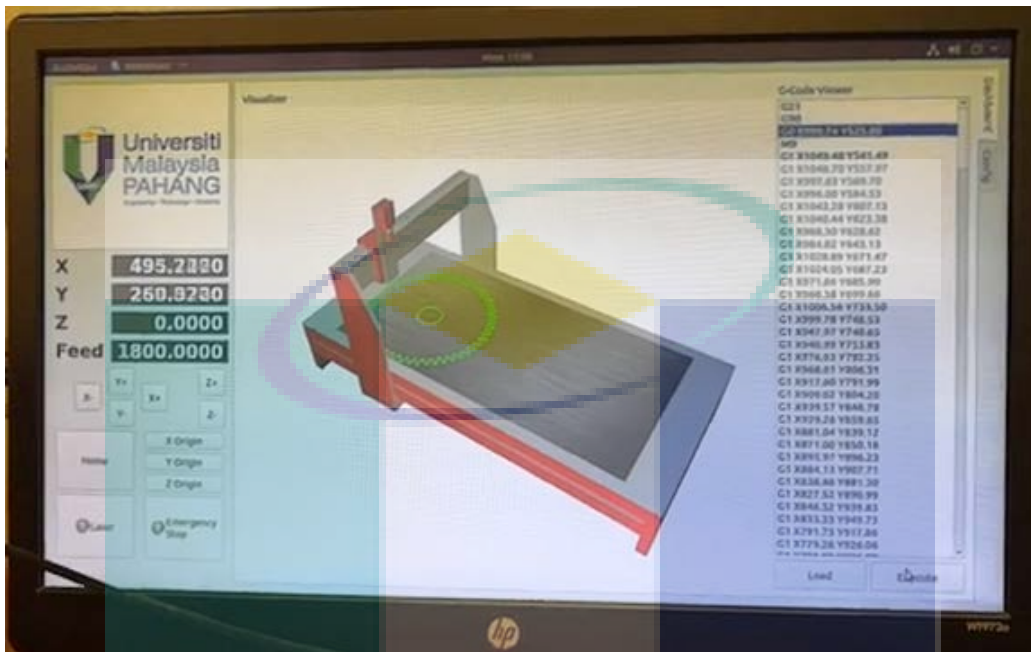
Composition,	Sample	A	B	C
--------------	--------	---	---	---

wt%		Element		
Spectrometer	B	0.002	0.002	0.00
	C	0.140	0.132	0.02
	Si	0.092	0.106	0.381
	Mn	1.13	1.21	0.565
	Fe	98.5	98.4	98.6
	EDX	B	3.89	5.10
	C	7.47	7.45	6.34
	Si	0.32	0.23	0.43
	Mn	1.29	1.29	0.55
	Fe	87.03	85.92	92.69

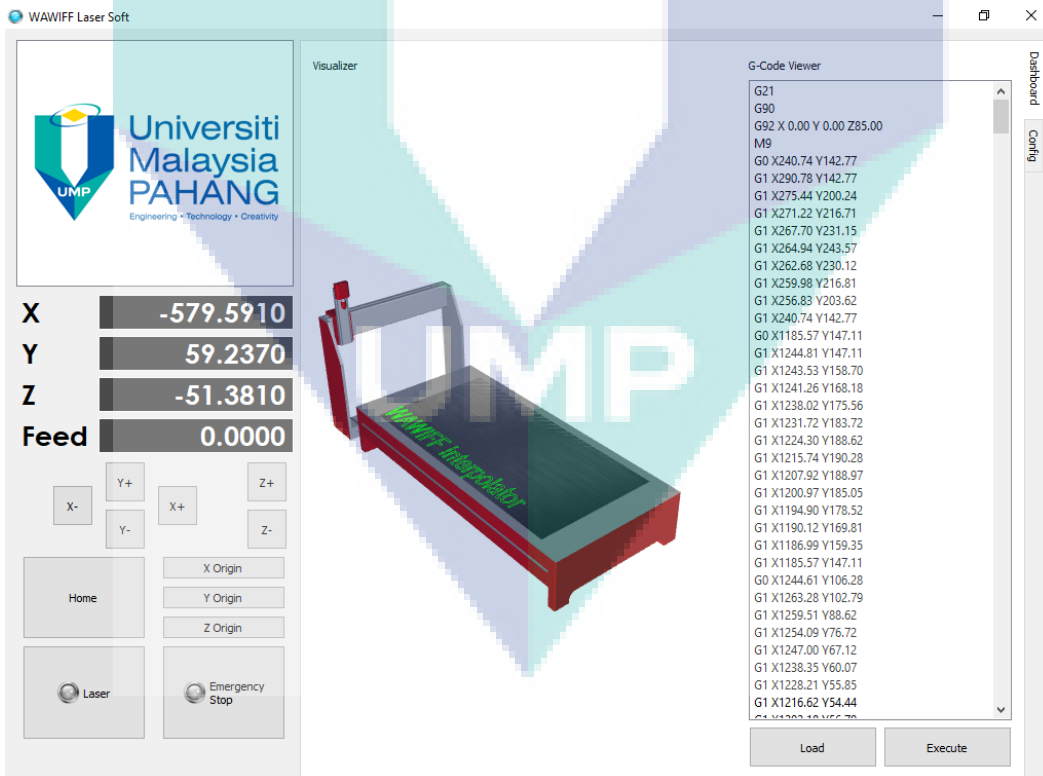


UMP

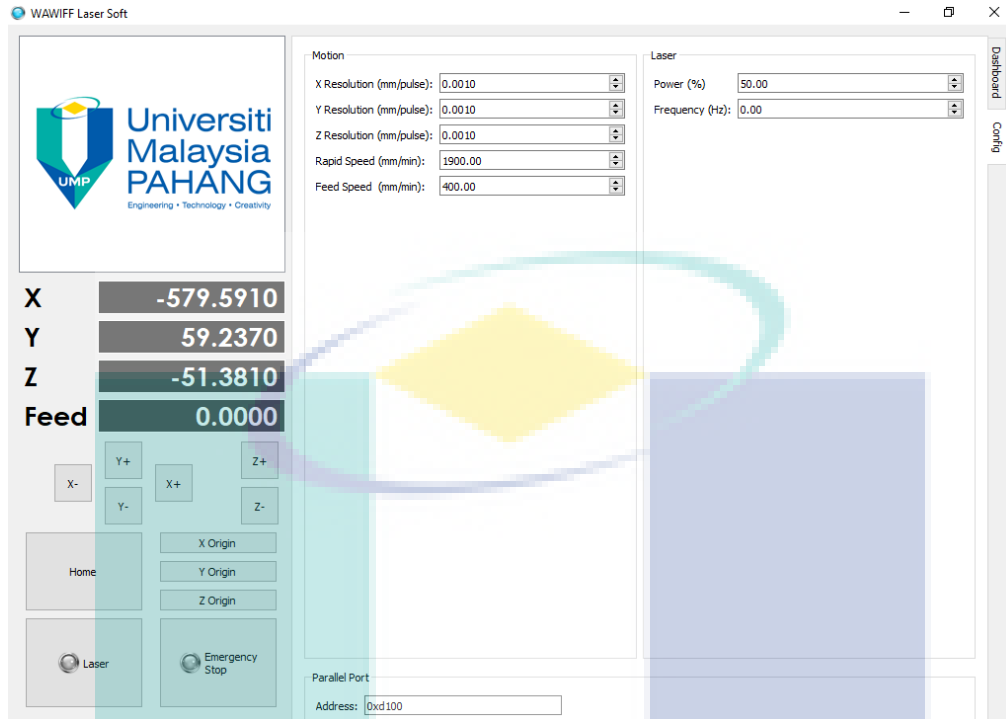
4.3 Software Testing – Alfa Version



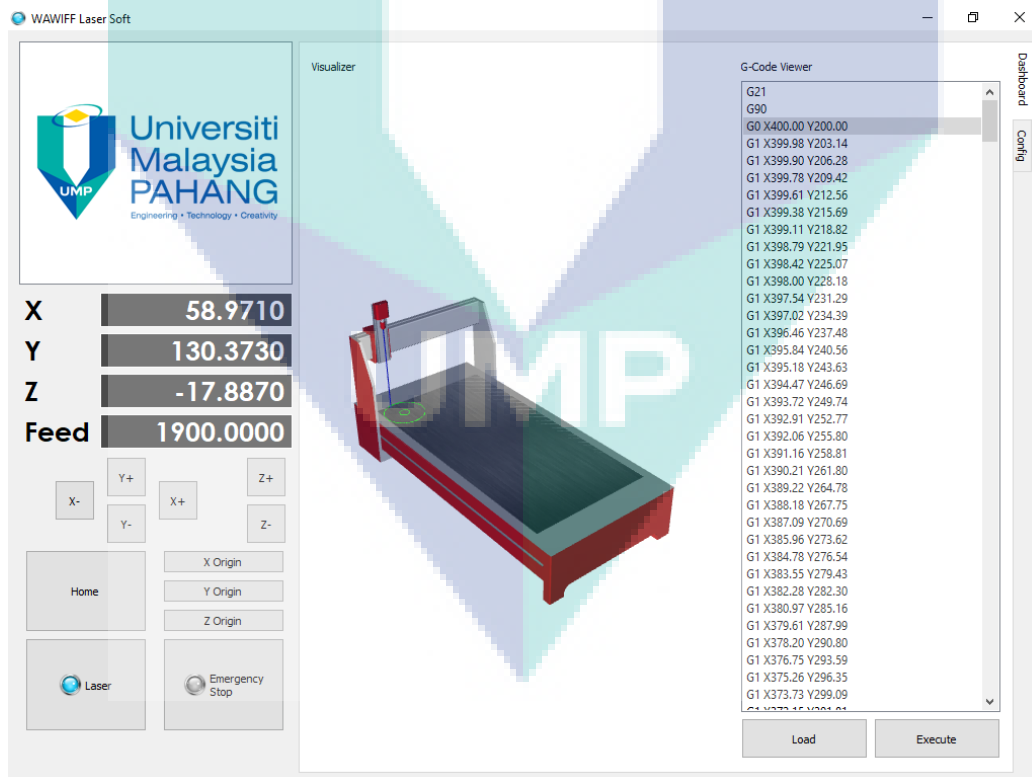
TWB CNC Laser Software Overview



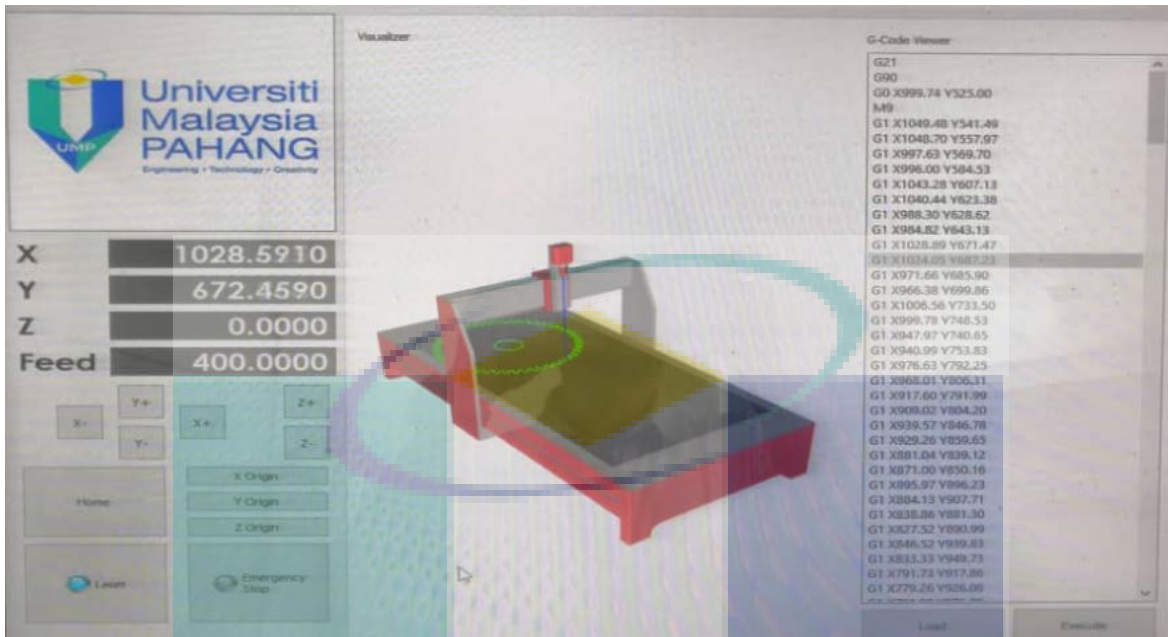
Main Page of the Software Controller



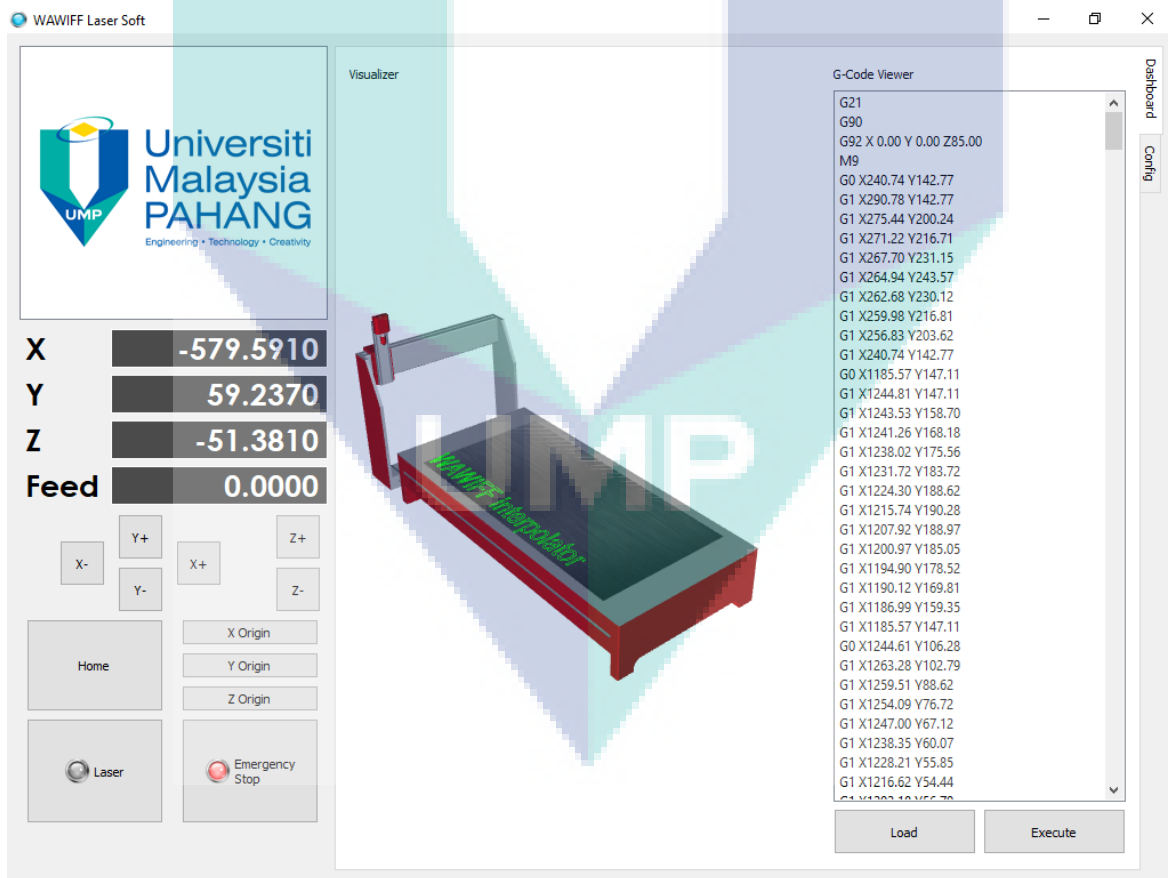
Motor Speed Control of X, Y and Z Axis by Rapid and Feed Rate Input



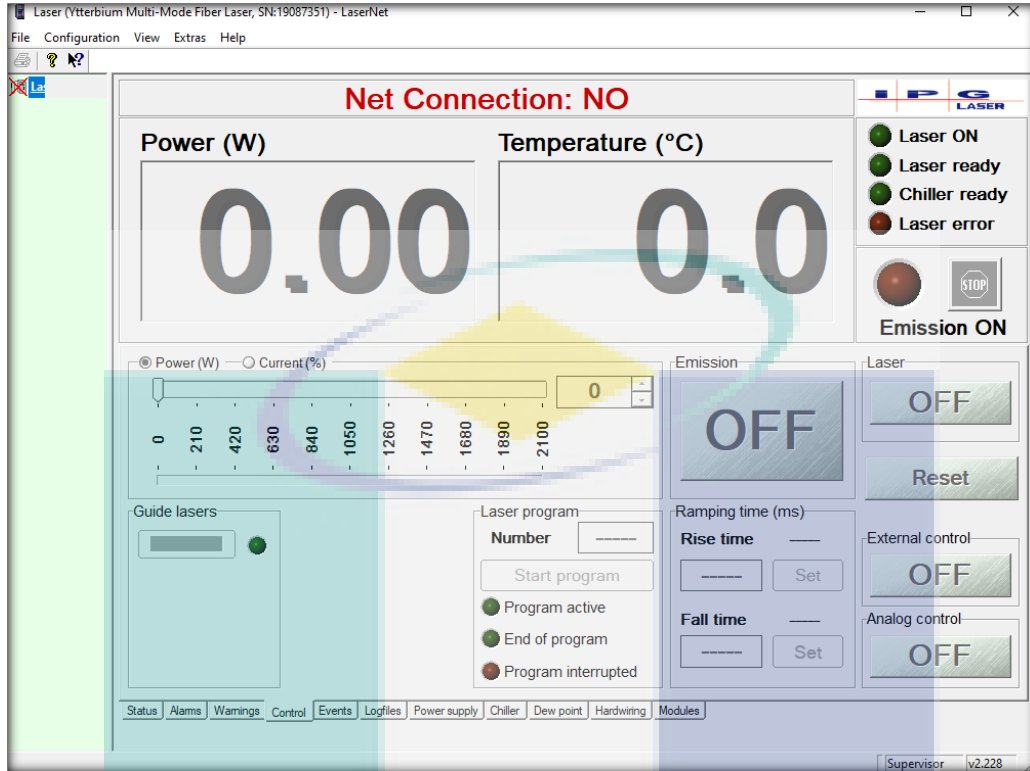
Load and Execute G-Code with On-Off Laser Input



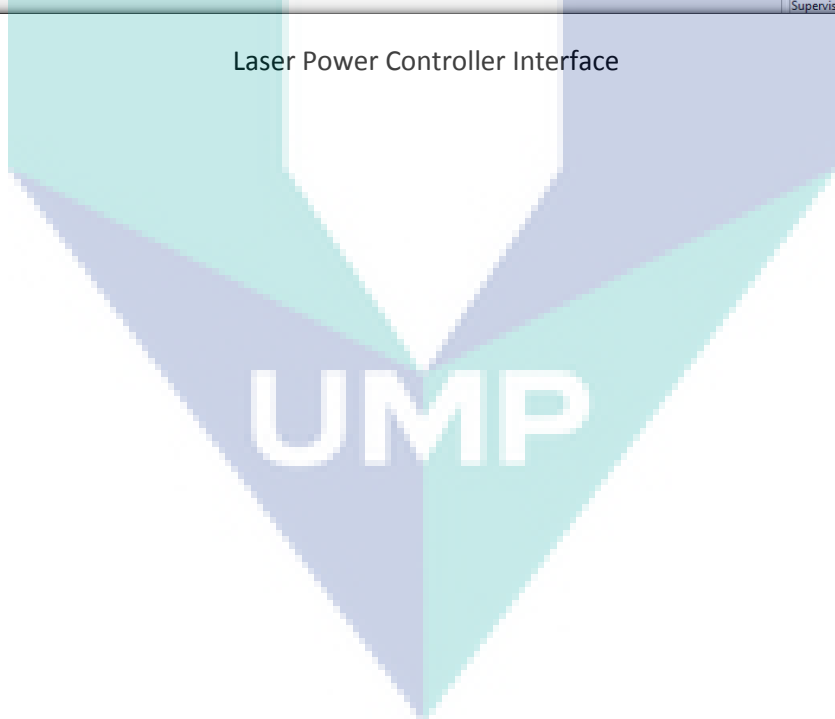
Laser On-Off Switch Capability



Emergency Stop Button

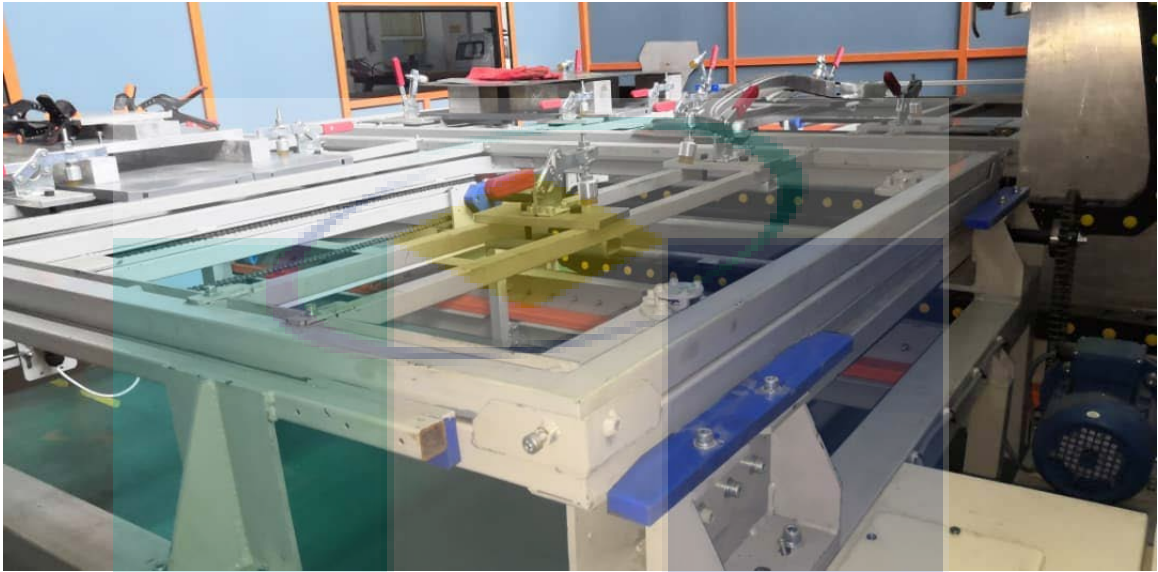


Laser Power Controller Interface



MILESTONE 5: TRIAL RUN

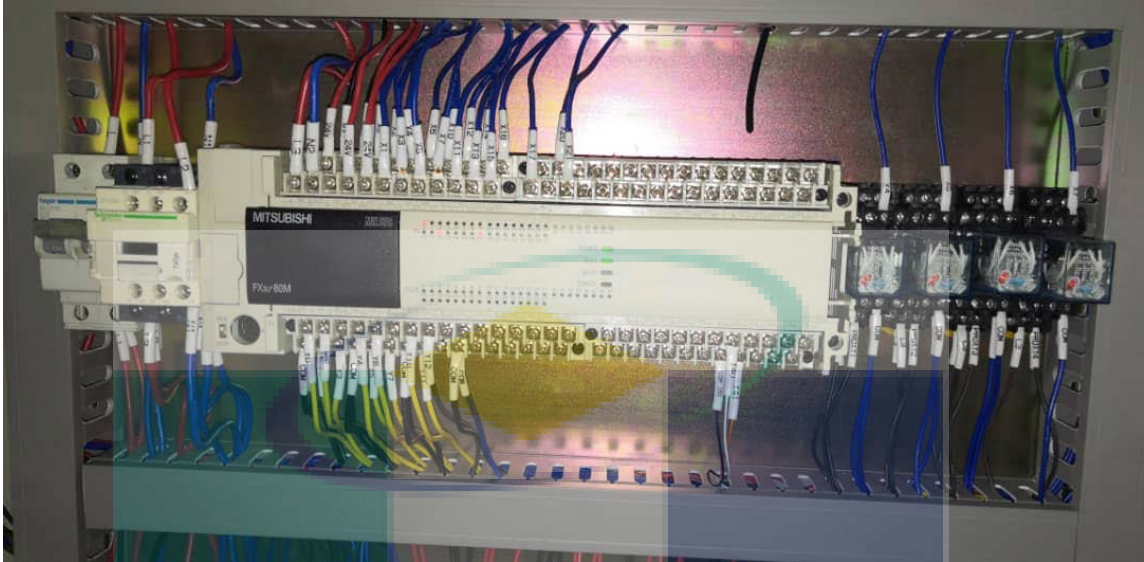
5.1 Jig Tuned Up – TWB Part Fabrication



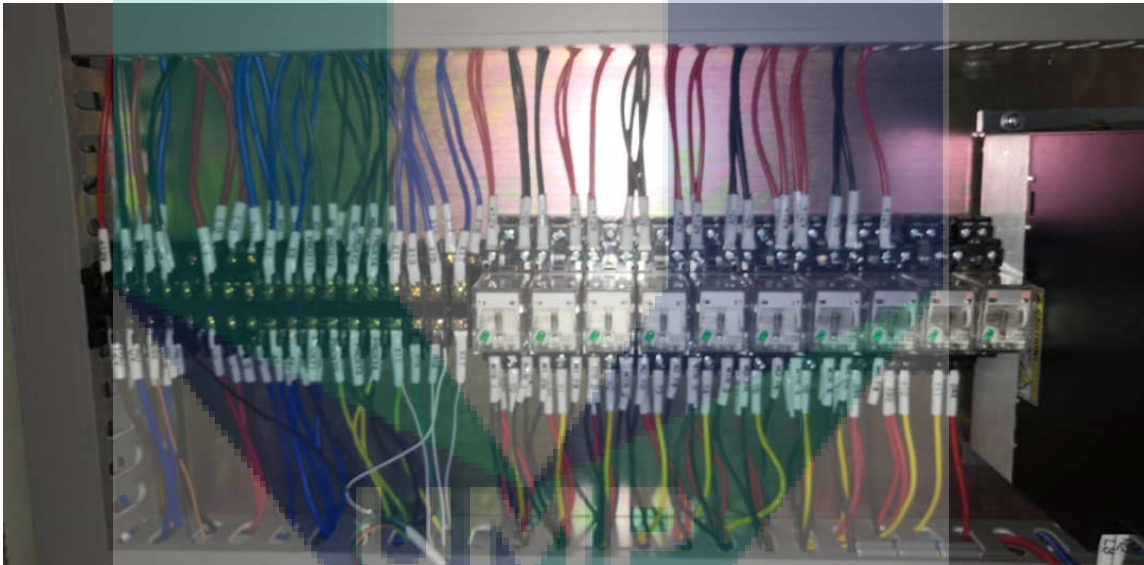
Overview of the Palette Jig for TWB Laser Welding Joining Parts



AC Motor for Palette Transfer with Limit Switch Position Control Capability



PLC Controller for Palette Jig Controller



Palette Jig Relay Wiring



AC Motor Inverter for Motor Speed Control

5.2 Performance Measurement – QC report on Mechanical Test

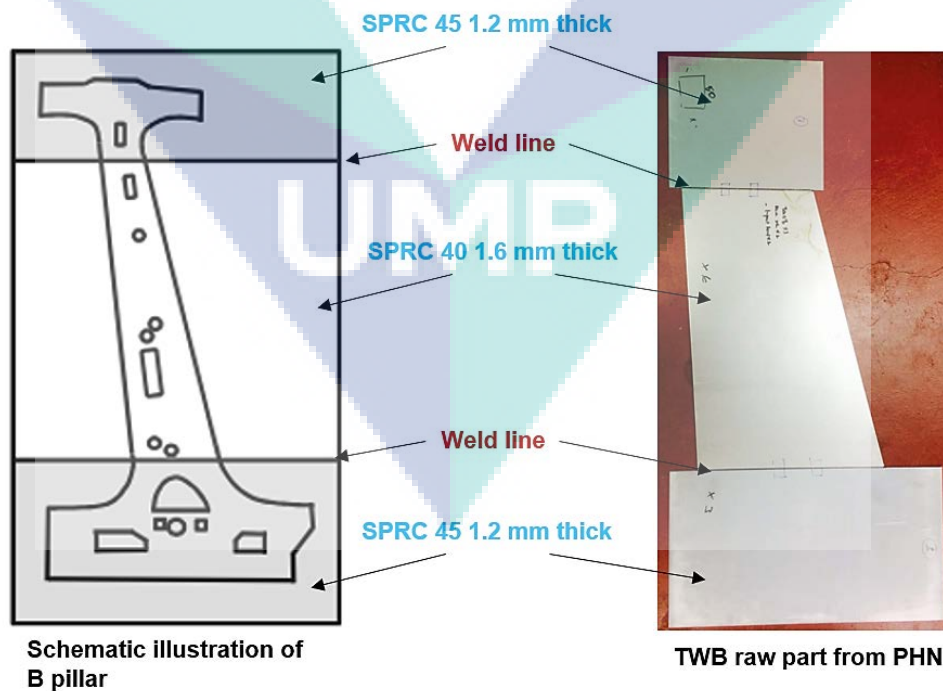
Receiving raw materials used for TWB part from PHN Industry Sdn Bhd. Table 5-1 and Table 5-2 show the information for the materials received for this project. The thickness variation of materials are; 1.2 mm for SPRC 45, and 1.6 mm for SPRC 40. These types of materials are known as cold-reduced high strength steels.

Table 5-1. Chemical Composition of as-received materials

Material	Element	C	Mn	P	S	Si
SPRC 40	Wt %	0.03	0.254	0.069	0.01	0.104
SPRC 45	Wt %	0.08	0.72	0.065	0.05	0.09

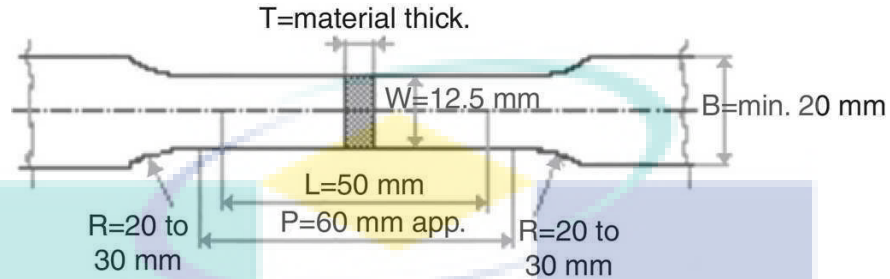
Table 5-2. Mechanical Properties of as-received materials

Material	UTS (MPa)	YS (MPa)	E, 50 GL (%)
SPRC 40	401	281	39
SPRC 45	454	337	37



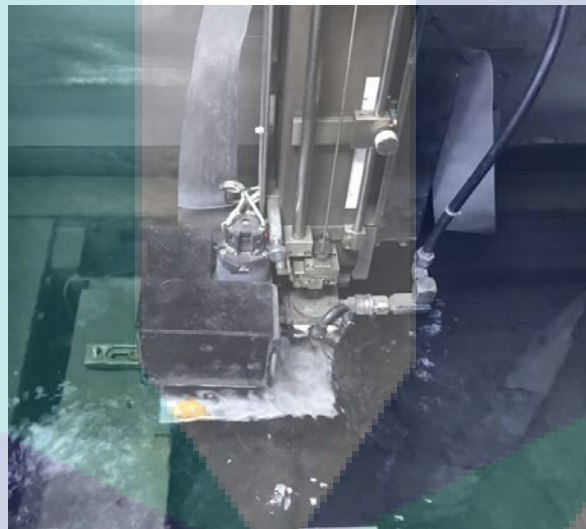
SPRC 40 and 45 application in TWB raw products of B-pillar

Base metal for both materials were subjected to the Electro Discharge Machine (EDM) wire cut to produce a precise measurement for tensile test sample. Following industrial standard used by PHN, tensile test sample from Japan Industrial Standard (JIS Z2201 (13b)) was used in this research.

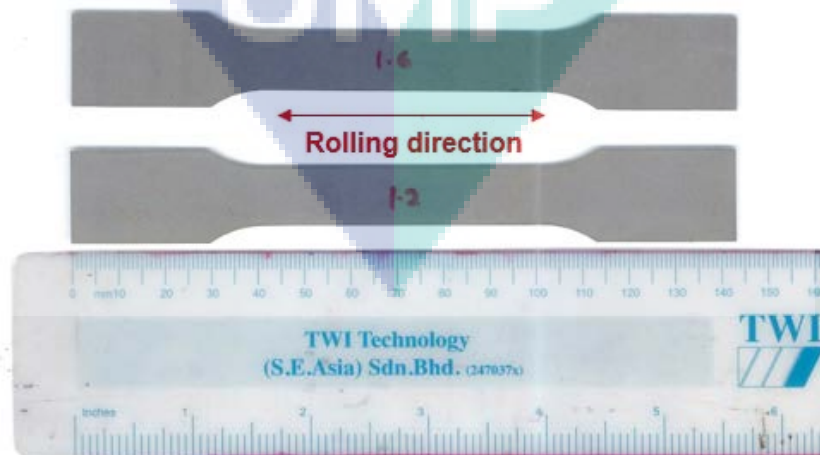


Journal of Applied Research and Technology. 2016;14:148-53

Schematic Illustration of JIS Z2201 (13b) tensile sample dimensions

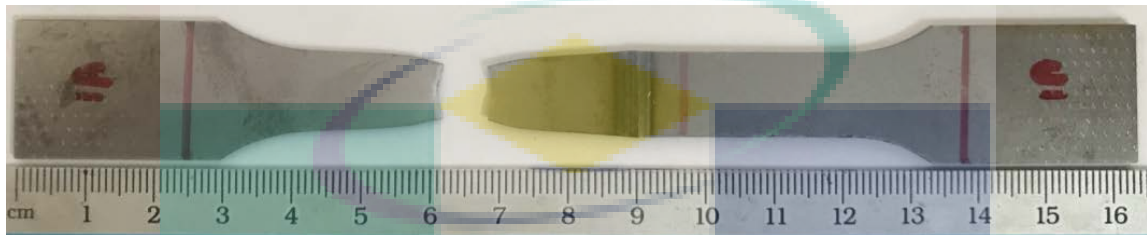


EDM wire cut process of producing JIS Z2201 (13b) tensile sample of base metal



JIS Z2201 (13b) tensile test sample for both as-received materials

As received metals were then subjected to the joint strength test. The tension tests were conducted using Instron Universal Testing machine. The average ultimate tensile strength were considered in account, (MPa). Out of total 25 welded samples are tested on the joint strength. Note that: LHS is 1.2 mm thick SPRC 45; RHS is 1.6 mm thick SPRC 40. JIS Z2201 (13b) standard tensile test sample was used.



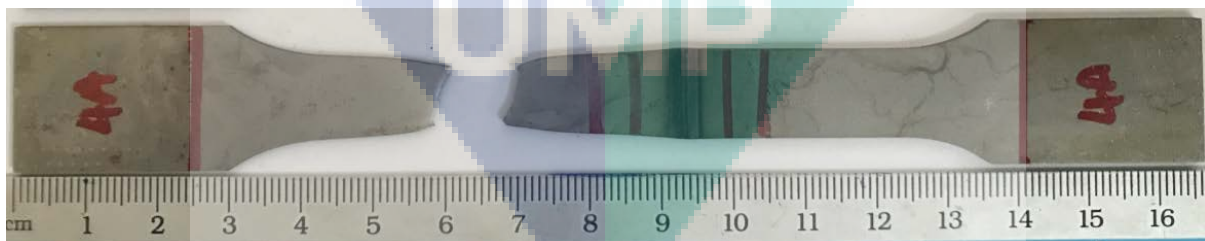
Sample 1



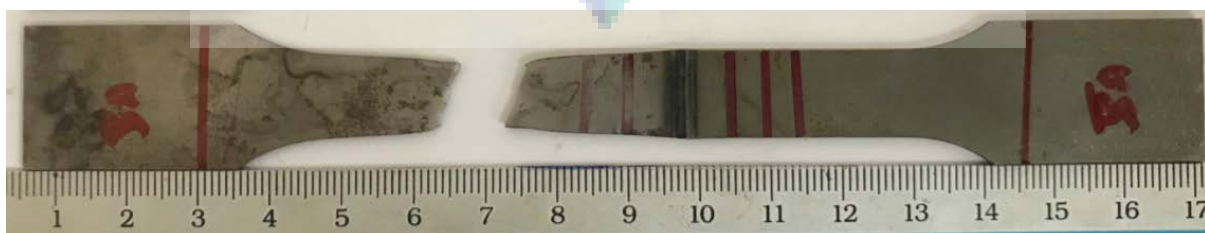
Sample 2



Sample 3



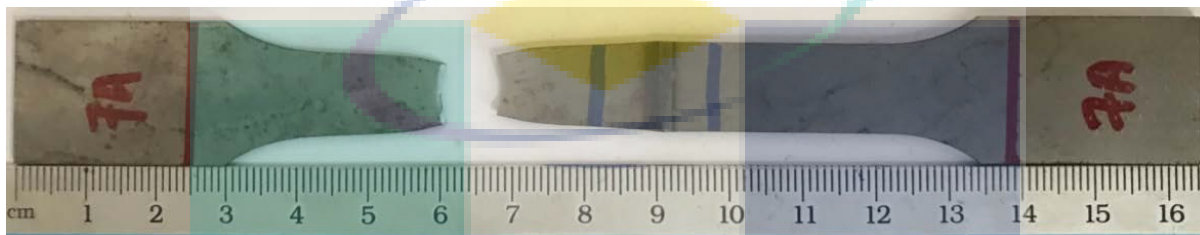
Sample 4



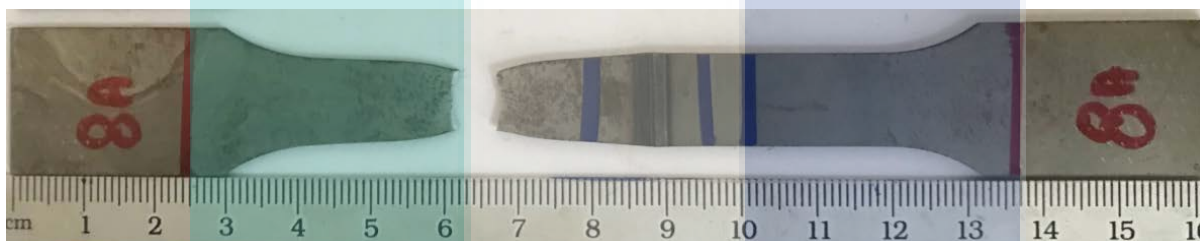
Sample 5



Sample 6



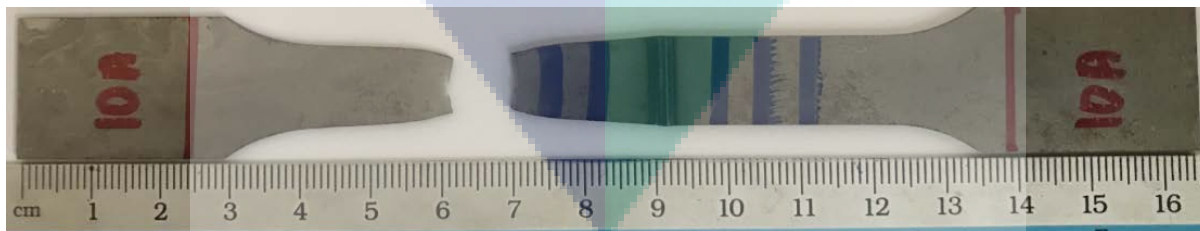
Sample 7



Sample 8



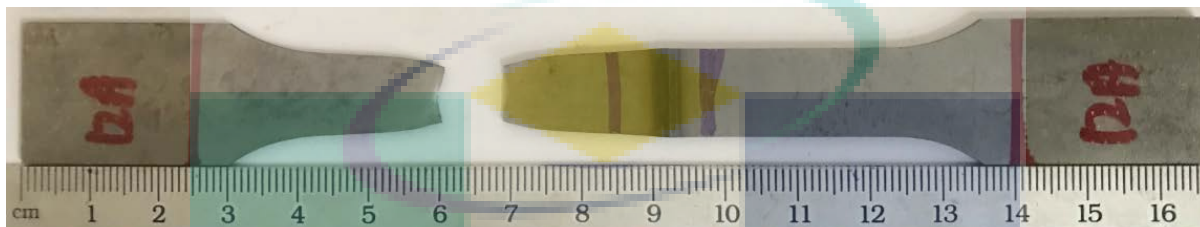
Sample 9



Sample 10



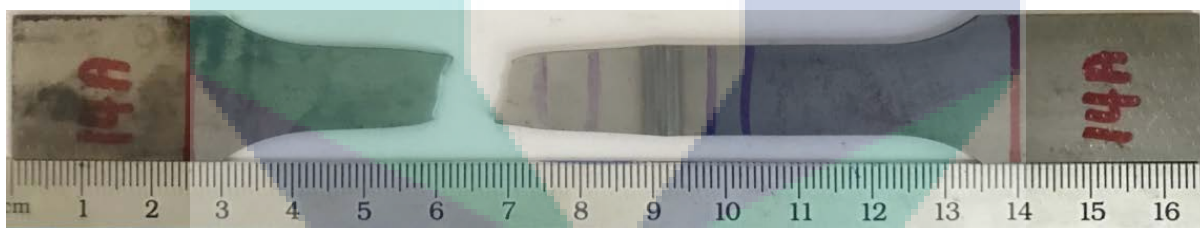
Sample 11



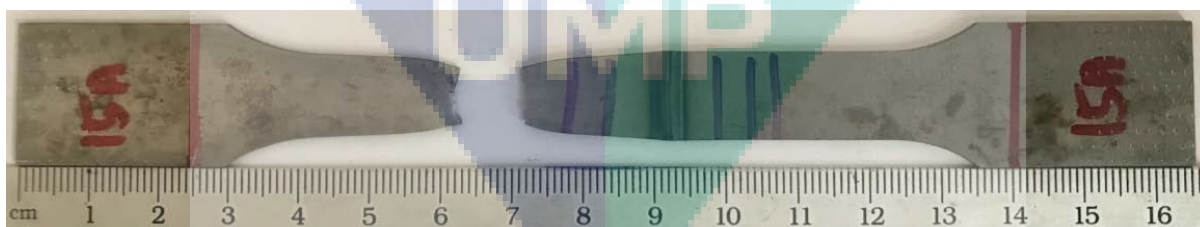
Sample 12



Sample 13



Sample 14



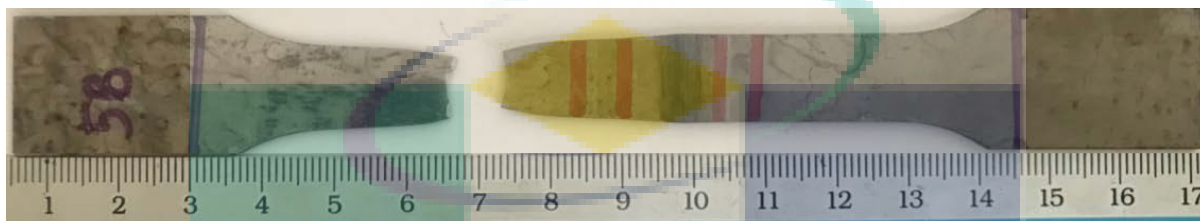
Sample 15



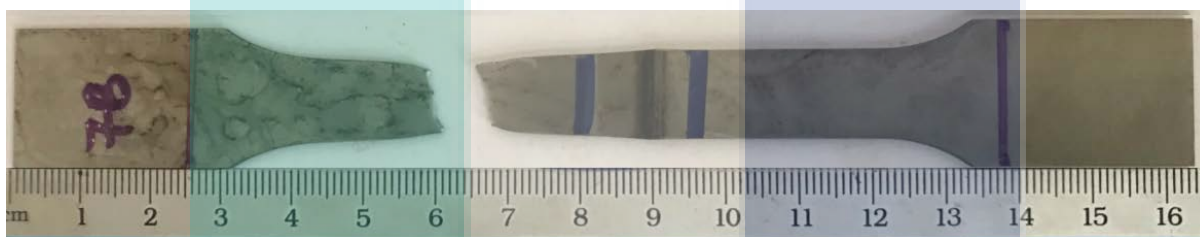
Sample 16



Sample 17



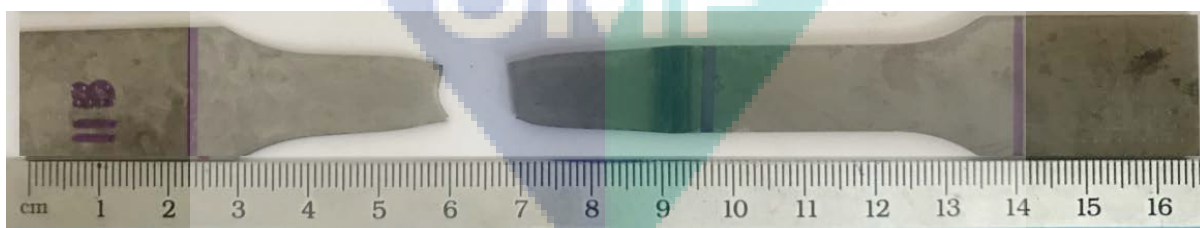
Sample 18



Sample 19



Sample 20

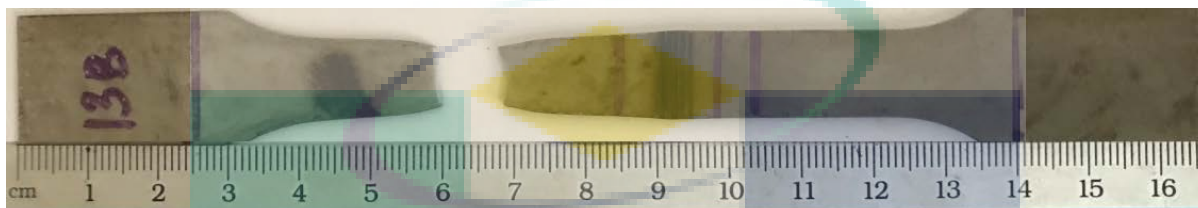


Sample 21

UMP



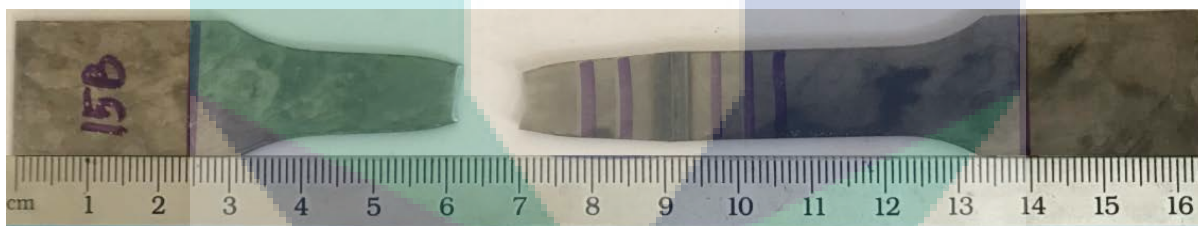
Sample 22



Sample 23

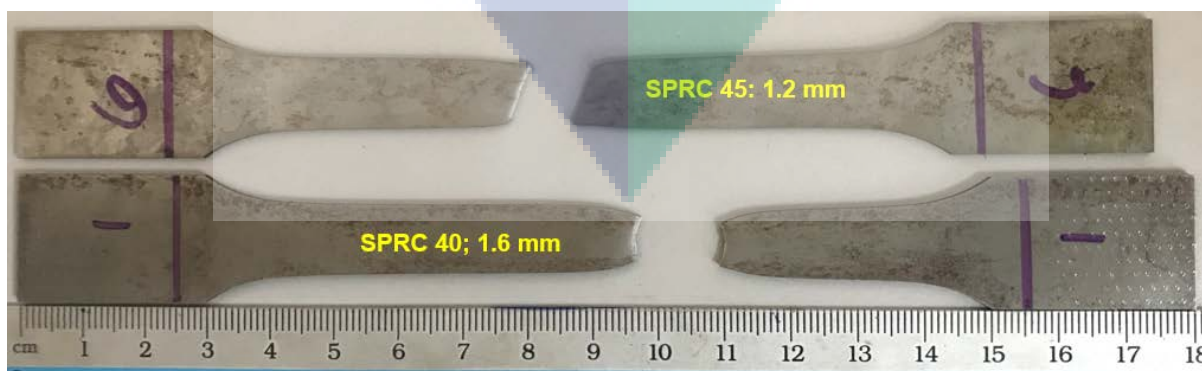


Sample 24



Sample 25

Base metal for both metals and thicknesses were carried out using three samples for more accurate results. Base metal fractured samples are indicated in the figure below.



Sample base metal

Note that: all welded sample were fractured at base metal of 1.2 mm thick SPRC 45, presenting a high strength laser weld joint.

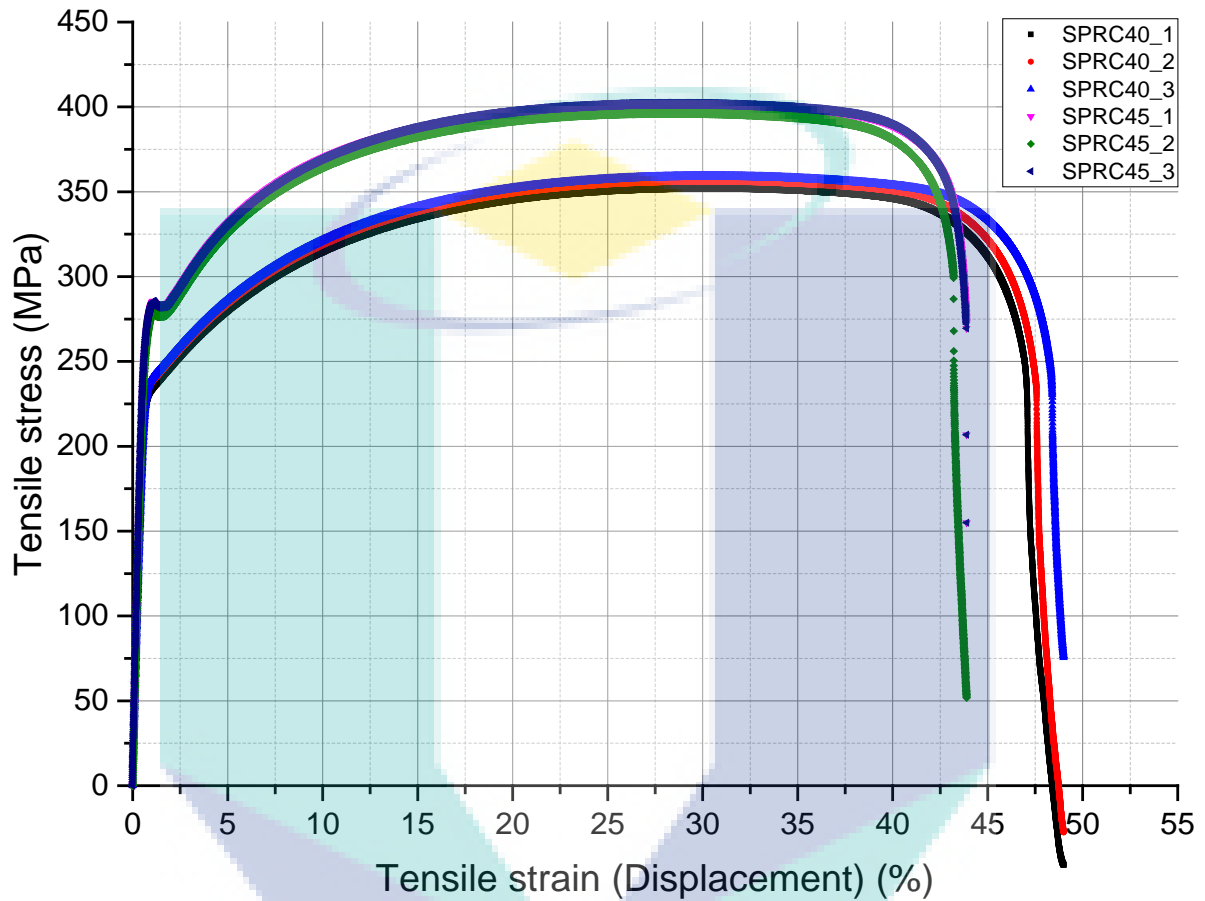
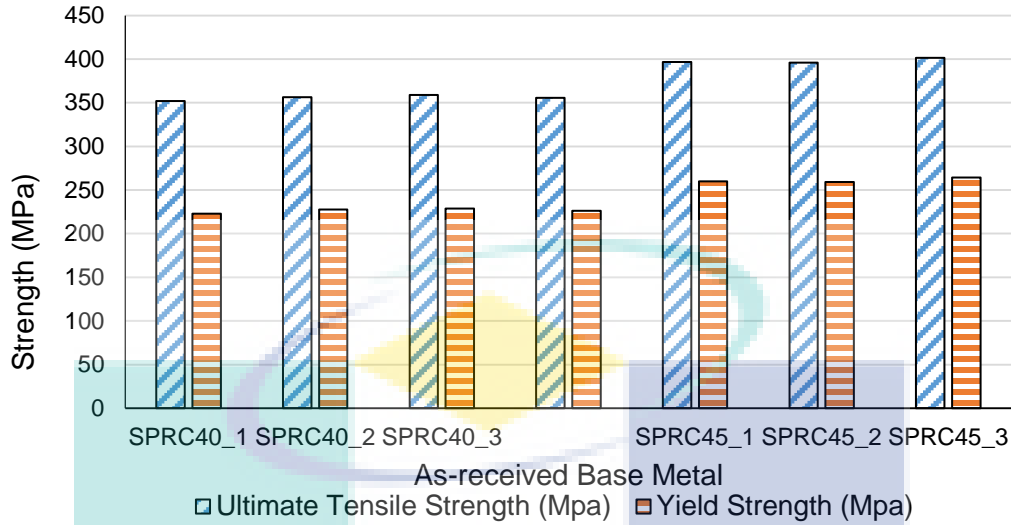
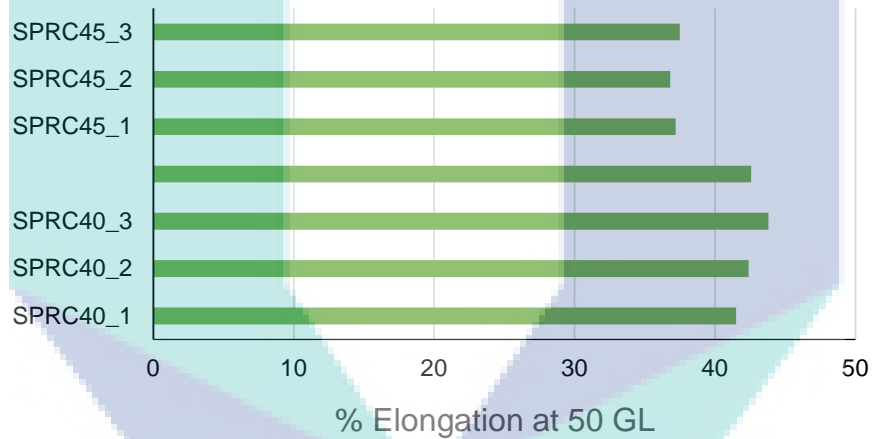


Table 5-3. Tensile test results for as-received base metal of SPRC 40 and 45

Specimen	Ultimate Tensile Strength (Mpa)	Yield Strength, 0.2% offset (Mpa)	% Elongation at 50 GL
SPRC40_1	351.99	222.86	41.5
SPRC40_2	356.29	227.51	42.4
SPRC40_3	359.09	228.75	43.8
SPRC45_1	396.79	259.79	37.2
SPRC45_2	396.06	259.23	36.8
SPRC45_3	401.56	264.27	37.5



Bar graph showing the results of UTS and Yield strength of tested as received base metal



Bar graph showing the percentage of elongation of base metals at 50 mm Gauge Length

These results from the tension testing following JIS Z2201 (13b) standard tensile testing for sheet metal showing results approximately equally to the mill certification retrieved from the company. SPRC 40 sample showing lower UTS value with higher percentage of elongations. Meanwhile, SPRC 45 sample shows higher UTS value with lower percentage of elongation at fracture.

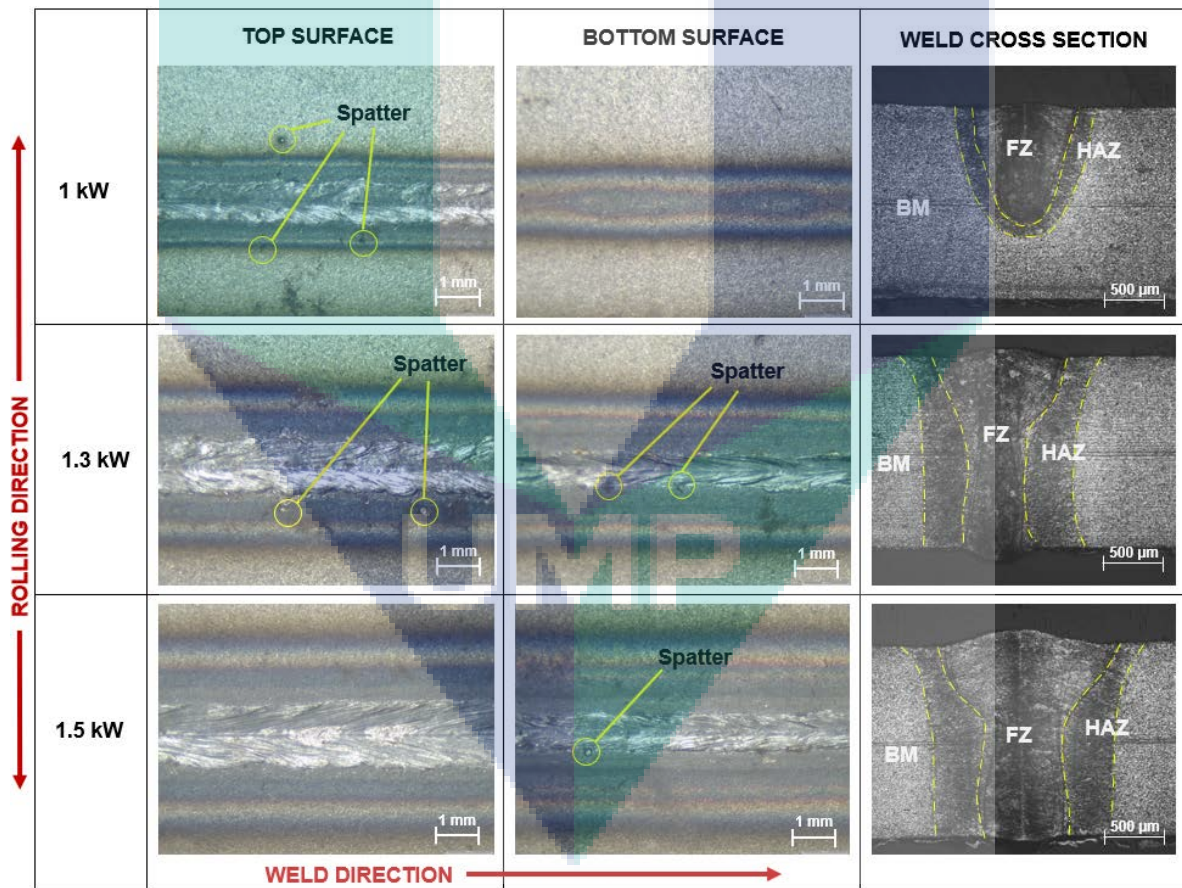
Table 5-4. Average results for strength and elongation of base metal

Material	Average UTS (MPa)	Average YS (MPa)	Average E, 50 GL (%)
SPRC 40	356	226	42
SPRC 45	398	261	37

Preliminary experiment was done for parameters screening before conducting the systematic experiment order. This stage was applied to get the range of parameters which will be used in the design of experiment (DOE). Bead-on-plate (BOP) welding was performed on 1.6 mm thickness sample.

Table 5-5. Power Screening parameters setup

Experiment	Laser Power, Watt (kW)	Scanning Speed (mm/min)	Focal length (mm)	Ar gas (L/min)
1	1.0	2000	82 (at focus position)	12
2	1.3			
3	1.5			



Macrostructure images at top, bottom, and cross section of 1.6 mm thickness SPRC 40 at different laser power

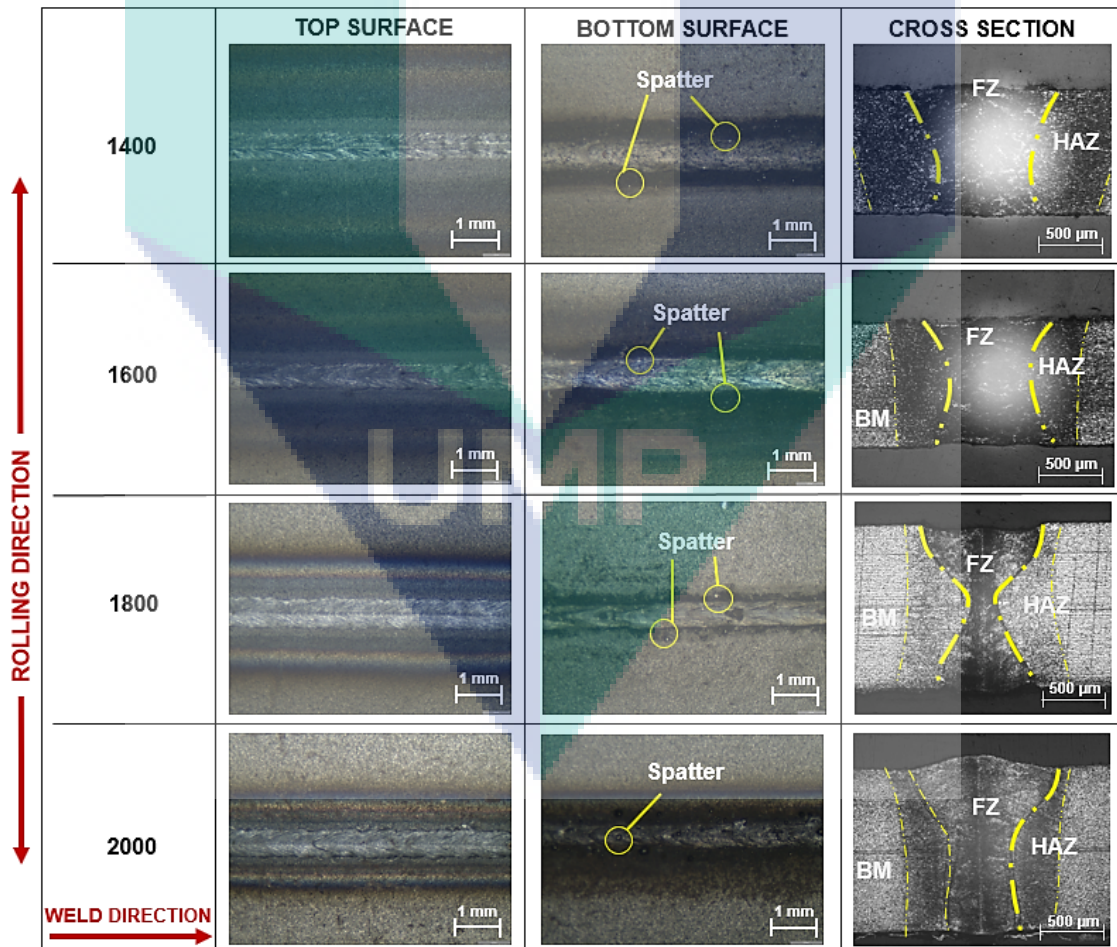
Table 5-6. Results of observation for laser power screening

Experiment	Laser Power, (kW)	Penetration	Spatter	Notes
1	1.0	Partial	Yes (top)	Reject
2	1.3	Full	Yes (top, bottom)	Accept
3	1.5	Full	Yes (bottom)	Accept

From the results of observation, 1kW power is not enough to produce full weld penetration for the welding joint. Laser power 1.3 and 1.5 kW are acceptable to produce full weld penetration. Next pre-experiment was done for scanning speed (welding speed) parameter screening using 1.5 kW laser power.

Table 5-7. Scanning Speed screening parameters setup

Experiment	Scanning Speed (mm/min)	Power (kW)	Focal position (mm)	Ar gas (L/min)
1	1400	1.5	82	12
2	1600			
3	1800			
4	2000			

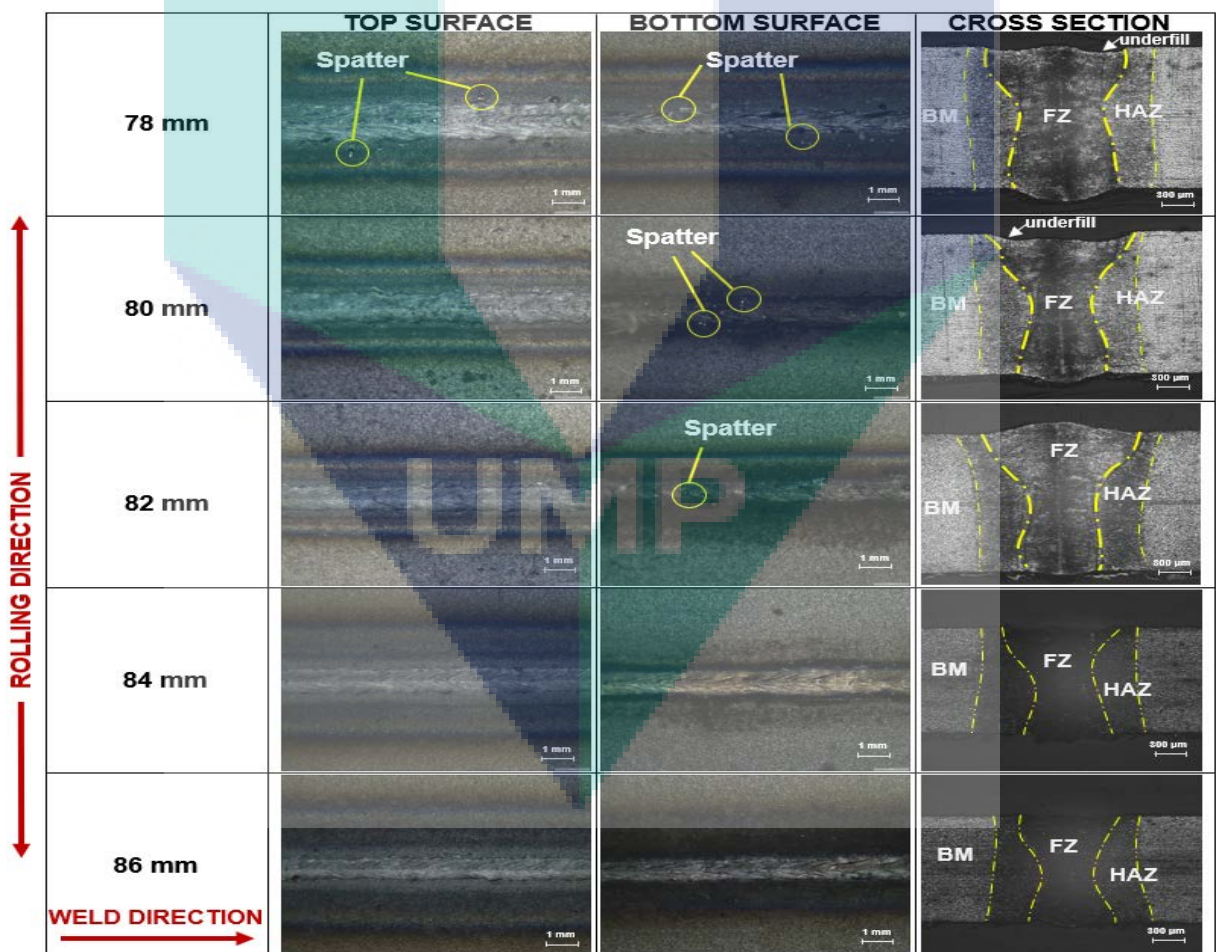


Macrostructure images at top, bottom, and cross section at different scanning speed

Table 5-8. Results of observation for scanning speed screening

Experiment	Scanning speed (mm/min)	Penetration	Spatter	Notes
1	1400	Full	Yes (bottom)	Reject (HAZ too large)
2	1600	Full	Yes (bottom)	Accept
3	1800	Full	Yes (bottom)	Accept
4	2000	Full	Yes (bottom)	Accept

From the observation results, scanning speed at 1400 mm/min is not suitable for high speed welding since it produces larger heat affected zone (HAZ) which can lead to weaker joint strength. Scanning speed 2000 mm/min with 1.5 kW laser power are used for focal length screening parameters.



Macrostructure images at top, bottom, and cross section at different focal length

Table 5-9. Focal length screening parameters setup

Experiment	Focal position (mm)	Power (kW)	Scanning Speed (mm/min)	Ar gas (L/min)
1	78	1.5	2000	12
2	80			
3	82			
4	84			
5	86			

Table 5-10. Observation results for focal length screening parameters

Experiment	Focal Position (mm)	Penetration	Spatter	Underfill	Notes
1	78	Full	Yes (top, bottom)	Yes	Accept
2	80	Full	Yes (bottom)	Yes	Accept
3	82	Full	Yes (bottom)	No	Accept
4	84	Full	No	No	Accept
5	86	Full	No	No	Accept

Experiment 1 and 2 produced weld zone with underfill defects. However, in term of dissimilar welding, small underfill defects is acceptable. The parameters then were set to the parameters range setup in order to be used in design of experiment (DOE) for a systematic order of experiment. Box-Behnken design (BBD) from the response surface method (RSM) was selected in this experiment.

Table 5-11. Parameters range based on the parameters screening

Factors	Design matrix range (BBD)		
	-1	0	+1
Power, P (W)	1300	1400	1500
Scanning Speed, S (mm/min)	1600	1800	2000
Focal Length, F (mm)	78	82	86

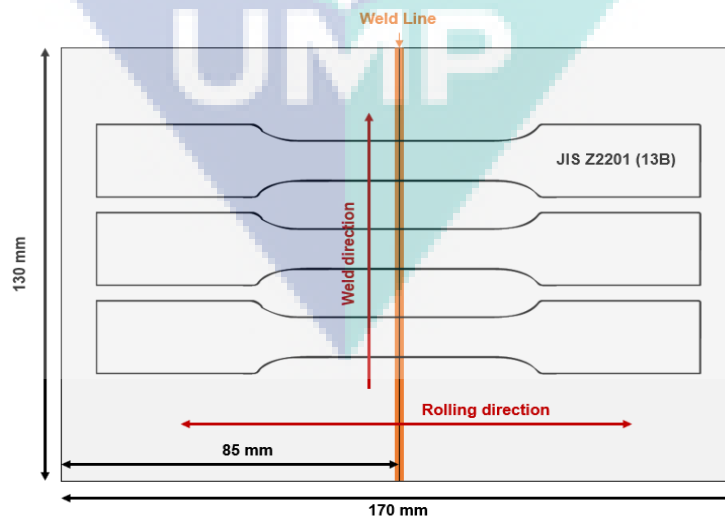
Design Summary

Factors: 3 Replicates: 1
 Base runs: 15 Total runs: 15
 Base blocks: 1 Total blocks: 1

Design summary based on the BBD setup

Table 5-12. Sets of experiment order from BBD design

Exp No.	Input Voltage, V	Power, P (W)	Scanning Speed, S (mm/min)	Focal Length, F (mm)
1	7.2	1300	1600	82
2	8.3	1500	1600	82
3	7.2	1300	2000	82
4	8.3	1500	2000	82
5	7.2	1300	1800	78
6	8.3	1500	1800	78
7	7.2	1300	1800	86
8	8.3	1500	1800	86
9	7.7	1400	1600	78
10	7.7	1400	2000	78
11	7.7	1400	1600	86
12	7.7	1400	2000	86
13	7.7	1400	1800	82
14	7.7	1400	1800	82
15	7.7	1400	1800	82

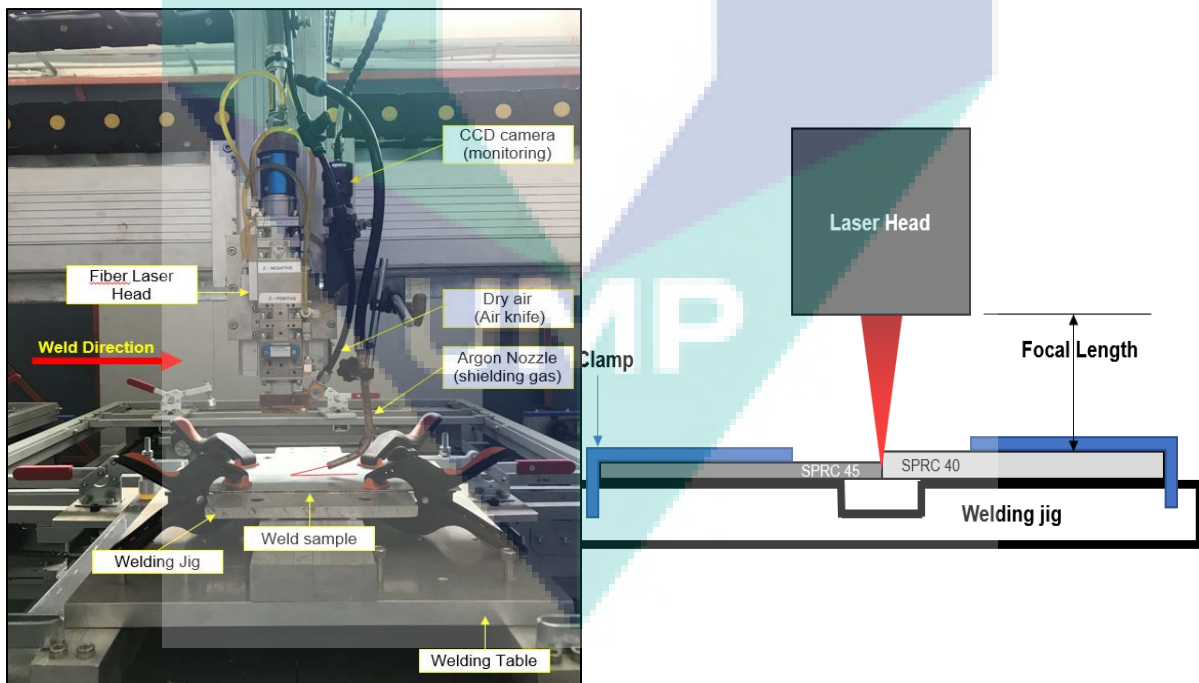


Schematic illustration tensile sample cut from the welded product

Prior to laser welding, base metal from both samples (SPRC 40; 1.6 mm thickness and SPRC 45; 1.2 mm thickness) was prepared by the dimension of 130 × 85 mm. Before laser welding process started, the edge of the sample (weld area only) was prepared by surface grinding method in order to avoid large gap at the butt joint configurations and to obtain smooth edge surfaces.

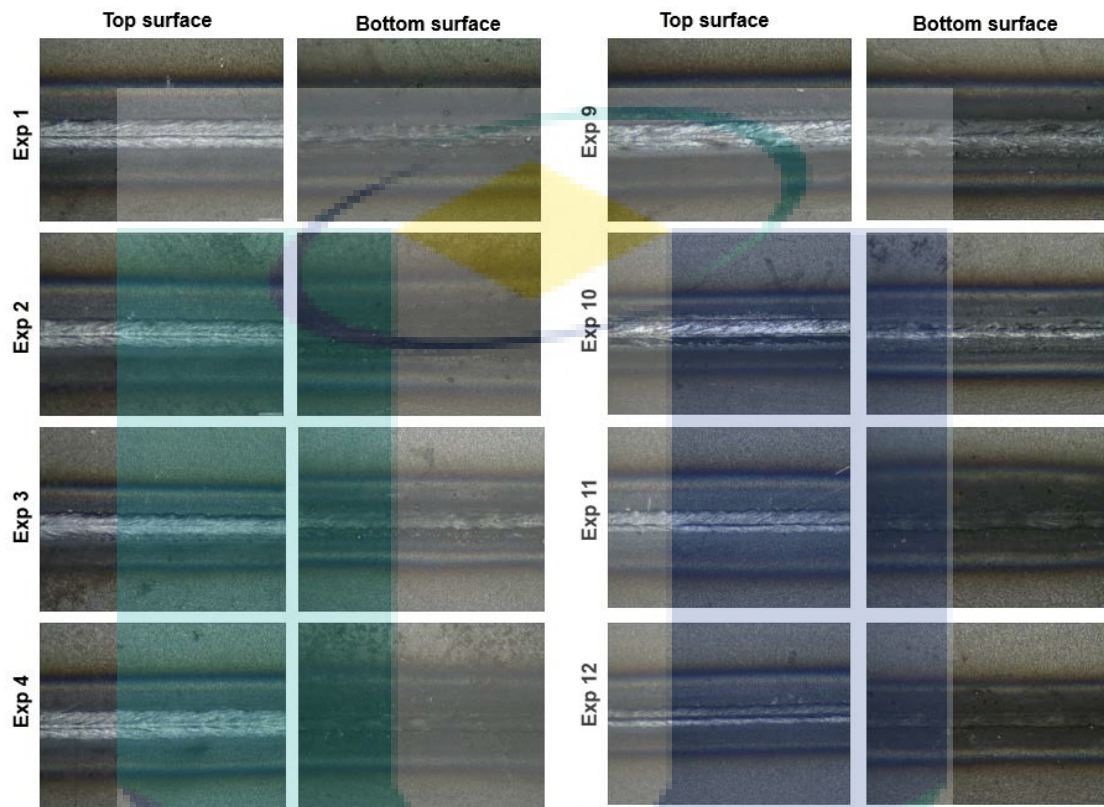


Surface grinding process at the edge (weld area only) of base metal sample

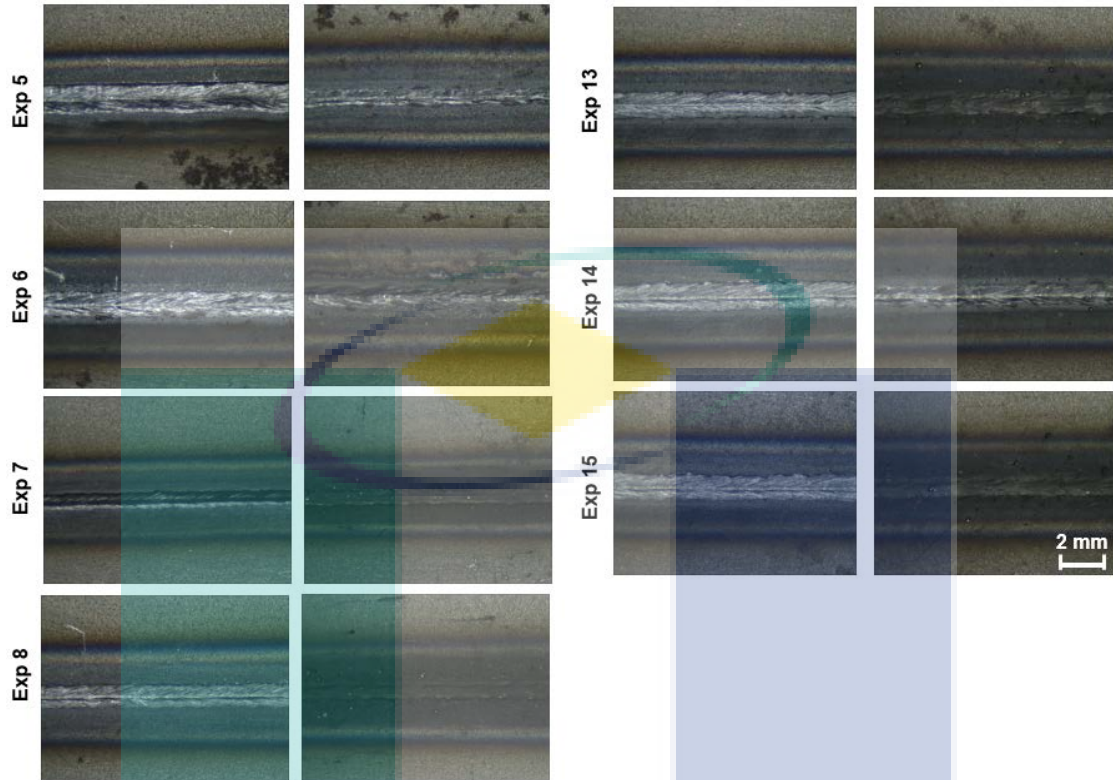


Laser welding setup for dissimilar welding (SPRC 40 and SPRC 45)

All 15 samples were welded according to the design table retrieved from the BBD design for a better systematic experimental process. Weld area was cleaned using ethanol to avoid foreign object and dirt.



UMP



Macro-images at top and bottom surface of TWB welded samples

6

Full penetration weld achieved successfully with low spatter defects for all 15 TWB samples of SPRC 40 and 45 materials. Samples then were cut by EDM wire cut according to the JIS Z2201 (13b) for tensile test.

Table 5-13. Result of UTS and YS from the tension test

Exp No.	Ultimate Tensile Strength, UTS (MPa)				Yield Strength, YS (MPa)				Avg % E at 50 GL
	A	B	C	Average	A	B	C	Average	
1	428.5	419.06	439.0	428.9	275.3	284.0	306.9	288.7	27.0
2	411.3	417.6	429.1	419.3	272.9	286.2	300.8	286.6	26.3
3	415.3	409.0	442.7	422.3	272.8	270.2	303.8	282.3	26.7
4	413.6	410.2	435.3	419.7	285.2	284.8	312.2	294.1	26.7
5	410.4	413.7	431.4	418.5	266.07	272.2	292.3	276.9	26.7
6	414.8	415.8	439.0	432.2	279.0	281.4	306.0	288.8	29.0
7	423.5	418.4	443.1	428.3	280.4	277.9	308.3	288.9	27.3
8	420.7	421.2	446.4	429.4	293.8	293.6	318.8	302.9	26.3

9	414.9	417.4	437.5	423.3	273.5	278.9	303.1	285.2	26.7
10	419.9	423.0	442.2	428.4	287.6	289.8	315.0	297.5	27.0
11	411.5	433.3	446.0	430.3	278.3	302.5	316.0	298.2	27.3
12	413.8	433.1	439.0	428.6	281.5	305.5	312.8	299.9	29.0
13	418.6	432.4	439.4	430.1	272.3	293.1	304.6	290.0	29.3
14	420.6	431.8	441.2	431.2	276.9	289.7	306.2	290.9	28.0
15	419.7	427.8	434.7	427.4	285.9	298.6	305.8	296.7	27.0

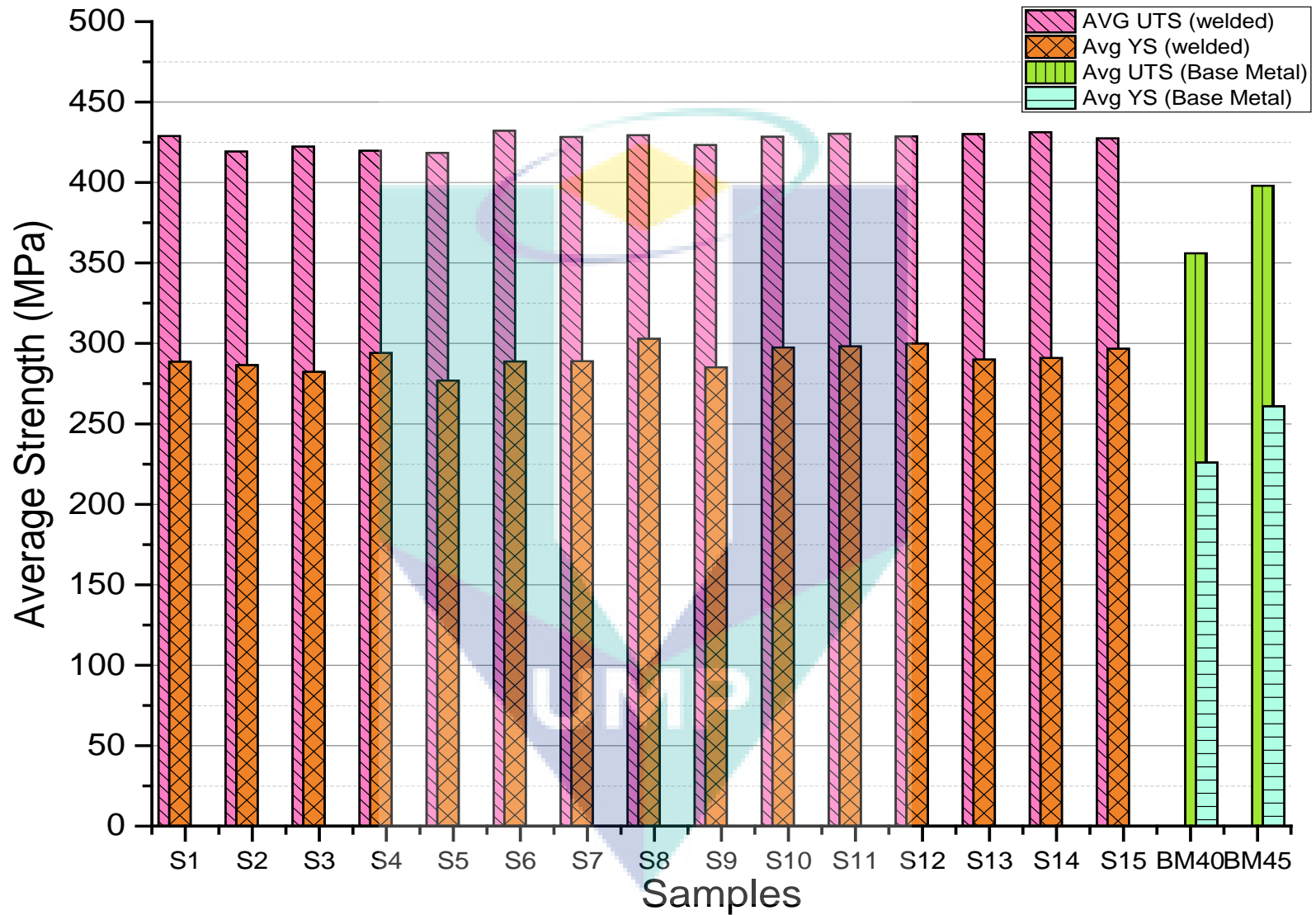
All 15 welded samples with three tensile samples (total of 45 tensile samples) were fractured at the SPRC 45 location, which having 1.2 mm thickness. The average tensile strength and yield strength for the welded parts was calculated and then compared with the base metals' strength for both metals (SPRC 40 and SPRC 45).

A bar graph was constructed based on the strength results. It was observed that UTS and YS of welded parts were all higher compared with the UTS and YS of both base metals. The highest average UTS was possessed by sample number 6 (welded; P=1.5 kW, S=1800 mm/min, F=78 mm), which having average UTS of 432.2 MPa and average YS of 288.8. However, other 14 samples possessed approximately similar UTS value since all samples fractured at 1.2 mm thickness base metal.

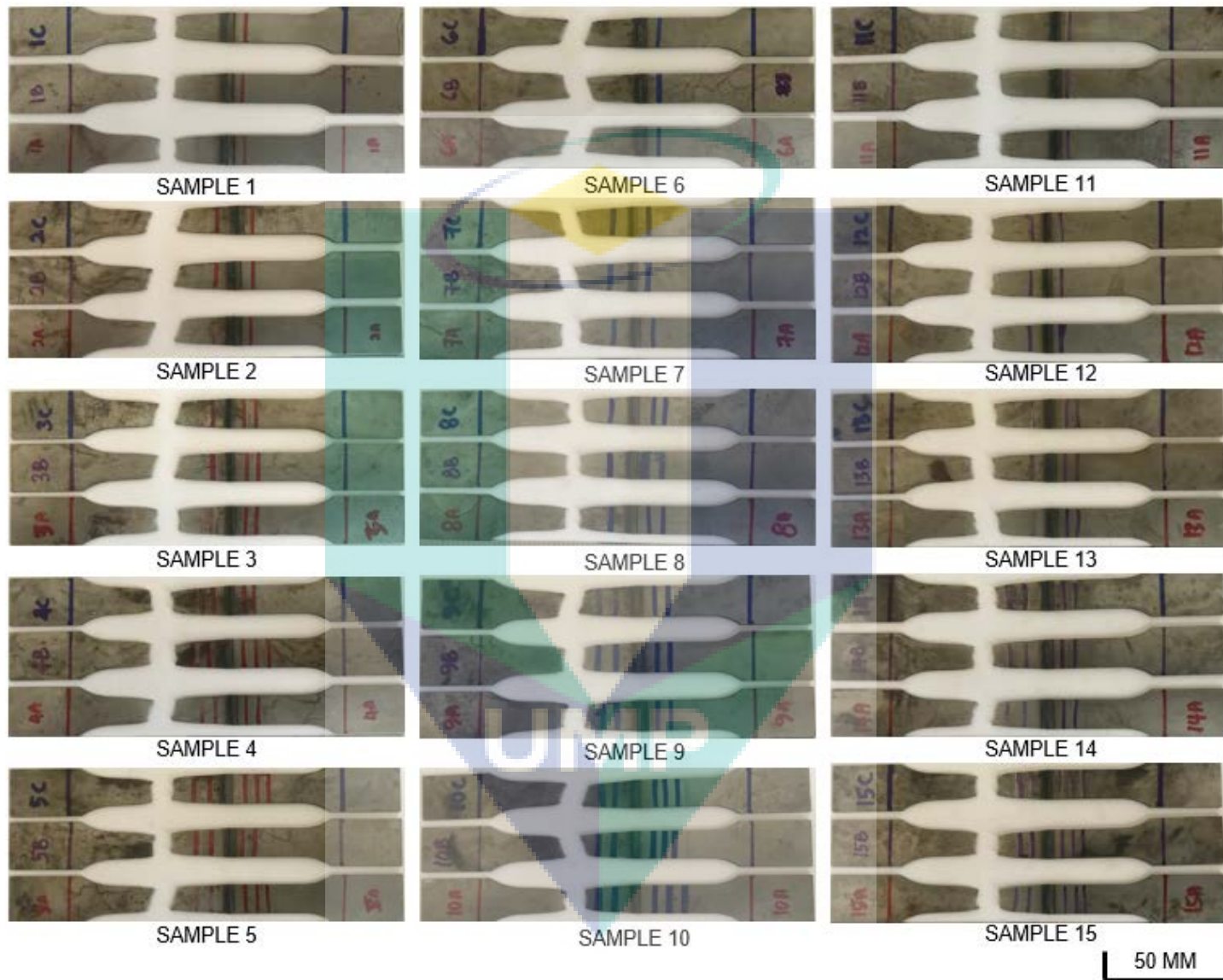
The increment of UTS value after been weld was calculated based on sample 6 and base metal of SPRC 40 and 45; 8.54% higher (sample 6-SPRC 45), 21.3% higher (sample 6-SPRC40).



UMP



Bar graph shows the results of 15 welded samples compared with the SPRC 40 and 45 base metals strength

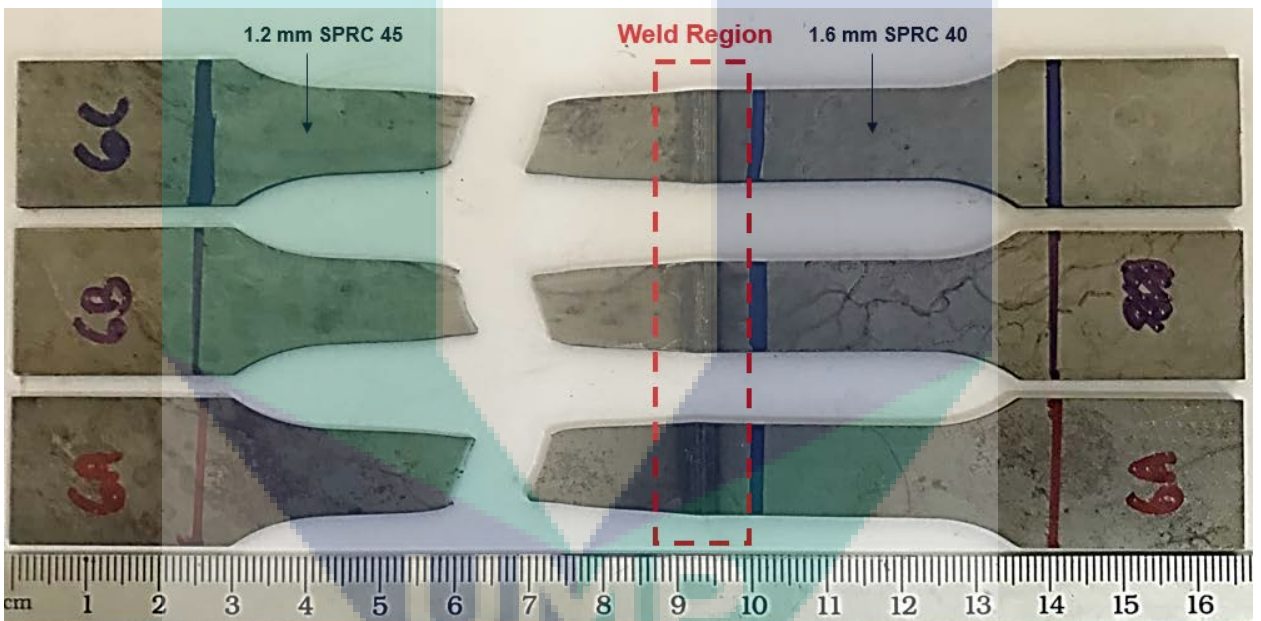


Fractured samples for 15 sets of experiment, three tensile sample for average measurement



Fractured sample of base metal SPRC 40 and SPRC 45

From figure above, SPRC 40 showing a criterion of high ductility which possessing higher percentage of elongation compared than SPRC 40. However, SPRC 40 having lower ultimate tensile strength compared than the SPRC 45 UTS.



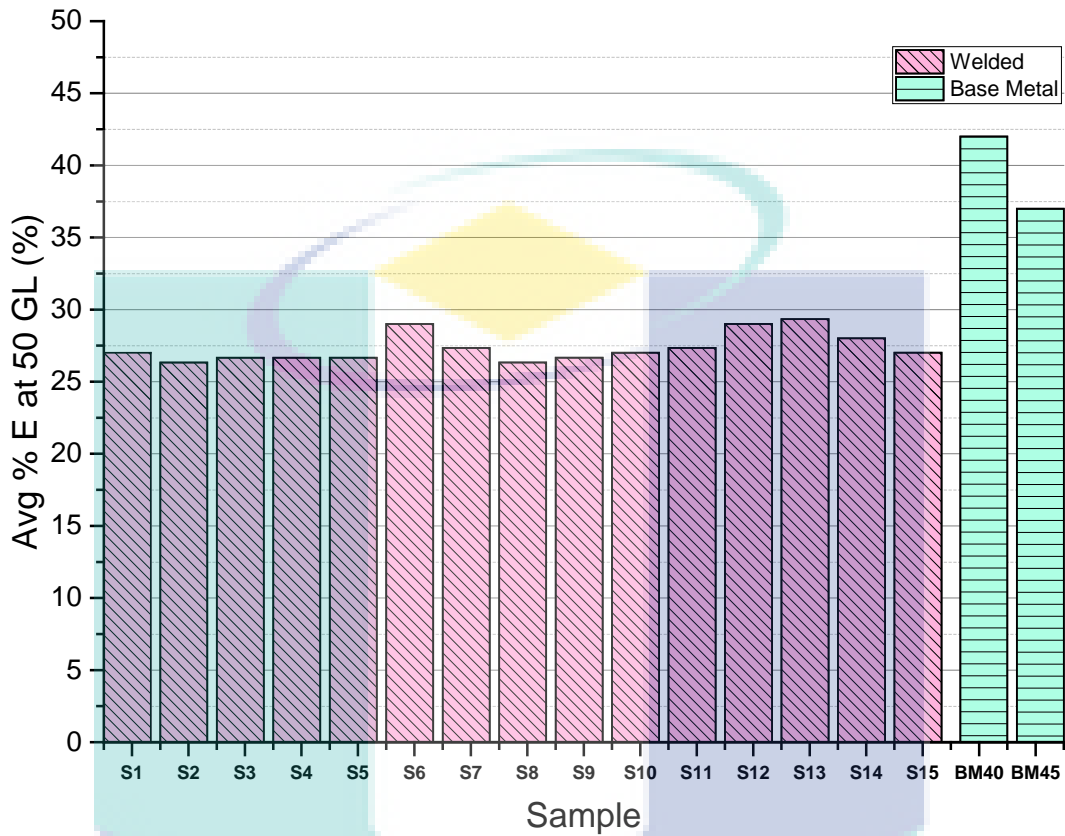
Fractured tensile sample from sample No. 6

Figure above showing the fractured sample of the highest UTS among the 15 sets of welded samples. It was observed that the welded product fractured at the base metal of 1.2 mm thickness side (SPRC45), without harming the welded region. It proves higher joint strength when the welded product fractured at the base metal.

The fracture behavior for sample 6 is approximately similar to the fracture behavior of base metal SPRC 45, which showing the character of lower ductility with high strength results.

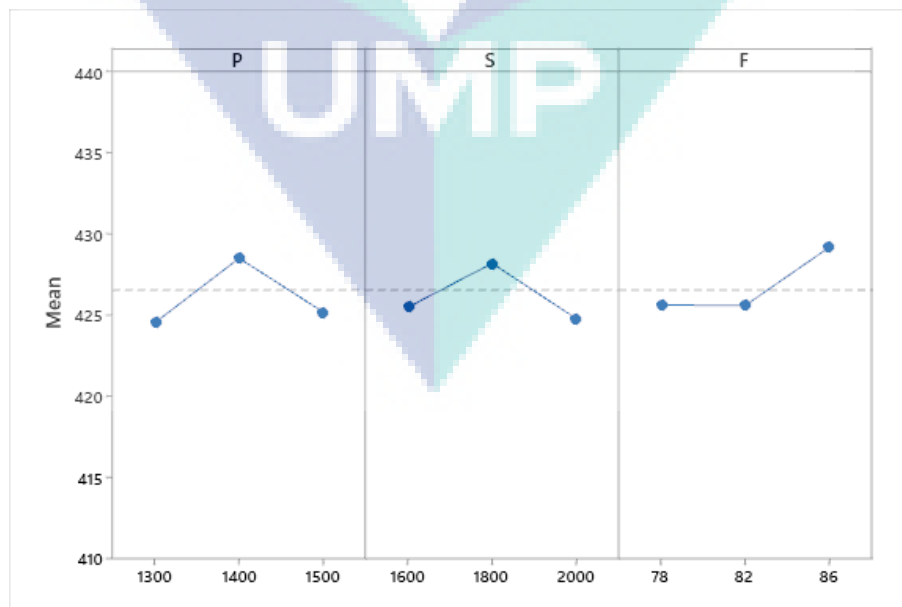
Bar graph shows the comparison of percentage of elongation of welded samples with the base metals; SPRC 40 and SPRC 45. The elongation of welded product was decreased compared to the base metal percentage of elongation. This is due to the effect of the heat affected during the

welding process which may alter the microstructure of the metals. However, the UTS and YS values are higher after been laser welded with high speed welding.

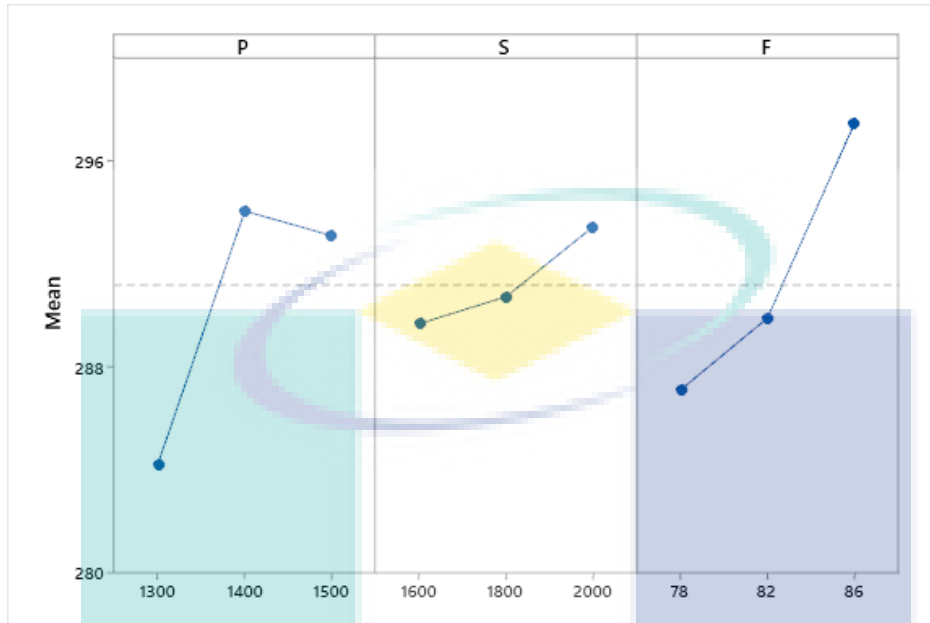


Bar graph of comparison between percentage of elongation (% E) of base metal and welded samples

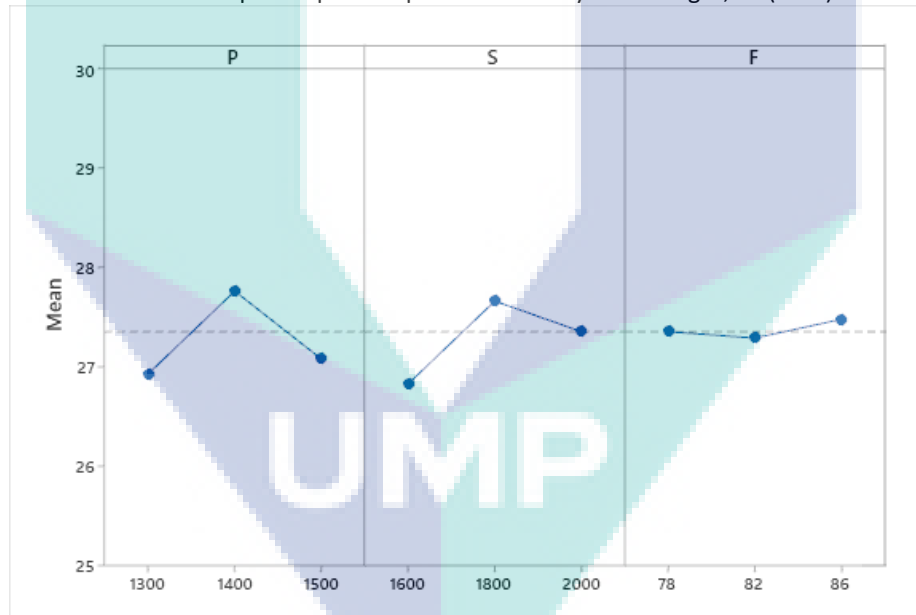
The effect of the welding parameters also was studied using mean effect plot (MEP) method from the DOE.



Mean effect plot of process parameters for ultimate tensile strength, UTS (MPa)



Mean effect plot of process parameters for yield strength, YS (MPa)



Mean effect plot of process parameters for yield strength, YS (MPa)

From the MEP graph based on this experiment, when the laser power increased, the UTS, YS, and % E increased above the mean value. However, the values of that three responses drop significantly below mean value as the laser power increased. 1.4 kW laser power was the most effective set up in this experiment for the laser power factor.

For scanning speed factor, the UTS and % E increased above mean value as the scanning speed increased from 1600 to 1800 mm/min. However, UTS value drops below mean after the speed increased to 2000 mm/min. % E still acceptable region since the percentage drops, but still above the mean value. It is a different situation with yield strength, as the yield strength keep increasing as the scanning speed increased.

From the focal length factor, the three response were stable when at F 78 and 80 mm. The three responses increased as the focal length increased from 78 to 86 mm. It could be observed that the most significance parameters in this experiment was focal length where it shows a trend above the mean line for all responses (UTS, YS, % E). Table below shows the setup for desired higher UTS, YS, and % E for this SPRC 40 and SPRC 45 dissimilar thickness joint.

Table 14 Main effective parameters for desired responses values

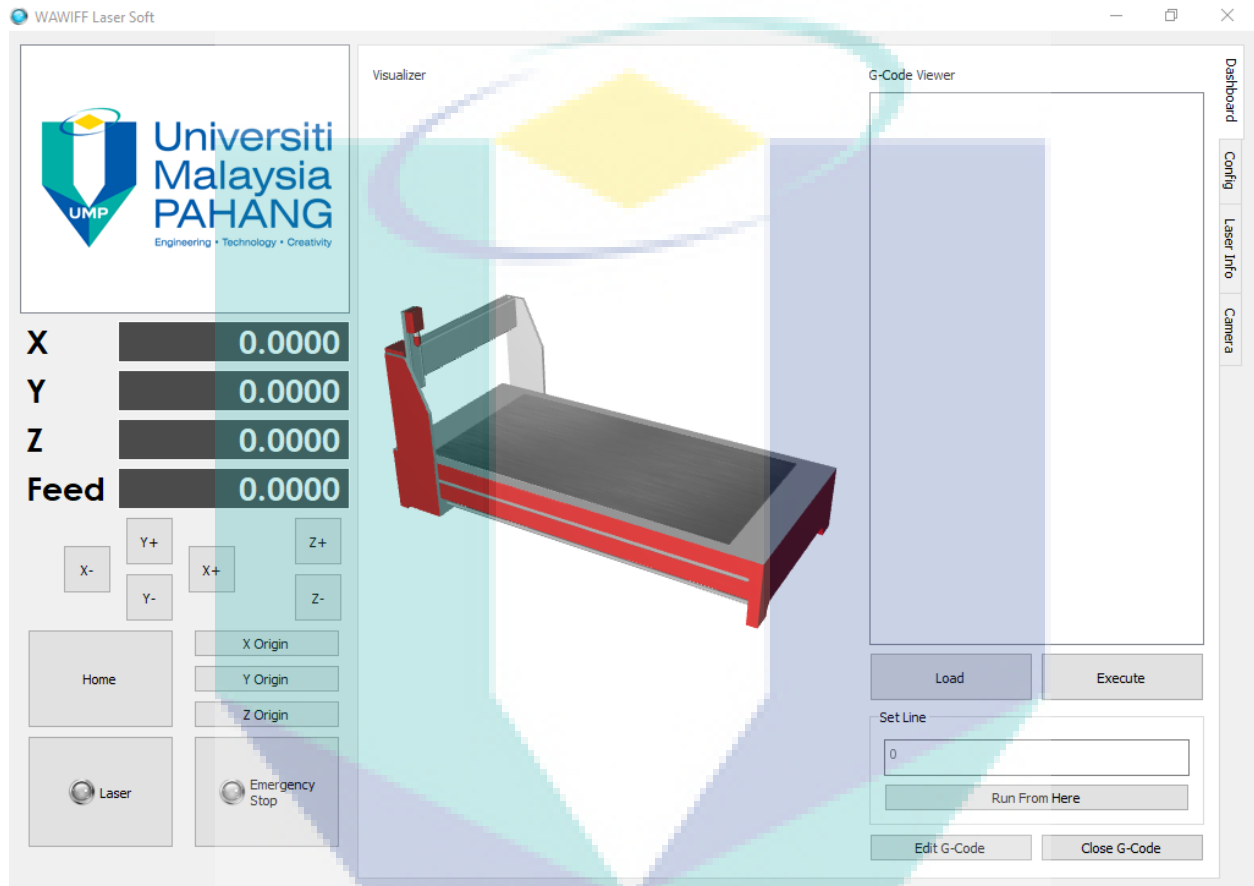
Responses	Target	Laser Power, P (W)	Scanning speed, S (mm/min)	Focal length, F (mm)
UTS (MPa)	High	1400	1800	86
YS (MPa)	High	1400	2000	86
% E at 50 GL (%)	High	1400	1800	86

The experiment of joining dissimilar thickness with different materials, SPRC 40 and SPRC 45 were successful using in-house high power fiber laser machine in Universiti Malaysia Pahang. The joint strength was high for all 15 samples, retrieved from the destructive testing (tension test), where sample break at the base metal instead of break at the joint itself.

UMP

5.3 Software Finalizing – Release Version

Release Version of CNC TWB Laser Welding Software



[TAILOR WELDED BALNKS (TWB) EQUIPMENT DEVELOPMENT-TF0713D278]
PROGRESS REPORT: MILESTONE 6 Patent and Documentation

The screenshot displays the WAWIFF Laser Soft control interface. At the top left, the logo for Universiti Malaysia PAHANG (UMP) is visible, with the tagline "Engineering • Technology • Creativity". The main interface is divided into several sections:

- Motion Control:** Parameters for X, Y, and Z resolutions (all set to 0.0010 mm/pulse), Rapid Speed (400.00 mm/min), and Feed Speed (400.00 mm/min).
- Laser Control:** Parameters for Laser Power (50.00%), Frequency (0.00 Hz), Laser Pulse (0.00 ms), Rise time (0.00 ms), and Fall time (0.00 ms).
- Laser Status:** A vertical column of buttons for Laser Power, Aim Beam, Analog control, External Control, and Emission, all currently set to OFF.
- Positioning:** A central area with a yellow diamond indicating the current position, surrounded by a blue circular path. Below this are buttons for X-, Y-, Z- (negative movement), X+, Y+, Z+ (positive movement), X Origin, Y Origin, Z Origin, Home, Laser, and Emergency Stop.
- Configuration:** A section at the bottom right for the Parallel Port Address and Config File, with Save and Load buttons.

The interface also features a sidebar on the right with navigation options: Dashboard, Config, Laser Info, and Camera.

[TAILOR WELDED BALNKS (TWB) EQUIPMENT DEVELOPMENT-TF0713D278]
 PROGRESS REPORT: MILESTONE 6 Patent and Documentation

WAWIFF Laser Soft

Universiti Malaysia PAHANG
 Engineering • Technology • Creativity

Laser ON
 Laser Ready
 Chiller Ready
 Lasser Error

Laser Power (W)
OFF

Laser Temperature (Degree)
31.5 °C

X: 0.0000
 Y: 0.0000
 Z: 0.0000
 Feed: 0.0000

Y+ X+ Z+
 X- Y- Z-

Home X Origin Y Origin Z Origin
 Laser Emergency Stop

OverHeat
 Laser Emission On
 High Back Reflection
 External Mode Enable
 Module Disconnected
 Module Fail
 Airing Beam On
 Power Supply Off
 Modulation Enabled
 Power Out Of Limit

Emission Starting
 Hardware Emission
 Power Supply Failure
 Low Temperature
 Power Supply Failure 2
 GND Leakage
 Critical Error
 Optical Interlock
 Communication Lost

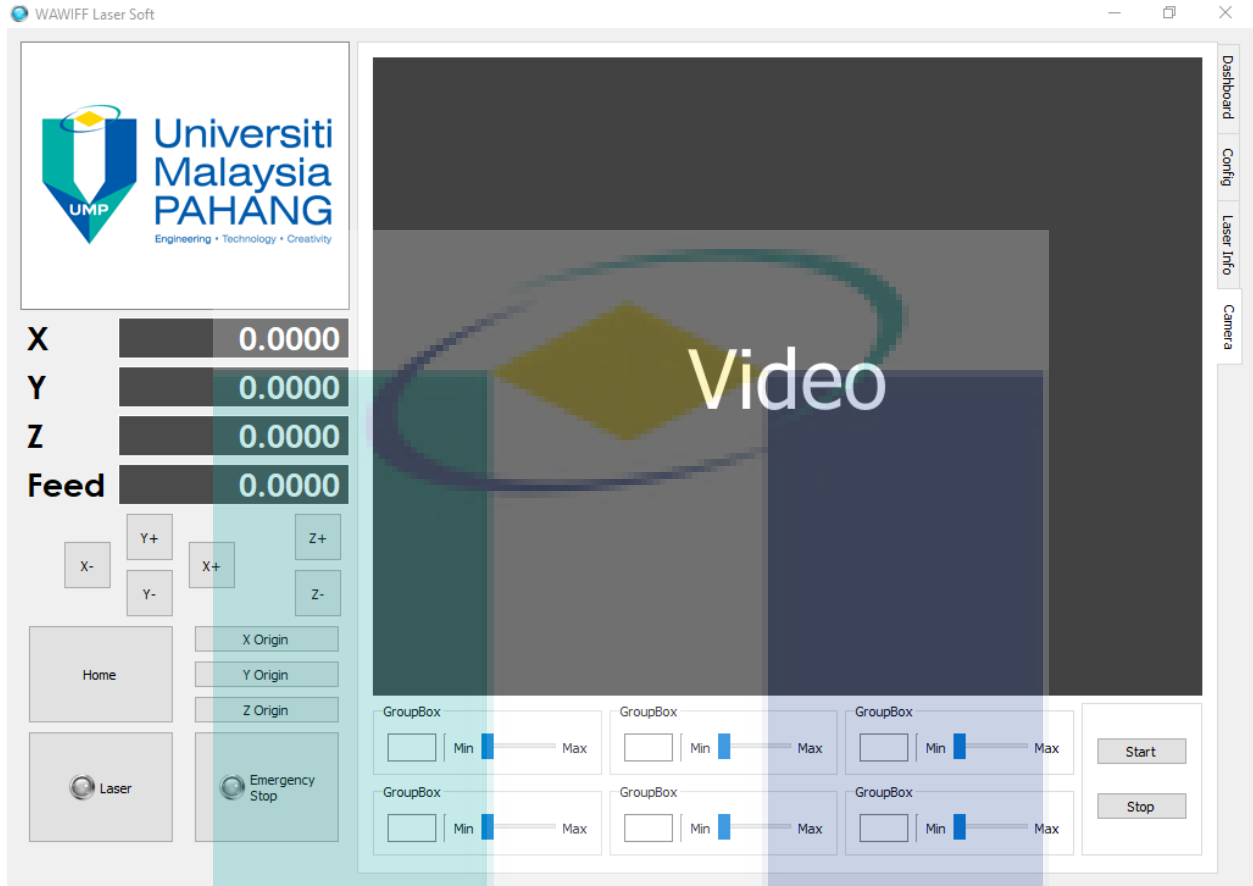
Temperature(Mean) [----] °C
 Temperature (max) [----] °C
 Temperature (min) [----] °C
 Module (Temp. max) [----]
 Module (Temp. min) [----]

Current [----] %
 Power [----] W
 Water flow: FF [----] l/min
 U control [----] V

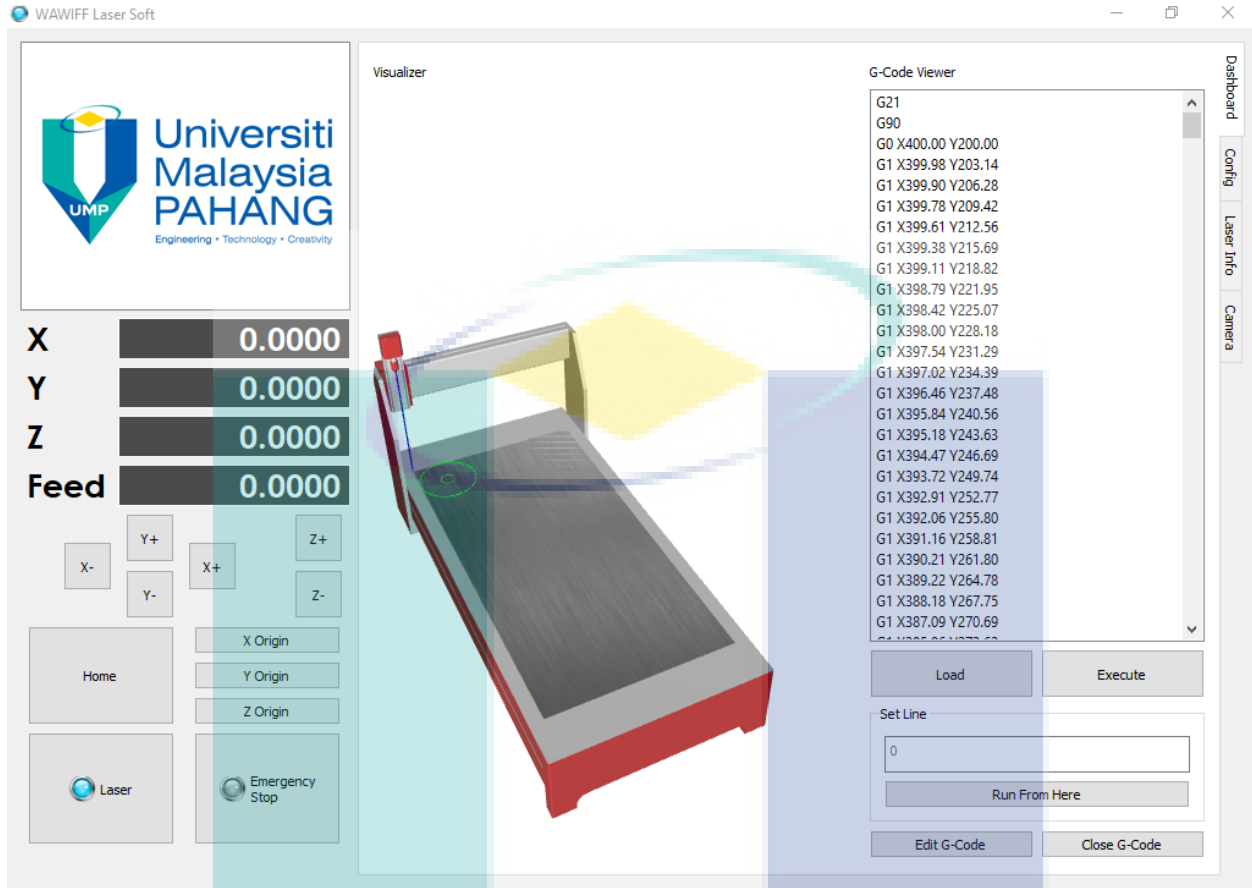
Operating Hours [----]
 Operating Hours Today [----]

Status Alarms Warning Events Power supply Chiler Dew point Hardwiring Modules

[TAILOR WELDED BALNKS (TWB) EQUIPMENT DEVELOPMENT-TF0713D278]
PROGRESS REPORT: MILESTONE 6 Patent and Documentation



[TAILOR WELDED BALNKS (TWB) EQUIPMENT DEVELOPMENT-TF0713D278]
PROGRESS REPORT: MILESTONE 6 Patent and Documentation

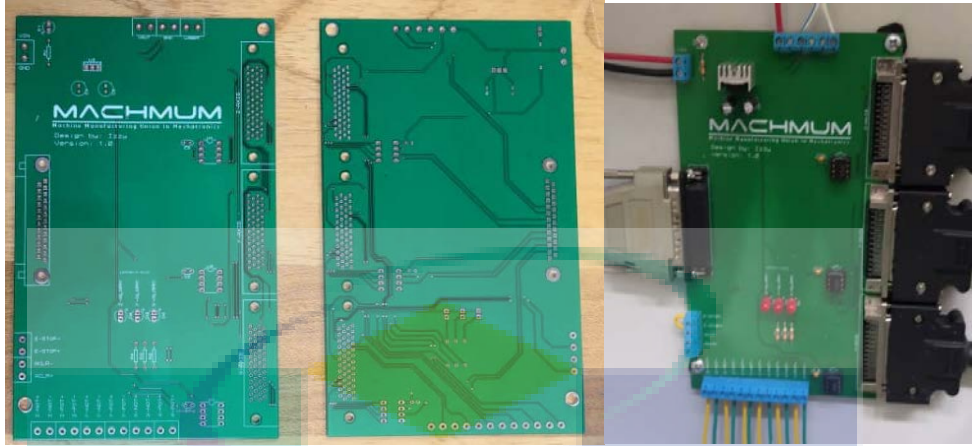


Features: Software Integrate with Laser Source and Monitoring Camera

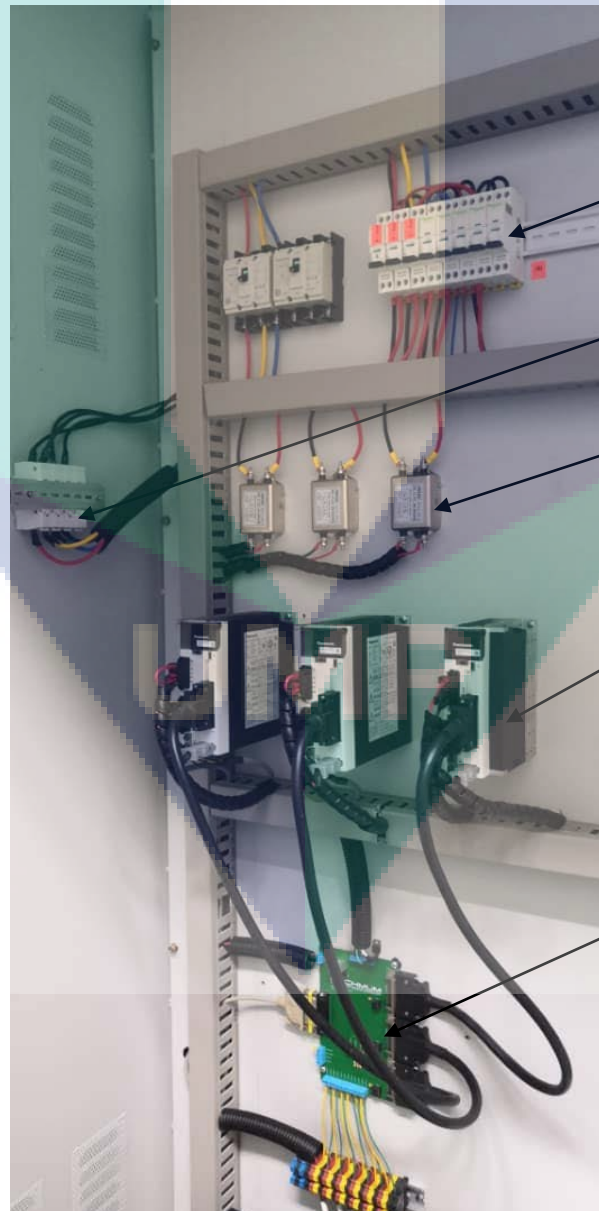


Analog laser power controller that synchronized with CNC software

[TAILOR WELDED BALNKS (TWB) EQUIPMENT DEVELOPMENT-TF0713D278]
PROGRESS REPORT: MILESTONE 6 Patent and Documentation



Laser and motor integration PCB controller board for CNC motion



Circuit braker

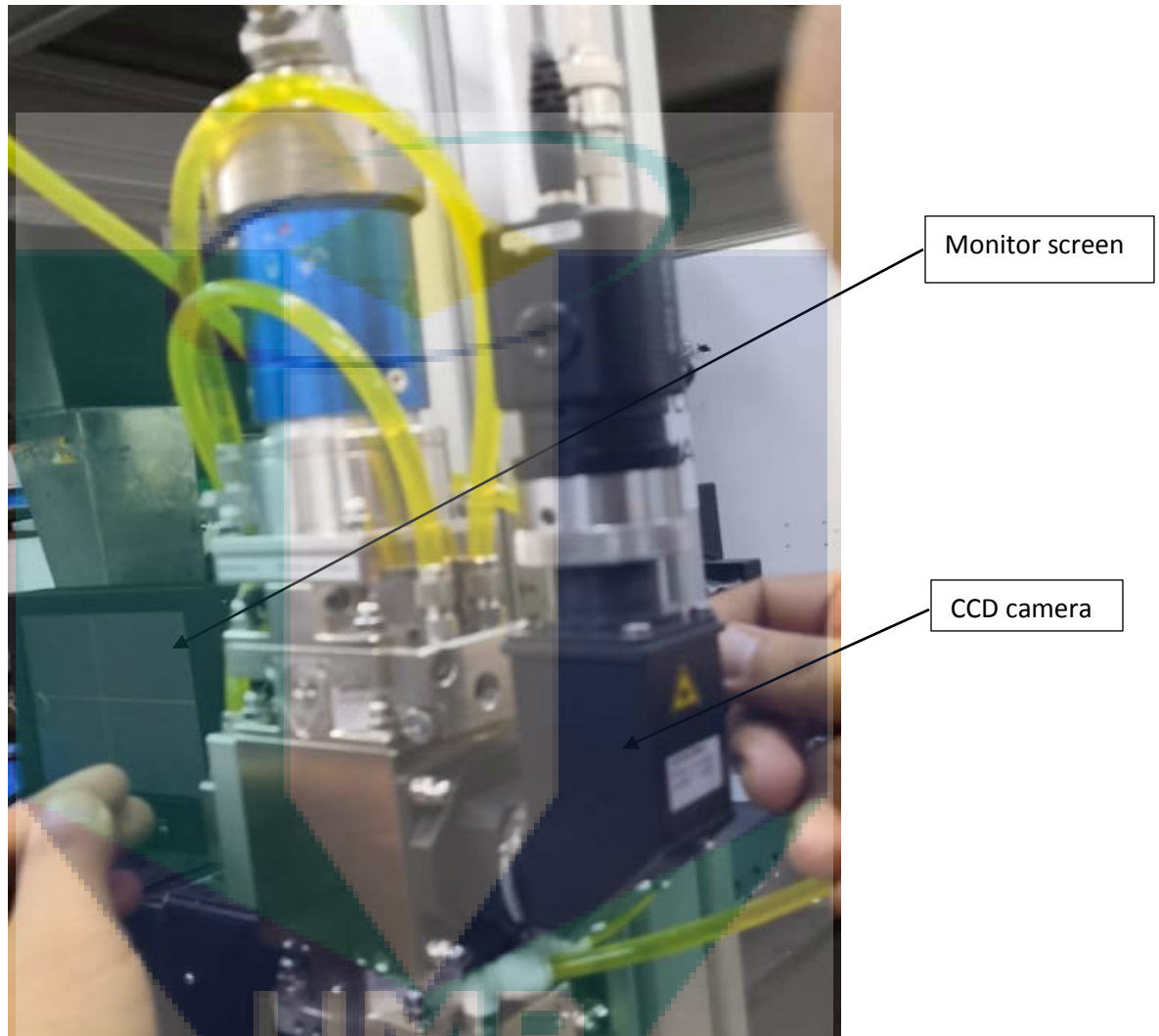
Emergency
switch switch

Signal filter

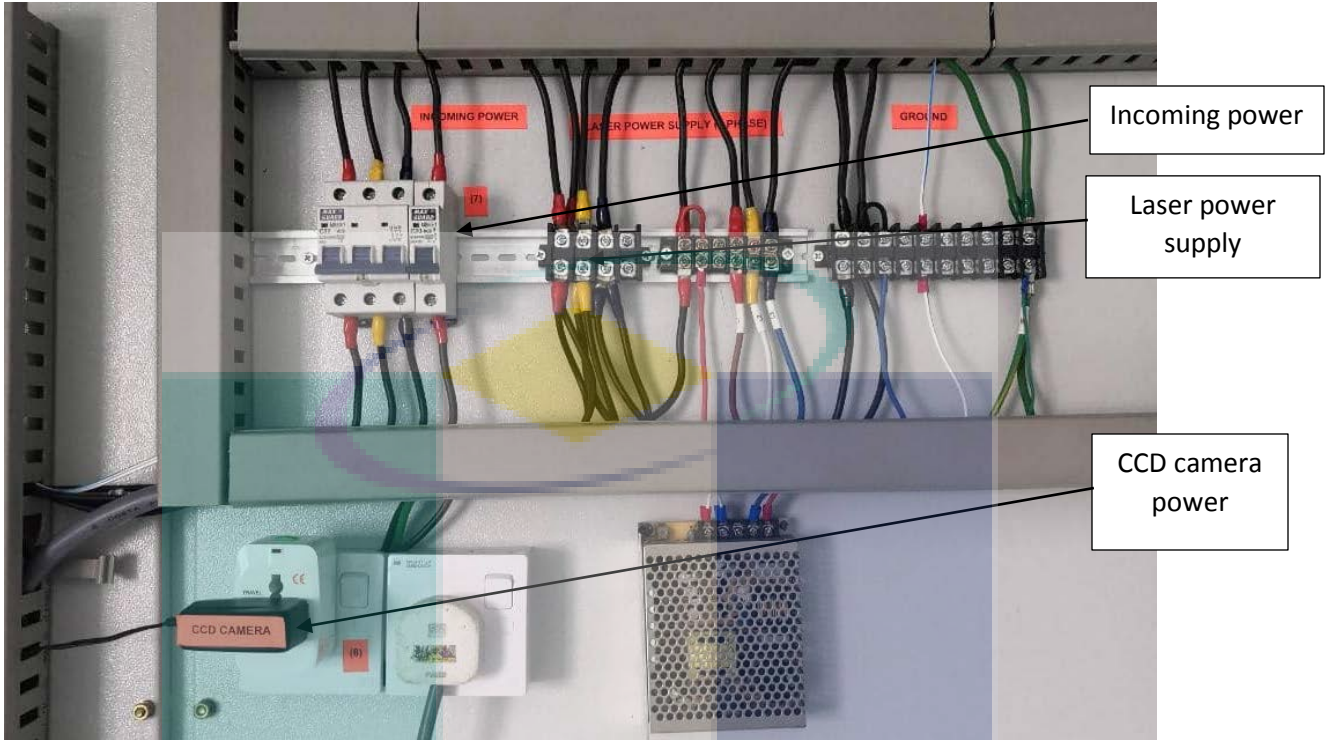
Motor driver

CNC integration
PCB board
controller

Overall wiring of the CNC laser welding integration PCB board



CCD camera and monitor screen for monitoring system



Laser power source and CCD camera integration to the system

UMP

MILESTONE 6

6.1 PATENT AND DOCUMENTATION

Filing No. PI2020000460

Title: Predefined Closest-Distance-Volume Reference-Pulse CNC Interpolator

E-STATUS Myipo: <https://estatus.myipo.gov.my/>

The screenshot shows the eStatus Myipo website interface. At the top, there is a search bar with the text "eStatus". Below it, a message states: "You may use this page to get the current status of your trademark, patent and industrial design. To begin please enter your application number or MyKad/company registration no, and the application type." The search form includes a "Domain" dropdown menu set to "Patent", a "Type" dropdown menu set to "Application No.", and an "Application" input field containing "PI2020000460". There are "Search" and "Reset" buttons. Below the search form, a "Result" section displays the following information:

Application No. : PI2020000460	Application Date : 28/01/2020	Priority Date : -
Patent No. : -	Grated Date : -	End of Protection Date : -
Expiry Date : -		
Owner : -		
Current Status : SUBMITTED		

ABSTRACT

This report presents an efficient interpolator algorithm for reference-pulse CNC controller. A 3-axis EMCO milling machine (31) was used as the platform to test the interpolator. The interpolator was executed in a PC-NC controller (32) and reference pulse signals are sent to the X (33), Y (34) and Z (35) axes drives. The positions and speeds information are acquired using another PC equipped with data acquisition system (36). The developed algorithm permits higher maximum allowable feed rate by reducing the number of required evaluated terms and employing less-extensive mathematical operations. Unlike existing interpolator which utilizes true distance calculation, the proposed interpolator is using the concept of predefined closest-distance-volumes whereby if the next point on curve is known and always resided into one of the volumes, the next interpolated point is identified. Results from computer simulations and experiments show that the developed algorithm is more efficient at least 2.5 times.

Technical Field

This invention describes an efficient interpolator algorithm for reference-pulse CNC controller. The developed algorithm permits higher maximum allowable feed rate by reducing the number of required evaluated terms and employing less-extensive mathematical operations.

Background Art

There are two types of CNC system: reference-pulse system and sampled-data system (Yang and Hong 2001). The two systems differ mainly in interpolation method and servo control loop implementation (Koren 1983).

Reference-pulse CNC system utilises incremental curve interpolator together with phase-lock servo control loop while sampled-data CNC system employs sampled-data interpolator and data-driven servo control loop.

Interpolator, or sometimes called, command generation is defined as algorithm that generates real-time reference commands to servo control loop in order to produce simultaneous multi-axis motion prescribing the shape of a mathematically defined curve (Lim et. al 1992, Lo 1992, Koren 1983, Danielsson 1970).

The inputs to the interpolator are coordinates between the end points, the required speed and the mathematically-defined cutting path. Interpolator computes and generates commands to the machine-axis servo control loops in real-time such that the relative motion between the cutting tool and the work-piece follows closely to the specified cutting path and speed (Lim et. al 1992).

On the other hand, servo control loop, or sometimes called, command realization is defined as servo-drive control loop that controls the positions and velocities of machine tools axes in accordance with commands generated by CNC interpolators (Srinivasan and Tsao 1997).

Reference-pulse interpolator is an incremental curve generation method in which the curve is traced by series of machine-tool smallest position resolution called basic length-unit (BLU). Using reference-pulse system, the interpolator is implemented in computer while the servo control loop is implemented by independent hardware.

Reference-pulse interpolator generates sequence of reference pulses as position commands to the servo control loop axes. Each pulse represents one basic length-unit (BLU) of axis motion. At the same time, the frequency of the pulse represents the speed command to the servo control loop. Using up-down counter, servo control loop compares the reference-pulses with the actual pulses from the encoder and the difference represents position error, which is utilised by the position controller to drive the axes.

In contrast, sampled-data interpolator is based upon approximating curve by series of straight-line determined by specified speed and sampling time (Lim et. al 1992). Using sampled-data system, computer is used as interpolator as well as part of the servo control loop by replacing the up-down

counter with a software comparator. The computer samples the actual pulses at fixed sampling time and compares with the reference positions provided by interpolator.

The difference represents position error and is utilised by software position controller, which calculates and transmits to digital-to-analogue converter (DAC) at fixed sampling time, the appropriate signal value to drive the axes (Koren 1983). The performances of CNC systems are based on three factors: maximum allowable feed rate, maximum contour error and maximum feed rate error (Lo 1992).

Maximum allowable feed rate is defined as the maximum allowable speed that the work-piece is brought into contact with the cutting tool (Krar et. al 1998). Higher maximum allowable feed rate allows higher material removal rate, which reduces machining time and cost. Maximum allowable feed rate is limited by the maximum allowable feed rate command and the maximum allowable speed of the servo-drive system.

On the other hand, maximum contour error is the maximum deviation of cutter location from the desired curve (Lo 1992, Koren 1997). Contour error is a source of dimensional inaccuracies of machining part. Contour error is contributed by interpolator error (position command error and chordal error) and axial error caused by imperfection of position controller inside the servo control loop of the servo drives (Ni 1997).

Finally, the maximum feed rate error is the maximum difference between the actual feed rate and the desired feed rate along the contour (Lo 1992, Koren 1997). Feed rate error is caused by feed rate command error and the imperfection of speed controller of the servo control loop.

In terms of performance, sampled-data CNC system permits higher maximum allowable feed rate and smaller feed rate error than reference-pulse CNC system (Yang and Hong 2001, Huang 1992, Lim et. al 1992, Koren 1983, Koren 1979). Nevertheless, the contour error for sampled-data CNC system is larger as well as dependent on feed rate, path curvature and sampling time. As a result, sampled-data system requires complicated servo control loop (Yang and Hong 2001, Huang 1992, Lim et. al 1992, Koren 1983, Koren 1979).

Although contour error for reference-pulse system is smaller and is independent of feed rate, path curvature and sampling time, the maximum allowable feed rate is limited and the feed rate error is bigger (Yang and Hong 2001, Huang 1992, Lim et. al 1992, Koren 1983). The maximum allowable feed rate of the reference-pulse system is determined by the maximum reference-pulse frequency generated by the reference-pulse interpolator to the servo control loop.

Reference-pulse interpolator is based upon iterative technique. During iteration, interpolator algorithm is executed and appropriate reference-pulse is generated to the servo control loops (Koren 1983, Koren 1979).

Clearly, the generated reference-pulse frequency is limited by the iteration speed - higher iteration speed corresponds to higher reference-pulse frequency.

Disclosure of Invention

Using reference-pulse system, there are two methods to increase the iteration speed: by means of utilizing faster microprocessor and by using efficient interpolator algorithm. The way to increase iteration speed is by employing efficient-algorithm reference-pulse interpolator. Obviously, the more efficient the algorithm the less central processing unit (CPU) time is required during interpolator iteration, which results in higher iteration speed.

Higher in iteration speed will result in higher reference-pulse frequency, which will permit higher maximum allowable feed rate.

Unlike existing interpolator which utilizes true distance calculation, the proposed interpolator is using the concept of predefined closest-distance-volumes whereby if the next point on curve is known and always resided into one of the volumes, the next interpolated point is identified.

The invention of using predefined closest-distance-volume interpolator technique is claimed which perform better than the commonly used Newton-Raphson interpolator technique.

Efficiency comparison between the two interpolators is then compared. Results from computer simulations and experiments show that the developed algorithm is more efficient at least 2.5 times.

Description of Drawings and Best Mode for Carrying Out the Invention

Based on FIG. 1, a curve is represented by a parametric equation r . Starting from an interpolated point P_k , there are 26 possible next interpolated points 1 - 26.

Interpolated point means a point where the motion can possibly move because each motion axis can only move in an incremental size. For instance, one possible next interpolated point is to move one step in X direction, one step in Y direction and one step in Z direction.

Considering all possibilities, there are 26 possible next interpolated points. Notice that the interpolated point may not coincide with the point on curve. Thus, the interpolator problem can be described as finding the next interpolated point based the current interpolated point, the current point on the curve and the direction of the curve in order to trace the curve.

FIG. 2 shows the summary of the steps for the predefined closest-distance-volume interpolator. The predefined closest-distance-volume interpolator consists of 4 major program.

First program 27. Determine the possible pierced plane based on tangent vector direction of the curve. In this step, the derivative of the curve at the current point on curve is calculated. From this information, the direction of the curve can be determined and thus the set of possible enclosing plane, pierced by the curve, can be determined.

Second program 28. Determine the possible pierced plane based on geometric ratio between tangent vectors of the curve. In this step, the tangent line at the point on curve is extended to the pierced plane. The geometric ratio between the X, Y and Z coordinates will indicate the set of possible enclosing planes pierced by the curve.

Third program 29. Determine the pierced plane by combining the possibility of the pierced plane set. Combining (union operation) the two sets of possible enclosing planes will uniquely determine the pierced plane. From the pierced plane, determine the next point on curve. Knowing the pierced plane, the next point on curve can be determined.

Forth program 30. From the next point on curve, determine the interpolated point. Based on the next point on curve – that is sitting inside an enclosing volume (based on the pierced plane), the next interpolated point can be determined.

Fig. 3 shows the hardware setup for the algorithm operation. A 3-axis EMCO milling machine 31 was used as the platform to test the interpolator. The interpolator was executed in a PC-NC controller 32 and reference pulse signals are sent to the X 33, Y 34 and Z 35 axes drives. The positions and speeds information are acquired using another PC equipped with data acquisition system 36.

CLAIMS:

A pre-defined closest-distance volume interpolator is claimed to increase the performance of reference pulse CNC interpolator. It is based on conditional criteria calculation instead of calculation intensive Newton Raphson algorithm.

The closest-distance volume technique uses little calculation but more conditional (Boolean) types operations whereas the Newton-Raphson's technique uses real computation like squaring and square rooting. This will make the Newton-Raphson technique calculation intensive.

The claim of algorithm 1 is efficient at least 2.5 times the popular Newton-Raphson algorithm.

The machining time for the pre-defined closest-distance volume interpolator is faster 3 times than the Newton-Raphson interpolator.

The logo for UMP (Universiti Malaysia Perlis) is a large, stylized shield shape. It is divided into four quadrants by a white 'V' shape pointing downwards. The top-left and bottom-right quadrants are light blue, while the top-right and bottom-left quadrants are light green. The letters 'UMP' are written in a large, white, sans-serif font across the center of the shield.

UMP

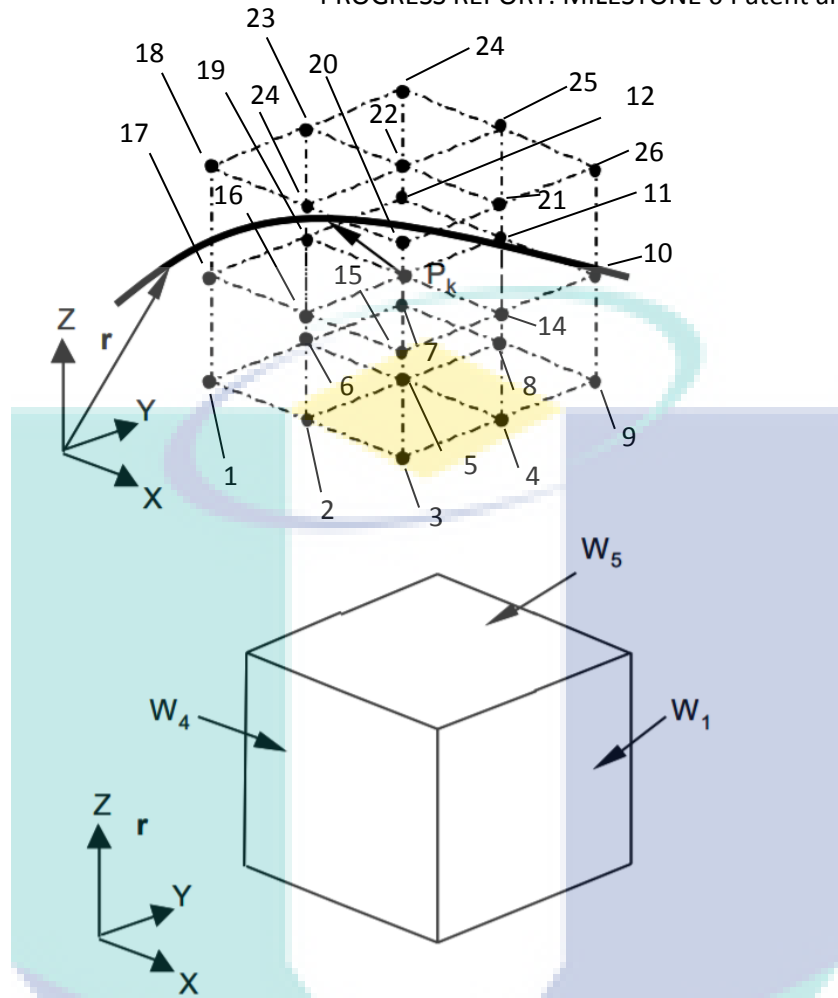


Fig. 1: The 26 Possible Next Interpolated Points and the 6 Enclosing Planes

UMP

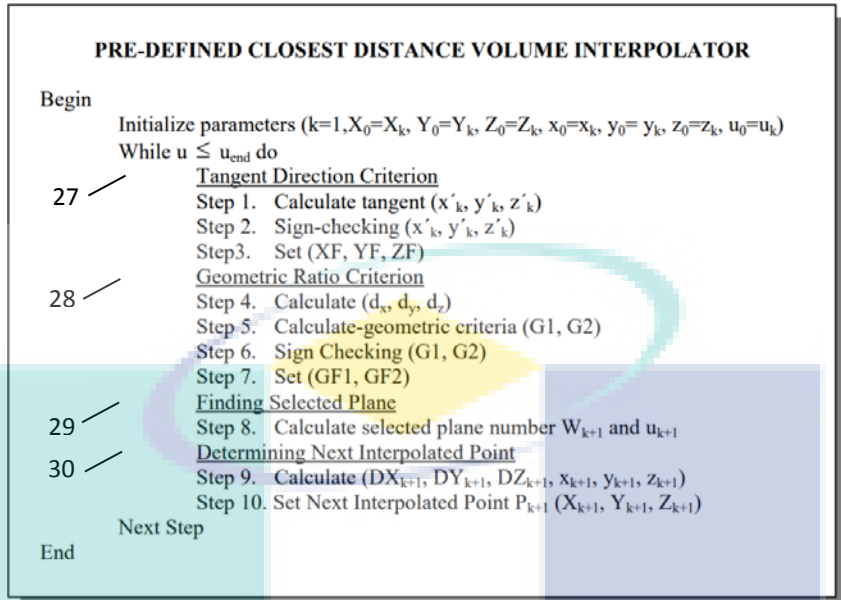


Fig. 2: The predefined closest-distance-volume interpolator

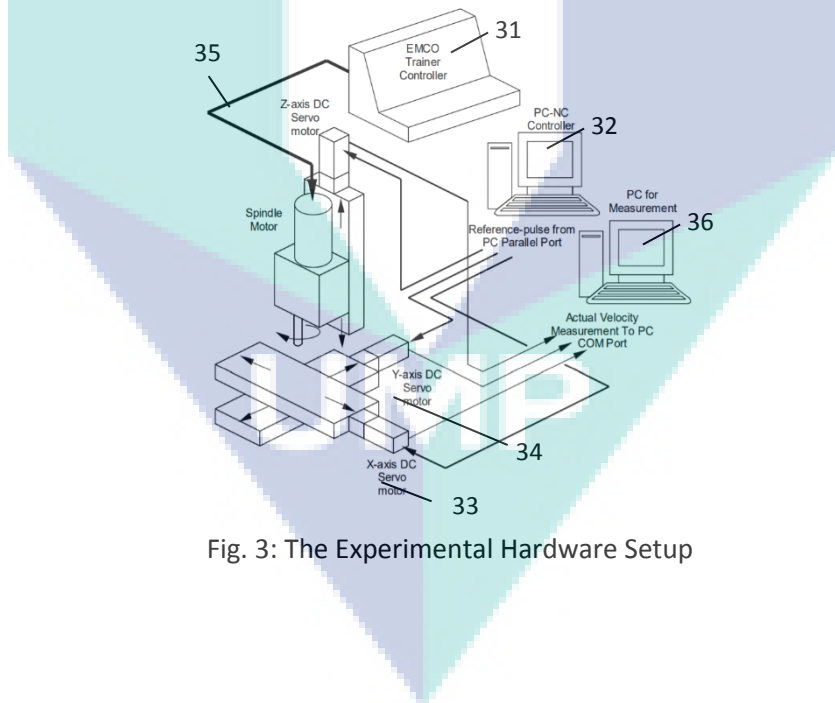


Fig. 3: The Experimental Hardware Setup

FUTURE PROSPECT OF THE TWB TECHNOLOGY

Manufacturing sector is one of the major contributor sectors that driving the Malaysian economy nowadays. The manufacturing sector is targeted by the government to grow 5.6% annually and to contribute 28.5% to gross domestic product (GDP) in the year 2020 with the total investment of RM27.5 billion annually (MITI, 2006).

Overall, sales value performance of manufacturing sector in 2009 posted an increment growth as shown in Figure 1.1 to register a total of RM468.8 billion sales value. The sales value of the manufacturing sector in December 2009 posted a double digit sales of RM43.2 billion as compared to RM33.6 billion reported in January 2009. This good performance is the proof of the stable environment for the manufacturing sector to be grown up in Malaysia.

Regarding to the Third Industrial Master Plan (IMP3) 2006-2020 which was launched on 18 August 2006 by Malaysian Ministry of International Trade and Industry, machine tools industry will be one of the main sub-sectors for the economic growth in manufacturing sector (MITI, 2006).

This justification based on the increment of machine tools import and export value in a period of 1996-2005 as shown in Figure 1.2. Based on the report, Malaysian machine tools industry activity increased consistently during the period of the Second Industrial Master Plan (IMP2) 1996-2005. The performance was continuing increase at the beginning of IMP3 period. The export value in 2008 of IMP3 marked the highest with RM 44 billion and close to double increment if the comparison is made between the years of 1996.

Extending from the IM2 report, total exports of machine tools those produced by local manufacturers increased dramatically from RM5.1 billion in 1996 to RM18.3 billion in 2005. Most of the Malaysian's export countries were China, Singapore, Thailand and United State. This shows the potential of machine tools industry to the country.

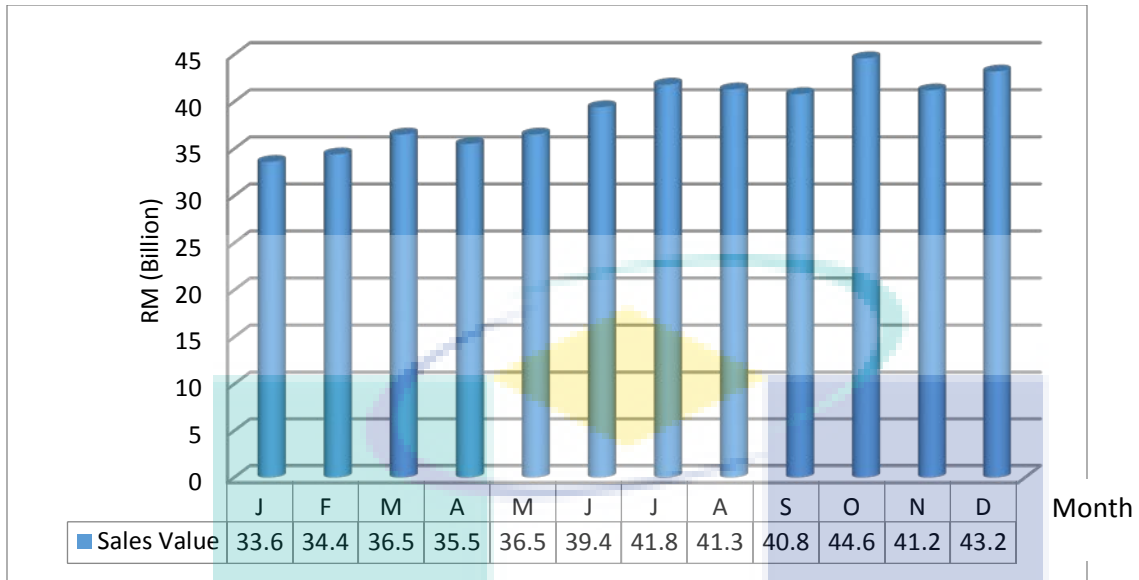


Figure 1.1: Sales Value of the Manufacturing Sector

Source: MITI (2010)

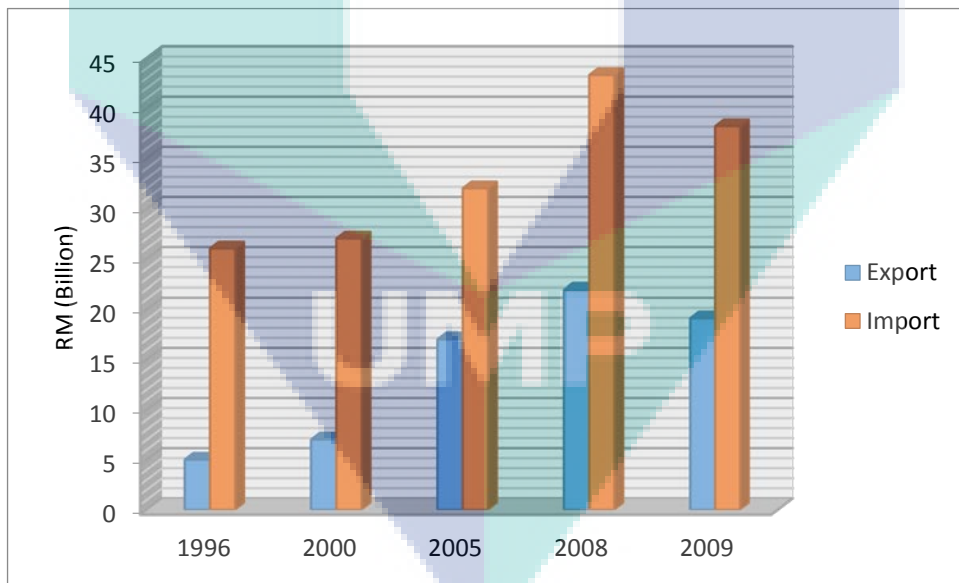


Figure 1.2: Export and Import of Machine Tools

Source: MITI (2010)

However, in IMP2 and IMP3 progress above, it is clearly illustrated that, Malaysia still depends on imports of machine tools from overseas. Average rate of yearly growth for imports of machine tools expands to 1.5%, which is from RM26.7 billion in 1996 to RM32.4 billion in 2005 (MITI, 2006). The situation happens because Malaysia has less expertise in high-tech machine tools builder and this issue is great importance to be highlighted.

The developed CNC welding machine is readily for commercial welding services that fall under the metal manufacturing industry. The performance of the final product with the accurate and precise welding output let the equipment developed positioned at the industry standard of practice. The complexity of welding demand process such as tailor welded blank and profile welding curve can be executed by the developed CNC machine.

The developed CNC machine structure and mechanism are capable for industrial specification; 4 x 8 feet of blank welding with material handling assisted system. Pipe welding with additional custom jig will make the machine more flexible for various welding application.

The developed CNC controller and software are capable to provide fully automation welding process with precise and accurate machine motion. The fully power can achieve until 2kWatt laser welding finishing.

The developed CNC welding machine can be extended for different field of industries such as oil and gas fabrication, various automotive part welding and other heavy machinery fabrication. The developed CNC machine controller and software are possible to be customized for another type of CNC machine such as laser cutting, plasma cutting and water jet cutting. Only some additional cutting accessories will make the machine more reliable to the industry.

The developed machine successfully reduced the machine cost since the design and assembly are integrated locally. The know-how of the CNC machine integration is successfully developed with fully local expertise. Local expertise will make the product developed easily to adapt the latest technology update.

REFERENCES

- [1] Schrek A., Đvec P., and Brusilová A. (2017). Formability of Tailor-Welded Blanks From Dual-Phase and Bake-Hardened Steels With A Planar Anisotropy Influence. *Journal of Strength of Materials*, Vol. 49, No. 4. Pp. 550-554.
- [2] Retrieved on 25th of January 2018. <http://www.twbcompany.com/products/tailor-welded-blanks>.
- [3] Gajendra J., Sourav D., Subhasis S. , Arijit L., and Arunansu H. (2013). Design and development of precipitate strengthened advanced high strength steel for automotive application. *Journal of Materials Science & Engineering A* 561. Pp. 394 – 402.
- [4] Salzgitter Flachstahl Handbook for 22MnB5 Page 1 from 3 Edition: 01/14.
- [5] Benjamin G., Uwe R., and Simon O. (2016) Laser Welding of Ultrahigh Strength Steels at Subzero Temperatures. 9th International Conference on Photonics Technologies (LANE).
- [6] Wei Y. N. and Jian Y. B. (2014) Microstructure and mechanical properties of fiber laser welded joints of ultrahigh-strength steel 22MnB5 and dual-phase steels. *Journal of Materials Research*. 29(21). Pp. 2565-2575.
- [7] F. Jovane, 1998, “Open Architecture Control Systems - Summary of Global Activity”, ITIA Series.
- [8] Harry H. Cheng, Frederick Proctor, John L. Michaloski and William P. Shackleford, 2001, “Real-Time Computing in Open Systems for Manufacturing”, March 2004, Vol. 1, *Journal of Computing and Information Science in Engineering* 92-99.
- [9] Proctor, F., 1998, “Practical Open Architecture Con- trollers for Manufacturing Applications”, in: “Open Architecture Control Systems”, ITIA Series.